SEISMIC BEHAVIOR OF FIBER REINFORCED CEMENTITIOUS COMPOSITE BEAM-TO-COLUMN CONNECTIONS

A THESIS SUBMITTED TO
THE GRADUATE SCHOOL OF NATURAL AND APPLIED SCIENCES
OF
MIDDLE EAST TECHNICAL UNIVERSITY

BY

YUNUS KANTEKİN

IN PARTIAL FULFILLMENT OF THE REQUIREMENTS
FOR
THE DEGREE OF MASTER OF SCIENCE
IN
CIVIL ENGINEERING

MAY 2023

Approval of the thesis:

SEISMIC BEHAVIOR OF FIBER REINFORCED CEMENTITIOUS COMPOSITE BEAM-TO-COLUMN CONNECTIONS

submitted by **YUNUS KANTEKİN** in partial fulfillment of the requirements for the degree of **Master of Science** i**n Civil Engineering, Middle East Technical University** by,

Prof. Dr. Halil Kalıpçılar
Dean, Graduate School of **Natural and Applied Sciences** _____

Prof. Dr. Erdem Canbay
Head of the Department, **Civil Engineering** _____

Assoc. Prof. Dr. Burcu Burak Bakır
Supervisor, **Civil Engineering Dept., METU** _____

Examining Committee Members:

Prof. Dr. Erdem Canbay
Civil Engineering Dept., METU _____

Assoc. Prof. Dr. Burcu Burak Bakır
Civil Engineering Dept., METU _____

Prof. Dr. Murat Altuğ Erberik
Civil Engineering Dept., METU _____

Prof. Dr. Afşin Sarıtaş
Civil Engineering Dept., METU _____

Asst. Prof. Dr. Halit Cenan Mertol
Civil Engineering Dept., Atılım University _____

Date: 26.05.2023

I hereby declare that all information in this document has been obtained and presented in accordance with academic rules and ethical conduct. I also declare that, as required by these rules and conduct, I have fully cited and referenced all material and results that are not original to this work.

Name Last name : Yunus Kantekin

Signature :

ABSTRACT

SEISMIC BEHAVIOR OF FIBER REINFORCED CEMENTITIOUS COMPOSITE BEAM-TO-COLUMN CONNECTIONS

Kantekin, Yunus
Master of Science, Civil Engineering
Supervisor: Assoc. Prof. Dr. Burcu Burak Bakır

May 2023, 178 pages

Beam-to-column connections in reinforced concrete moment-resisting frame structures are vulnerable to high horizontal shear stresses during seismic events. Ensuring integrity, shear strength, and ductility in these critical regions often involves complex detailing and reinforcement congestion. To overcome this problem, fiber reinforced cementitious composites (FRCC) have been proposed as an alternative material for beam-to-column connections. However, there is a lack of a comprehensive model for FRCC joint behavior. In this study, a shear strength prediction equation and a parametric shear stress-strain model are developed for FRCC beam-to-column connections, based on an extensive database of experimental data. The proposed models are validated against experimental data, existing equations, and code estimations, demonstrating their accuracy and applicability. This research enhances understanding and provides practical guidance for designing efficient and resilient FRCC beam-to-column connections, paving the way for safer and more sustainable structures.

Keywords: Beam-to-Column Connections, Fiber Reinforced Cementitious Composite, Joint Shear Strength, Joint Shear Deformation, Analytical Model.

ÖZ

LİF TAKVİYELİ ÇİMENTO ESASLI KOMPOZİTTEN YAPILAN KOLON-KİRİŞ BİRLEŞİM BÖLGELERİNİN SİSMİK DAVRANIŞI

Kantekin, Yunus
Yüksek Lisans, İnşaat Mühendisliği
Tez Yöneticisi: Doç. Dr. Burcu Burak Bakır

Mayıs 2023, 178 sayfa

Betonarme çerçeve yapılardaki kolon-kiriş birleşim bölgeleri, deprem etkileri nedeniyle yüksek kayma gerilmelerine maruz kalır. Bu kritik bölgelerde kayma dayanımı ve süneklik sağlamak için genellikle uygulaması zor donatı detayları kullanılır. Bu sorunları aşmak için, kolon-kiriş birleşim bölgelerinde alternatif bir malzeme olarak lifli kompozit kullanımı önerilebilir. Ancak, literatürde bu tür lifli kompozit birleşim bölgeleri için kapsamlı bir davranış modeli bulunmamaktadır. Bu çalışmada, deney verilerine dayanan kapsamlı bir veritabanı kullanılarak, lifli kompozitlerden yapılan kolon-kiriş birleşim bölgeleri için yeni bir kayma mukavemeti tahmin denklemi ve parametrik bir kayma gerilimi-birim şekil değiştirme modeli geliştirilmiştir. Önerilen denklem ve model, deneysel verilerle, mevcut araştırmaların ve yönetmeliklerin denklemleriyle karşılaştırılarak doğruluk ve pratik kullanılabilirlik açısından doğrulanmıştır.

Anahtar Kelimeler: Kolon-Kiriş Birleşim Bölgeleri, Lifli Kompozit, Birleşim Bölgesi, Kayma Dayanımı, Birleşim Bölgesi Kayma Şekil Yer Değiştirmesi, Analitik Model.

To My Lovely Family

ACKNOWLEDGMENTS

I wish to extend my deepest appreciation to my supervisor Assoc. Prof. Dr. Burcu Burak Bakır for her guidance, advice, criticism, encouragements, and insight throughout the research. Never would this study have been completed without her support, patience, and precious contributions.

I would like to express my heartfelt gratitude to my dear wife, Beste, whose steadfast love, support and encouragement have been the cornerstone of my journey throughout this thesis. Her patience, understanding, and unwavering belief in my abilities have been a constant source of inspiration.

Words alone cannot capture the depth of my gratitude towards my beloved family for the immeasurable love, unwavering support and encouragement they have provided me throughout this process.

I am grateful to my dear friend and colleague, Evrim Özkuzucu, for his support and motivation as well as enlightening discussions throughout the course of this thesis. His profound expertise, keen insights, and unwavering dedication have been instrumental in shaping the direction of my research and fostering a stimulating academic environment.

I would like to extend my sincerest gratitude to Salim Azak for his precious mentorship and insightful advice throughout this journey. His guidance and wisdom have played a pivotal role in shaping my understanding and approach. I am truly grateful for his unwavering support and dedication to my growth and development.

I would like to express my deepest appreciation and heartfelt thanks to Dr. Tuba Eroglu Azak. Her unwavering support, encouragement, and invaluable contributions have played a pivotal role in the successful completion of this thesis. Her guidance and insightful feedback have been instrumental in shaping the trajectory of my research.

TABLE OF CONTENTS

LIST OF TABLES

TABLES

LIST OF FIGURES

FIGURES

LIST OF SYMBOLS

SYMBOLS

A_g : Gross cross sectional area of column.

A_j : Effective joint area.

A_s : Cross sectional area of the beam longitudinal reinforcement.

A_{sv} : Total cross sectional area of transverse reinforcement.

A_0 : Cross sectional area of transverse reinforcement

a_s' : Distance between the outermost compression fiber and the centroid of compression reinforcement.

b_b : Beam width.

$b_{c,core}$: Column core width.

b_j : Effective joint width.

b_c : Column width.

d'' : Distance between outermost tension and compression reinforcement of beam.

D_f : Fiber diameter.

E_s : Modulus of elasticity of the beam reinforcement.

f_c' : Compressive strength of the composite.

f_y : Yield strength.

f_t : Tensile strength of the fibers.

h_b : Beam depth.

h_c : Column depth.

$h_{c,core}$: Column core depth.

$h_{b,core}$: Beam core depth.

h_j : Effective joint depth.

H : Column height.

k : Bond factor for fibers.

k_a : Adhesion coefficient of fibers.

L_f : Fiber length.

L : Beam length.

l_e : Effective length of the joint transverse reinforcement.

N : Axial force applied on the column.

n : Axial load ratio.

P : Applied force.

RI : Fiber reinforcing index.

R : Coefficient of correlation.

R^2 : Coefficient of determination.

s : Transverse reinforcement spacing.

s_{used} : Used joint stirrup spacing.

V_c : Shear carrying capacity of the composite.

V_{col} : Column shear force .

V_f : Volume fraction of fibers.

V_{fiber} : Shear carrying capacity of the fibers.

V_j : Joint shear strength.

V_{sv} : Shear carrying capacity of the transverse reinforcement.

σ_{cr} : Tensile cracking strength of the composite.

ε_y : Yield strain.

γ : Shear strength factor.

ρ_{gross} : Volumetric ratio of the joint stirrups based on gross joint volume.

ρ_{core} : Volumetric ratio of the joint stirrups based on core joint volume.

$\rho_{singlelayer}$: Volumetric ratio of the joint stirrups based on tributary volume of one stirrup.

$v_{j,cracking}$: Stress component of the cracking point.

$v_{j,inelastic}$: Stress component of the point at the onset of inelastic activity.

$v_{j,max1}$: Stress component of the initial point of the plateau.

$v_{j,max2}$: Stress component of the termination point of the plateau.

$v_{j,final}$: Stress component of the final point.

$\gamma_{j,cracking}$: Strain component of the cracking point.

$\gamma_{j,inelastic}$: Strain component of the point at the onset of inelastic activity.

$\gamma_{j,max1}$: Strain component of the initial point of the plateau.

$\gamma_{j,max2}$: Strain component of the termination point of the plateau.

$\gamma_{j,final}$: Strain component of the final point.

CHAPTER 1

INTRODUCTION

1.1 Overview

Beam-to-column connections in moment-resisting frame structures are highly susceptible to seismic loading, making them one of the most vulnerable regions in a structure. The main concern is the high horizontal shear forces they experience. Consequently, it is crucial to design these joints to withstand such shear forces without compromising their integrity. This entails preventing spalling off of concrete and diagonal cracking in the joint, ensuring that the joint remains intact during seismic loading.

The design of beam-to-column joints is influenced by numerous significant parameters, yet current design codes often oversimplify the requirements. They typically involve two basic aspects. Firstly, the shear strength of a joint is determined by a constant multiplied by the square root of the concrete compressive strength, that represents the tensile strength, with the requirement that it exceeds the horizontal joint shear demand. Secondly, a minimum ratio of moment capacities of the columns to the beams framing into the joint, typically set at 1.2, is specified. However, these simplified design requirements have been shown to be insufficient in addressing the complex nonlinear behavior of fiber reinforced composite beam-to-column connections, as demonstrated by previous studies in the literature.

Current design code requirements often impose the use of closely spaced reinforcement layouts in the joint region, leading to reinforcement congestion. However, workers on construction sites tend to avoid implementing such congested reinforcement layouts. This avoidance of proper reinforcement detailing is a significant factor contributing to the collapse of entire buildings during earthquakes.

The conflict between design code requirements and practical implementation underscores the need for more effective and practical solutions to ensure the safety and resilience of structures during seismic events.

The utilization of Fiber Reinforced Cementitious Composites (FRCC) in beam-to-column connections has drawn attention as a promising solution to relieve reinforcement congestion issues. Considering the favourable properties of FRCC, including crack bridging, enhanced ductility, and energy dissipation capacity, researchers have sought to optimize the performance of these critical regions. However, despite some experimental investigations, a noticeable gap persists in the field—a lack of a comprehensive model accounting for the shear behavior exhibited by FRCC beam-to-column joints. This compelling research gap underscores the pressing need for advanced studies to address this knowledge gap and reveal an understanding of FRCC joint behavior, enabling the realization of more conservative and resilient structural designs.

1.2 Research Objectives And Scope

This thesis aims to develop a practical and accurate model to predict the shear strength and capture the complex shear stress-shear strain relationship of FRCC beam-to-column joints under seismic loading. By considering various fiber types, the model's versatility extends to a wide range of FRCC applications in beam-to-column connections. Ultimately, this research seeks to establish a strong foundation that enhances the understanding of FRCC beam-to-column joints, making a significant contribution to the existing knowledge in this specialized area.

This study involves a compilation and analysis of a wide range of experimental data provided by previous research studies. First, a comprehensive literature review is conducted in Chapter 2. Based on this body of knowledge, an extensive database has been assembled, incorporating essential details such as specimen dimensions, fiber types, material properties, loading procedures, reinforcement specifications,

instrumentation methods, and the resulting outcomes, in Chapter 3. Special emphasis has been placed on including tests and studies that provide valuable insights into the shear stress vs. deformation characteristics of these joints, ensuring a comprehensive and in-depth analysis of the subject matter.

Within Chapter 4 of this thesis, a shear prediction equation is developed for the joints through the constructed database. The analysis is conducted using IBM SPSS to establish correlations between important parameters. Advanced regression techniques within IBM SPSS are then employed to optimize the equation and reduce discrepancies between predicted and experimental values. This methodical framework allows for a thorough exploration of the relationships involved, resulting in a reliable shear strength prediction equation.

After developing the shear strength prediction equation for the joints, in Chapter 5, the focus shifted to creating a comprehensive shear stress vs. strain model. A compilation of experimental data provided a basis for analysis. Patterns in joint behavior were extracted from the collected data, offering valuable insights into deformation characteristics. A mathematical model was then formulated to accurately represent the shear stress vs. strain behavior of the joints. Validation procedures were then implemented, incorporating additional experimental data, to ensure the model's robustness and accuracy.

CHAPTER 2

LITERATURE REVIEW

2.1 Overview

Fiber reinforced cementitious composites (FRCC) are an increasingly prevalent sustainable and high-performance construction materials that enhance the durability and resilience of structural elements. As such, it is imperative to possess a comprehensive understanding of their mechanics to gain insight into the seismic performance of beam-to-column connections constructed using these materials. Accurately predicting the behavior of FRCC joints under various loading conditions and developing effective design strategies to ensure their robustness and reliability is essential.

To provide a concise overview of the history of FRCC, it is worth noting that these composites have been studied and developed for several decades. Throughout the course of human history, a diverse range of fibers have been utilized to amplify the mechanical attributes of brittle materials. Evidence of this age-old practice can be traced back to ancient civilizations such as the Egyptians and Babylonians, who ingeniously employed straws to reinforce sunbaked bricks and mud-hut walls, and horsehair to reinforce plaster (Li, 2008).

In more recent times, academic research has increasingly focused on uniformly distributed discrete fibers, primarily steel fibers, which have ushered in the modern era of fiber reinforced composites (Li, 2008). Scholars from various regions around the world have also diligently studied the use of diverse fibers, in addition to steel, further advancing the field. As a result of these efforts, the utilization of steel fibers as an auxiliary reinforcement to improve the cracking resistance, flexural and shear strength, and impact resistance of reinforced concrete members has been well-

established since the 1970s, making it a commonly adopted practice in modern civil engineering (Nawy, 2008). Furthermore, a sustained influx of a great variety of fibers and fiber materials has been observed since that era, and this trend is expected to endure as inventive applications and pioneering breakthroughs come to light (Naaman, 2018).

This literature review section will illustrate the fundamental characteristics and properties of fiber reinforced cementitious composites, as well as the behavior and role of beam-to-column connections in current structural design specifications. Parameters impacting the behavior of the connections will be examined, drawing upon insights from recent research projects in the literature. Through this investigation, readers will attain a thorough comprehension of the latest developments in this field of research and the exploitation of the underlying mechanics of these materials and the inelastic behavior of beam-to-column joints to guarantee the safety, reliability, and resilience of structures in seismic zones.

2.2 Fiber Reinforced Cementitious Composites

Fiber reinforced cementitious composites (FRCC) are advanced composite materials that possess superior mechanical and durability properties compared to conventional cement-based materials (Naaman & Reinhardt, 1996). FRCCs consist of short, discrete fibers randomly distributed in a cementitious matrix, resulting in a homogenously dispersed, three-dimensional reinforcement network. The fibers act as a load-carrying component, providing tensile strength and ductility to the composite, while the matrix binds the fibers together and transfers the stresses between them. In structural applications, the cementitious matrix is typically made of concrete that includes coarse aggregates, resulting in the material being referred to as fiber reinforced concrete (FRC).

Fiber reinforced composites deploy a wide range of fibers based on their intrinsic properties to ensure that the composite material is optimal for various applications.

These fibers can be segregated into three broad categories: natural, synthetic, and metallic fibers. Flax, hemp, jute, and sisal are among the natural fibers that can be incorporated into FRCCs, use of which is attractive due to their affordability and recyclable properties (Faruk et al., 2014). Synthetic fibers, on the other hand, can be listed as polyethylene (PE), polypropylene (PP), poly vinyl alcohol (PVA), aramid, polyester, and carbon fibers (Zheng, 1995). Moreover, metallic fibers, such as steel and aluminum, can be utilized in FRCC applications. The mechanical properties of these fibers, such as their tensile strength and modulus of elasticity, determine their suitability for different applications. For example, carbon fibers are highly desirable for their superior stiffness and strength, rendering them suitable for applications in the aerospace and automotive industries (Faruk et al., 2014).

Finally, alkali-resistant glass fibers have been used since the late 1960s, thanks to their superior mechanical properties, such as high tensile strength and modulus of elasticity. Nonetheless, one of the drawbacks of glass-fiber products, apart from their tendency to fail in a brittle manner, is their susceptibility to degradation when exposed to outdoor environments, leading to a decline in strength over time. This factor has limited the use of glass fiber reinforced concrete (GFRC) in structural applications (Liu, 2006).

2.2.1 Mechanical Properties of FRCC

FRCCs possess several mechanical properties that are significantly different from traditional reinforced concrete. Firstly, the addition of fibers to the matrix enhances the tensile strength of the composite, providing ductility and energy absorption capacity. Moreover, the fibers can effectively resist cracking and limit crack propagation, thus improving the durability of the composite. Additionally, FRCC exhibits high toughness and impact resistance due to the crack-bridging ability of the fibers (Bentur & Mindess, 2006). Overall, the mechanical properties of FRCC make it a desirable material for various structural applications, especially for enhancing the performance of reinforced concrete structures.

2.2.2 Definition of FRCC and HPFRCC

In general, conventional plain concrete exhibits brittle behavior under tensile loading due to its inherent low tensile strength and the formation of microcracks that propagate quickly under applied stress. On the other hand, FRCCs exhibit enhanced tensile behavior due to the presence of short fibers that resist the formation and propagation of microcracks. The fibers bridge the microcracks and increase the composite's ductility and toughness. However, the tensile behavior of FRCC is still limited by the fiber distribution and orientation within the matrix. In contrast, high-performance fiber-reinforced cementitious composites (HPFRCC) show a more gradual and stable stress-strain response in tension due to their more uniform fiber distribution and optimized fiber-matrix interface (Naaman, 2008). The use of higher fiber volume fractions and tailored fiber types in HPFRCC can further enhance its tensile performance and strain-hardening behavior, which improves the ductility and energy dissipation capacity, as depicted in Figure 2.1. Therefore, HPFRCC has the potential to provide significant improvements in structural performance compared to conventional reinforced concrete and FRCC.

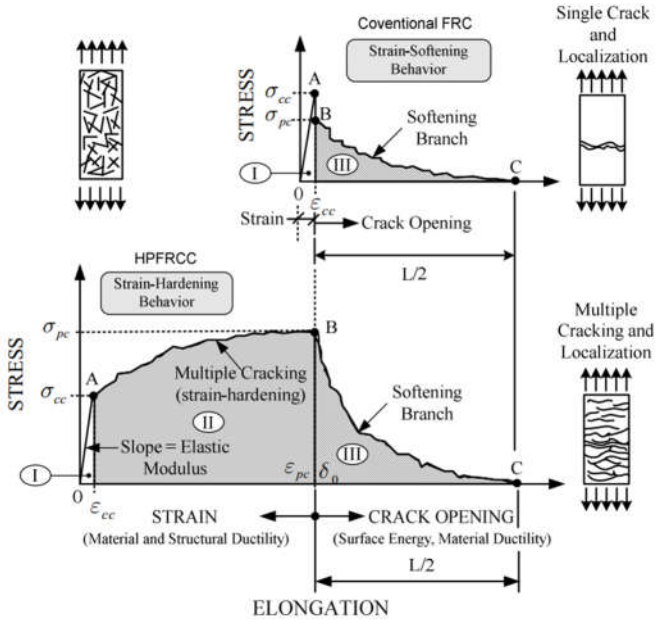

Figure 2.1. Comparison Tensile Behavior of FRCC & HPFRCC (Naaman, 2008).

In short, the tensile behavior of FRCC and conventional reinforced concrete is different due to the presence of fibers. The fibers in FRCC provide additional tensile strength and ductility, resulting in a more gradual post-cracking response compared to reinforced concrete. HPFRCC takes this behavior a step further by exhibiting strain-hardening response under tension, which provides enhanced ductility and energy dissipation capacity (Qudah & Maalej, 2014; Suwannakarn, 2009). The use of HPFRCC can lead to more durable and resilient structures that are better equipped to handle extreme loading conditions. As such, further research in the development and implementation of HPFRCC can lead to significant advancements in the field of construction industry.

In summary, the key factor that sets FRCC and HPFRCC apart is the ability to exhibit tensile strain hardening, which promotes the occurrence of multiple cracking, thus enhancing the capacity of the material to dissipate energy within the structure (Naaman & Reinhardt, 1996).

2.2.2.1 Cracking and Post-Cracking Tensile Strength

Naaman & Reinhardt (1996) conducted a numerical study to investigate the cracking and post-cracking strengths of high-performance fiber reinforced concrete, which is distinguished from regular fiber reinforced concrete based on its tensile behavior. As a result of their study, they developed equations for the cracking strength (σ_{cc}) and post-cracking strength (σ_{pc}) under tension. Cracking strength is obtained using Equation **(2.1)**.

$$\sigma_{cc} = \sigma_{mu}(1 - V_f) + \alpha_1 \alpha_2 \tau V_f \frac{L}{d} \quad \textbf{(2.1)}$$

The parameters involved in Equation **(2.1)** include the matrix tensile strength, σ_{mu}, as well as the coefficient, α_1, which represents the fraction of bond mobilized when the first matrix cracking occurs. The other coefficient, α_2, accounts for the efficiency of fiber orientation in the uncracked composite state. Additionally, the average bond

strength at the interface between the matrix and fiber, τ, is included as a parameter, along with the length, L, and diameter, d, of the fiber used. The aspect ratio of the fiber, which is represented by L/d, is also a factor in this equation, as well as the volume fraction of fibers, V_f.

Furthermore, the post cracking strength equation formulated by Naaman and Reinhardt (1996) can be represented by Equation **(2.2)**.

$$\sigma_{pc} = \lambda_{pc} \tau V_f \frac{L}{d} \quad \textbf{(2.2)}$$

In this expression, the coefficient, λ_{pc}, is given by the multiplication of three parameters, λ_1, λ_2, and λ_3. The first parameter, λ_1, is associated with the expected pull-out length ratio, and a value of 0.25 is recommended by the authors based on probability analysis. The efficiency of fiber orientation in the cracked composite state is expressed by λ_2, while λ_3 denotes the group reduction factor based on the number of fibers per unit area.

2.2.2.2 Critical Volume Fraction of Fibers

Naaman and Reinhardt (1996) have postulated that the critical volume fraction is the fiber volume fraction that specifies the transition from fiber reinforced cementitious composite (FRCC) behavior to high-performance FRCC (HPFRCC) behavior, characterized by tensile strain hardening. The authors derived the critical volume fraction by equating the expressions for cracking tensile strength and post-cracking tensile strength. This critical volume fraction is a fundamental parameter that impacts the mechanical properties of FRCCs and HPFRCCs, thereby providing insight into the optimum fiber content required to achieve superior performance. The identification of this parameter can aid in developing efficient strategies for optimizing the design and construction of structures using these materials (ACI 318-19, 2019).

In other words, the critical volume fraction is the minimum proportion required to achieve the tensile strain hardening behavior, for which the post cracking strength is higher than the cracking strength, that differentiates FRCC and HPFRCC. Thus, the minimum volume fraction required to achieve strain hardening behavior under tension, $V_{f,crit}$, which is defined by Equation **(2.3)**, serves as a transition point between the two behaviors.

$$V_{f,crit} = \frac{1}{1 + \frac{\tau}{\sigma_{mu}} \frac{L}{d} (\lambda_1 \lambda_2 \lambda_3 - \alpha_1 \alpha_2)} \quad \textbf{(2.3)}$$

2.3 Beam-to-Column Connections

Over the course of half a century, numerous research projects have been carried out to comprehend the seismic performance of beam-to-column connections. Thus far, a comprehensive understanding of the factors influencing their seismic behavior has been attained. The primary parameters that significantly impact the seismic response of connections primarily include joint transverse reinforcement, concrete grade used within the joint, joint geometry, effect of the floor system, bond strength, flexural strength ratio, joint type, axial load on the column and if FRCCs are used, the mechanical properties of the fibers.

2.3.1 Classification of Beam-to-Column Connections

Despite their often interchangeable usage, it is imperative to discern the contrasting definitions of the terms joint and connection. A beam-to-column joint can be explicitly defined as the segment of the column within the depth of the beam. On the other hand, a connection encompasses the joint in conjunction with the beam and column plastic hinge regions near the joint. (ACI 352-02, 2002). It is crucial to apprehend the distinction between these two fundamental concepts to ensure precise comprehension of structural behavior.

Apart from the detailed definitions given in contemporary seismic codes, beam-to-column connections are commonly classified as either interior or exterior connections in literature. The distinction between an exterior and an interior connection is primarily determined by the number of beams framing into the column in the loading direction. Specifically, an exterior joint is characterized by the presence of a single beam in the direction of loading, while an interior joint is identified by the presence of two beams in the longitudinal direction.

Moreover, since the classification of a joint is based solely on the number of longitudinal beams it connects to, the number of transverse beams attached to the joint has no bearing on its classification. In other words, regardless of the number of transverse beams framing to the joint, its classification remains the same. Some of the building codes such as ACI 318-19 (ACI 318-19, 2019) and ACI 352-02 (ACI 352-02, 2002) considered the confining effect of transverse beams and recommended different classifications based on the overall number of beams framing into the column as shown in Table 2.2 and Table 2.3, respectively. However, some of the transverse beams were considered not to confine the joint properly based on their relative width definitions.

In order to improve the categorization of interior and exterior joints, taking into account the confining effect of all beams in the transverse direction, a classification scheme has been proposed in this study as depicted in Figure 2.2. This approach ensures a coherent and systematic methodology that considers the number of transverse beams framing into the joint. The nomenclature used in this scheme is comprehensively elaborated in Table 2.1.

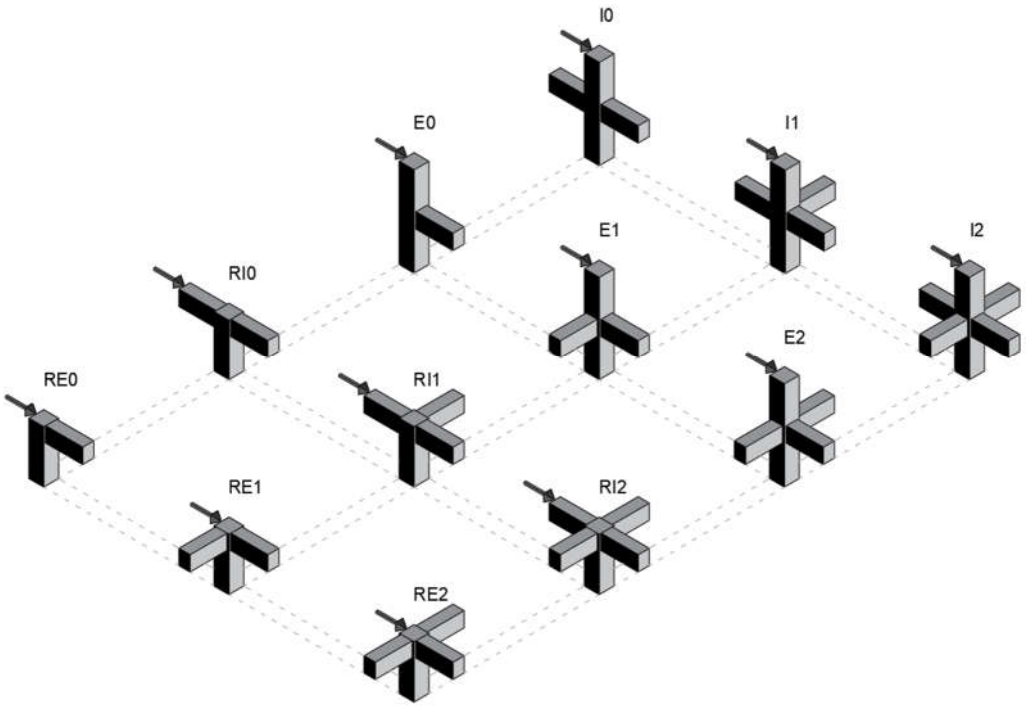

Figure 2.2. Beam-to-Column Joint Types proposed in this Study.

Table 2.1 Beam-to-Column Joint Types.

Abbreviation	Full designation		
	Number of columns framing into joint	Number of beams framing into joint	
		Longitudinal Direction	Transverse Direction
E0	2	1	0
E1	2	1	1
E2	2	1	2
I0	2	2	0
I1	2	2	1
I2	2	2	2
RE0	1	1	0
RE1	1	1	1
RE2	1	1	2
RI0	1	2	0
RI1	1	2	1
RI2	1	2	2

2.3.2 Structural Code Requirements for Beam-to-Column Joints

This section of the literature review aims to present a succinct overview of the design specifications for beam-to-column connections outlined in contemporary structural design codes. Notably, it should be emphasized that the ACI 544 Committee has yet to address the issue of FRCC beam-to-column connections. Consequently, the considerations discussed in this section will focus primarily on reinforced concrete beam-to-column connections.

2.3.2.1 **ACI 318-19** (ACI 318-19, 2019)

In accordance with the ACI 318-19 standard, '*Building Code Requirements for Structural Concrete*', a joint is defined as a structural element located at the intersection of two or more joining members. Conversely, a connection encompasses not only the joint but also the portions of the framing members that interface with it. The effect of the longitudinal and transverse beams on the confinement of the joint and consequently the joint shear is shown in Table 2.2. In this table, the term λ is recommended to be taken as 0.75 and 1.0 for lightweight concrete and normalweight concrete, respectively.

Table 2.2 Joint shear strength calculation according to ACI 318-19.

Column	Beam in direction of V_u	Confinement by transverse beams according to 15.2.8	V_n, lb[1]
Continuous or meets 15.2.6	Continuous or meets 15.2.7	Confined	$20\lambda\sqrt{f'_c}A_j$
		Not confined	$15\lambda\sqrt{f'_c}A_j$
	Other	Confined	$15\lambda\sqrt{f'_c}A_j$
		Not confined	$12\lambda\sqrt{f'_c}A_j$
Other	Continuous or meets 15.2.7	Confined	$15\lambda\sqrt{f'_c}A_j$
		Not confined	$12\lambda\sqrt{f'_c}A_j$
	Other	Confined	$12\lambda\sqrt{f'_c}A_j$
		Not confined	$8\lambda\sqrt{f'_c}A_j$

As shown by Equation **(2.4)**, the nominal joint shear strength, V_n, times the shear strength coefficient, Φ, must be higher than the joint shear force, V_u, for all joints. The nominal joint shear strength, V_n, can be calculated using the equations provided in Table 2.2.

$$\Phi V_n \geq V_u \qquad \textbf{(2.4)}$$

To obtain the A_j, given in Table 2.2, according to ACI 318-19 specifications, the joint depth is multiplied by the effective joint width, b_j, which is determined based on the overall depth of the column, in the direction of the considered joint shear.

In the case where the beam is wider than the column, the effective joint width is determined by the overall width of the column. However, if the column is wider than the beam, the effective joint width cannot exceed the lesser value of two options: the

sum of the beam width and the joint depth, or twice the perpendicular distance from the longitudinal axis of the beam to the closest side face of the column. Moreover, it is significant to emphasize that under no circumstance should the effective cross-sectional area of a joint, denoted as A_j, exceed the cross-sectional area of the column.

Effective joint width is a crucial parameter that significantly influences the behavior of beam-to-column connections under lateral loading. It represents the width of the joint area where the shear forces are transferred between the beam and column. The effective joint width is a function of the beam and column geometries and the joint configuration. As per the ACI 318-19 specification, the effective joint width is determined based on Figure 2.3, which outlines the calculation of the effective joint area, A_j.

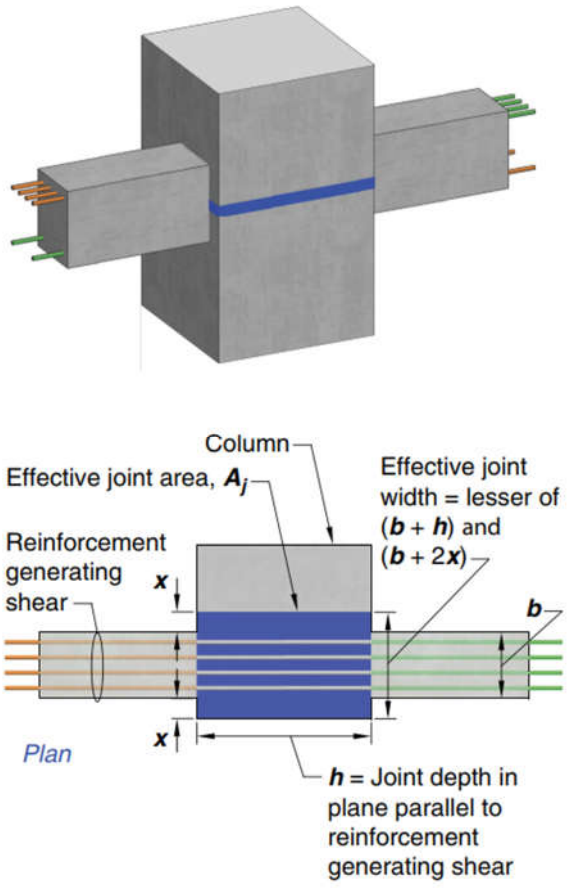

Figure 2.3. Calculation of effective joint area, A_j, according to ACI 318-19.

The ACI 318-19 code highlights the importance of verifying the horizontal joint shear strength in both principal directions. This requirement emphasizes the need to assess the connection's resistance to lateral loads that may occur in various directions. By mandating the evaluation of shear strength in both principal directions, the code aims to ensure the safety and stability of the structure for different loading conditions.

2.3.2.2 **ACI 352-02** (ACI 352-02, 2002)

As per the guidelines provided in ACI 352-02, '*Recommendations for Design of Beam-Column Connections in Monolithic Reinforced Concrete Structures*', which offer recommendations for designing beam-to-column connections in monolithic reinforced concrete structures, a total of six connection types have been identified and illustrated in Figure 2.4.

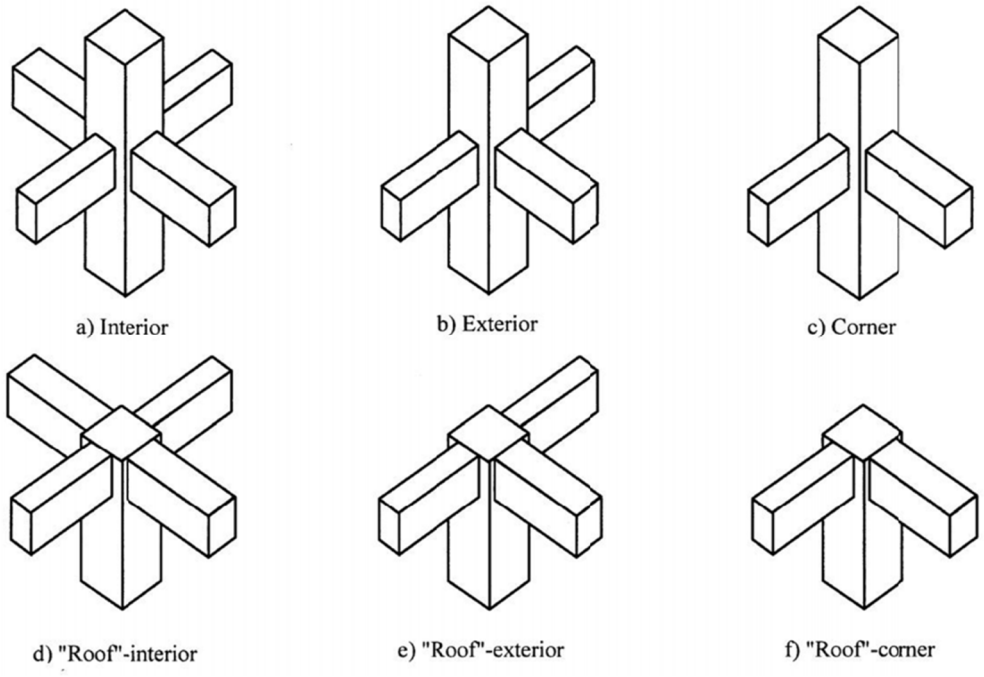

Figure 2.4. Connection types (ACI 352-02, 2002).

Moreover, the connections are further subdivided into two types, Type-1 and Type-2, based on loading. Type-1 connections are designed to sustain gravitational loads without experiencing inelastic deformations. On the other hand, Type-2 connections are designed to withstand seismic loads while experiencing significant inelastic deformations.

Figure 2.5 depicts the computation of shear forces exerted on both joint types, as specified by the code.

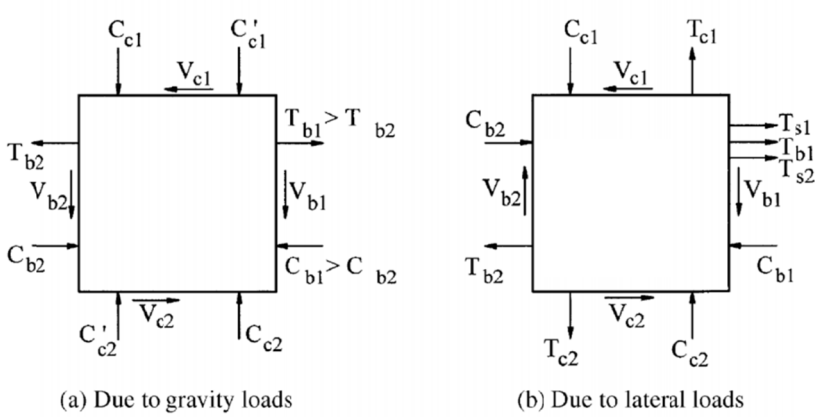

Figure 2.5. Loads applied on joints by ACI 352-02.

In Figure 2.5, T represents tensile force, C stands for compressive force, V represents shear force, the subscripts b, c, and s denote the beam, column, and slab, respectively.

ACI 352-02 offers an alternate definition of effective joint width as compared to ACI 318-19, incorporating the use of a coefficient, denoted as m, to determine the effective width of the joint transverse to the direction of shear. This definition was expressed mathematically using Equation **(2.5)**.

$$b_{j,ACI352} = \min \begin{cases} \dfrac{b_b + b_c}{2} \\ b_b + \sum m \dfrac{h_c}{2} \\ h_c \end{cases} \quad \textbf{(2.5)}$$

Specifically, the formula for the effective joint width given by ACI 352-02 includes the beam width, column width, and column depth, as well as the aforementioned coefficient. A value of 0.5 is assigned to m for connections with no eccentricity. The effective joint area, in turn, can be calculated by multiplying the effective joint width by the column depth. In contrast, the joint shear strength can be determined using Equation **(2.6)**, where the factor γ is utilized, which can be obtained from Table 2.3.

$$V_n = 0.083\,\gamma\,\sqrt{f_c'}\,A_j \qquad \textbf{(2.6)}$$

where, γ is shear strength factor and is given in .

Table 2.3 Shear strength factor by ACI 352-02.

Classification	Connection type	
	1	2
A. Joints with a continuous column		
A.1 Joints effectively confined on all four vertical faces	24	20
A.2 Joints effectively confined on three vertical faces or on two opposite vertical faces	20	15
A.3 Other cases	15	12
B. Joints with a discontinuous column		
B.1 Joints effectively confined on all four vertical faces	20	15
B.2 Joints effectively confined on three vertical faces or on two opposite vertical faces	15	12
B.3 Other cases	12	8

According to ACI 352-02, Figure 2.6 provides the necessary information to determine the horizontal joint shear, V_u, and the joint shear strength must satisfy the condition of $V_u \leq 0.85V_n$.

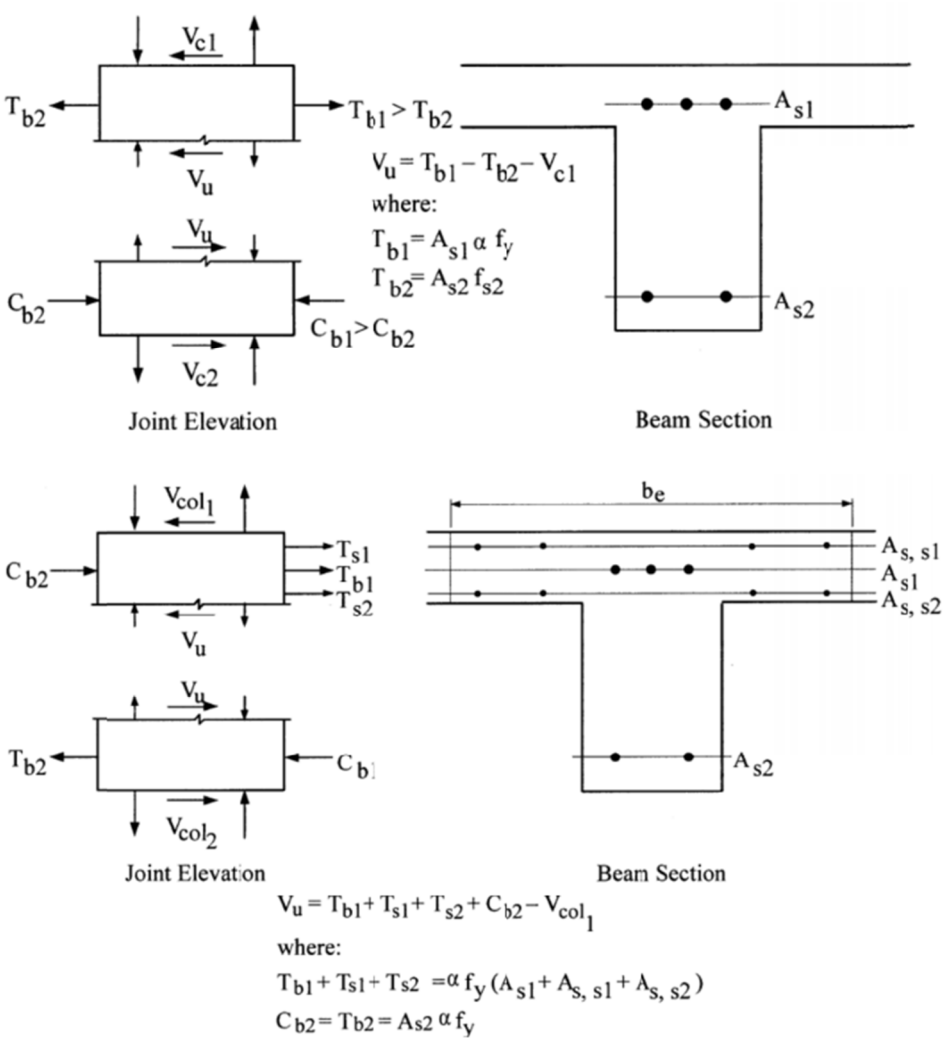

Figure 2.6. Horizontal joint shear calculation by ACI 352-02.

In this representation, several parameters are used to calculate the shear strength of the joint. Firstly, A_s represents the area of the beam longitudinal reinforcement, while $A_{s,s}$ represents the area of slab reinforcement. T_b and C_b are the tensile and compressive forces in the beam, respectively. The parameter α is a stress multiplier that takes into account the effect of strain hardening in the longitudinal bars of the beam. Additionally, V_{col1} and V_{col2} represent the shear forces acting on the top and bottom columns, respectively. Finally, b_e is the effective flange width.

2.3.2.3 **TSC2018** (TSC2018, 2018)

TSC2018, *'Turkish Building Seismic Design Code'*, is a regulatory framework that offers guidance for the design and construction of buildings in Turkey, aiming to ensure their resistance against earthquake loading and to provide life-safety. It includes a set of regulatory standards that outlines guidelines for designing and constructing buildings in Turkey, with the primary goal of enabling them to stand against seismic events and mitigate potential risks to human life.

As per TSC2018, beam-to-column connections are divided into two categories as confined and unconfined connections. According to the regulations set forth in this code, a beam-to-column joint is classified as confined when the beams surround the joint on all four faces, as shown in Figure 2.7 and the beam widths must be at least three-quarters of that of the column, If these criteria are not satisfied, the joint is considered as an unconfined joint.

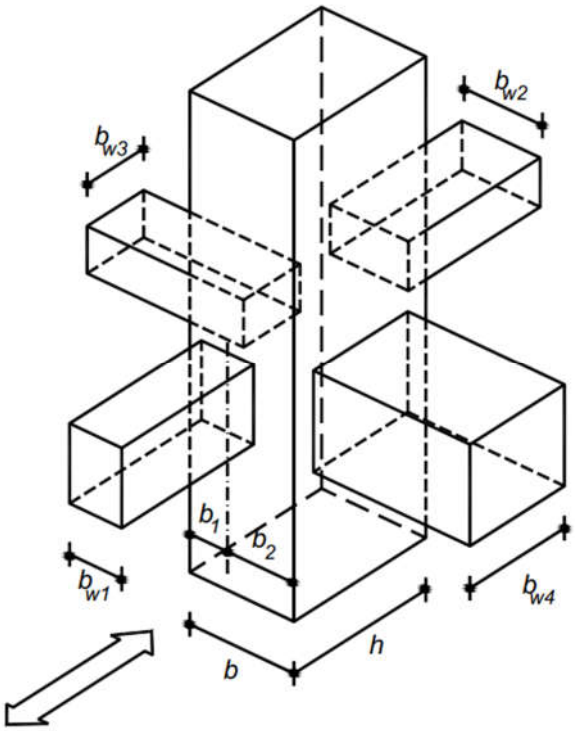

Figure 2.7. Geometric dimensions of beams and columns. (TSC2018, 2018).

Shear strength of the confined joints can be obtained by using Equation **(2.7)**.

$$V_e \leq 1.7 b_j h \sqrt{f_{ck}} \quad \textbf{(2.7)}$$

For unconfined joints, Equation **(2.7)** is modified to Equation **(2.8)**.

$$V_e \leq 1.0 b_j h \sqrt{f_{ck}} \quad \textbf{(2.8)}$$

Equations **(2.7)** and **(2.8)** involve the effective joint width, b_j, and the characteristic compressive strength, f_{ck}, while h represents the column depth in the direction of seismic loading.

Horizontal shear force applied on the joint, V_e, according to the TSC2018, is given in Equation **(2.9)**, considering the equilibrium of horizontal forces, presented in the Figure 2.8, illustrating the total reinforcement area of the top and bottom longitudinal bars, referred to as A_{s1} and A_{s2}, respectively. Moreover, the column shear force in the direction of seismic loading, denoted as V_{col}, is determined as the maximum of V_a and $V_{ü}$, which represent the shear forces at the bottom of the top column and at the top of the bottom column, respectively.

$$V_e = 1.25 f_{ck}(A_{s1} + A_{s2}) - V_{col} \quad \textbf{(2.9)}$$

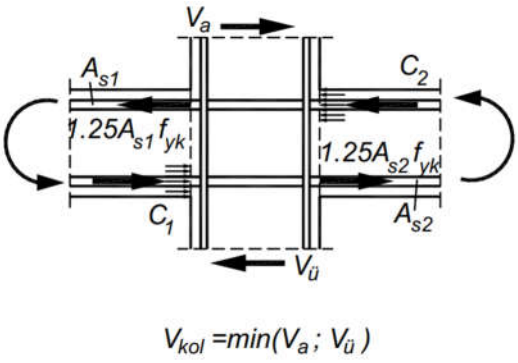

Figure 2.8. Horizontal forces exerted on an interior joint. (TSC2018, 2018).

The coefficient 1.25 in Equation **(2.9)** is utilized to account for the strain hardening of the beam's longitudinal bars, which is believed to result in an increase in the joint shear forces. This adjustment is similar to the approach specified in ACI 352-02.

The effective joint width is given in Equation **(2.10)**, based on the geometrical dimensions given in Figure 2.7.

$$b_{j,TSC2018} = \begin{cases} b & \text{if } b_{w1} \geq b \text{ and } b_{w2} \geq b \\ 2\min(b_1; b_2) & \text{if } b_{w1} < b \text{ and } b_{w2} < b \end{cases} \quad \textbf{(2.10)}$$

Furthermore, the effective joint width is constrained by an additional condition, which is specified in Equation **(2.11)**.

$$b_j \leq b_{w1} + h \qquad \text{if } b_{w1} < b_{w2} \quad \textbf{(2.11)}$$

Finally, the TSC2018 establishes a set of minimum requirements for the amount of joint transverse reinforcement. As per the code, in case of confined joints, it is required to utilize a minimum of 40% of the amount of transverse reinforcement designed for the confinement zone of the lower column along the joint region. It is significant to note that the diameter of the transverse reinforcement must not be less than 8 mm, and its spacing must not exceed 150 mm. On the other hand, for unconfined joints, at least 60% of the transverse reinforcement required for the confinement zone of the lower column shall be used along the joint depth. However, in this case, the diameter of the transverse reinforcement shall not be less than 8 mm and the spacing shall not exceed 100 mm. (TSC2018, 2018).

2.3.2.4 Other Code Definitions for Effective Joint Width

Up to this point, it has been established that design codes have comparable approaches, involving the determination of joint shear force, estimation of joint shear strength, and requirements related to joint transverse reinforcement. An important aspect is to determine the effective joint width adequately, which affects the joint shear strength. Consequently, this section will outline how different codes handle the determination of effective joint width.

Eurocode 8, *'Design of structures for earthquake resistance',* requires the use of Equation **(2.12)** to determine the effective joint width.

$$b_j = \begin{cases} \min\left(b_c; (b_w + 0.5h_c)\right) & \text{if } b_C > b_w \\ \min\left(b_w; (b_c + 0.5h_c)\right) & \text{if } b_c < b_w \end{cases} \quad \textbf{(2.12)}$$

In Equation **(2.12)**, b and h terms denote the width and depth, respectively. Moreover, the subscripts w and c stand for the beam and column, respectively. (Eurocode 8, 2004).

AIJ Guideline (1999), '*Design Guidelines for Earthquake Resistant Reinforced Concrete Buildings',* requires the use of Equation **(2.13)** to determine the effective joint width.

$$b_{j,AIJ} = b_b + b_{a1} + b_{a2} \quad \textbf{(2.13)}$$

In Equation **(2.13)**, b_b account for the beam width while b_{a1} and b_{a2} are calculated using Equation **(2.14)**.

$$b_{ai} = \min\left(\frac{x_i}{2}, \frac{h_c}{4}\right) \quad \textbf{(2.14)}$$

The expression given in Equation **(2.14)** defines x as the distance between the beam and column faces. Moreover, the AIJ Guidelines also define an effective joint depth. The determination of the effective joint depth is contingent upon the longitudinal beam bars' effectiveness in transferring shear forces. For interior joints, the effective joint depth is considered equal to the entire column depth. For exterior joints, the joint depth is limited by the top hooked beam bar depth as shown in Figure 2.9.

Figure 2.9 showcases how the effective joint width and effective joint depth are calculated according to the AIJ Guidelines. (AIJ Guidelines, 1999).

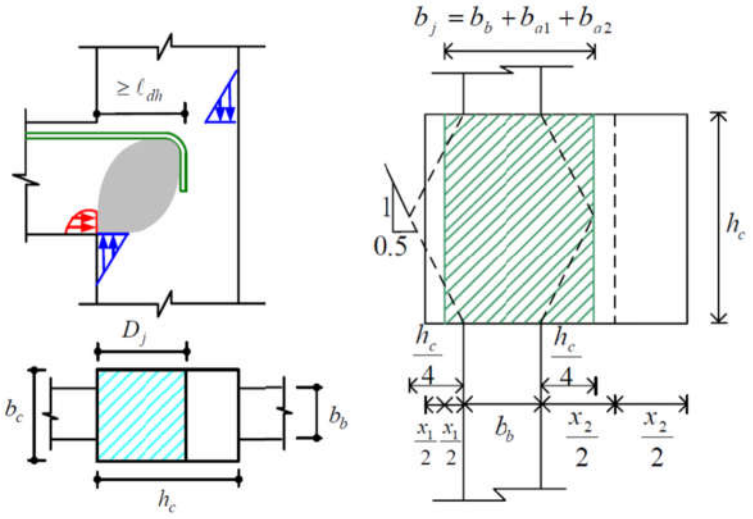

Figure 2.9. Effective Joint Area Definition. (AIJ Guidelines, 1999).

NZS 3101:2006, *'New Zealand Concrete Structures Standard',* utilized the similar approach as Eurocode 8, recommending the effective joint width to be taken as Equation **(2.15)**. (NZS 3101, 2006).

$$b_j = \begin{cases} \min(b_c; (b_w + 0.5h_c)) & \text{if } b_c \geq b_w \\ \min(b_w; (b_c + 0.5h_c)) & \text{if } b_c < b_w \end{cases} \quad \textbf{(2.15)}$$

2.3.3 Parameters Affecting Beam-to-Column Connection Behavior

The key factors influencing the performance of beam-to-column connections can be listed as the joint transverse reinforcement, the confinement provided by the slab, bond strength of the composite, the ratio of moment capacity of the columns to the beams, joint type, axial load applied to the column, and the fiber-related parameters such as fiber type, length, diameter, aspect ratio, volume fraction, reinforcing index and pullout strength. In this section experimental results showcasing the effects of these parameters on the seismic behavior of beam-to-column connections will be presented.

2.3.3.1 Joint Transverse Reinforcement

One of the key parameters that significantly influences the ductility and overall behavior of a beam-to-column joint is the joint transverse reinforcement. These stirrups are responsible for effectively carrying the shear forces exerted by earthquakes within the joint in the direction of seismic activity. Therefore, most contemporary seismic design codes enforce the utilization of joint stirrups with minimum required values.

However, implementing such amounts of joint stirrups in the relatively confined space of the joint can be challenging to achieve on the site, often leading to reinforcement congestion, aggregate segregation and lumping (Annadurai & Ravichandran, 2016; Ganesan et al., 2007; Liu, 2006; Muthupriya et al., 2014; Qureshi & Muhammad, 2018). These issues can lower the load carrying capacity of the members, posing a potential risk of total collapse of the structure. As a result, the practice of implementing the designed joint hoops is generally avoided. Moreover, even if the required amount of joint stirrups is installed, it could still result in aggregate segregation, further increasing the potential risks. In summary, while joint stirrups are critical in enhancing the seismic performance of beam-to-column joints, the challenges associated with their installation and their potential impacts on the load carrying capacity of members require careful consideration and appropriate measures to mitigate the associated risks.

Researchers proposed to eliminate the need for joint transverse reinforcement entirely by utilizing fiber reinforced concrete (FRC) in the vicinity of the joint (Henager, 1977; Parra-Montesinos et al., 2005; Saghafi & Shariatmadar, 2018; Yuan et al., 2013). On the other hand, some researchers believe that the application of FRC can only reduce the stirrup amount within the joint, rather than completely replacing the joint stirrups. (Liu, 2006). In other words, while the use of FRC can reduce the required amount of joint stirrups, it may not be sufficient to eliminate them (Bayasi & Gebman, 2002; Gefken & Ramey, 1989; Gencoglu, 2007; Rohm et al., 2012).

Thus, the use of FRC as a total substitute for joint stirrups is still a relatively evolving area of research, and more experimental and analytical studies are required to evaluate its effectiveness and practicality. Nonetheless, this approach presents an attractive alternative to conventional joint reinforcement, which are known to be difficult to install and can lead to issues such as reinforcement congestion and aggregate segregation.

Said (2016b) conducted a comprehensive experimental investigation on the behavior of FRC beam-to-column joints, composed of PVA and PE fibers, with a particular focus on the impact of joint stirrups on the performance. The primary objective of the study was to evaluate the efficiency of joint stirrups in enhancing the behavior of FRC exterior connections. The findings revealed that joint stirrups can significantly improve the ductility and energy dissipation capacity of FRC connections, providing insight into the design and optimization of FRC connections for use in seismic-resistant structures.

Hosseini et al. (2018) studied the impact of joint stirrups on the seismic behavior of 3-D ECC beam-to-column connections, subjected to bidirectional bending and torsion. Through a comparative analysis of the specimens with and without stirrups, the investigation concludes that the integration of joint stirrups increases the seismic resistance and overall performance of the connection regions. However, the specimens without joint stirrups had a substantial reduction in stiffness and increase in shear deformations of up to 300%. These outcomes indicate stirrups are important for withstanding the applied shear forces and adequate stirrup spacing is vital for the seismic performance of beam-to-column connections.

Liu (2006) also investigated the effect of joint transverse reinforcement on the behavior of reinforced concrete beam-to-column connections. The study included both experimental work and finite element analysis to obtain the response of connections under cyclic loading. The results of the study highlighted that joint transverse reinforcement played a crucial role in reducing deformations and the rate of stiffness degradation during cyclic loading for both conventional reinforced

concrete and fiber-reinforced concrete (FRC) joints. This highlights the importance of joint transverse reinforcement in enhancing the seismic resilience of structures.

Choi and Bae (2019) stated that the utilization of steel fibers instead of stirrups in exterior beam-to-column joints subjected to cyclic loading can lead to a considerable enhancement in the load carrying capacity of the joint. The experimental findings indicated the efficiency of steel fibers in increasing the joint strength and ductility, particularly when employed along with joint transverse reinforcement.

The investigation of the seismic behavior and shear strength of joints constructed with steel-fiber reinforced concrete, conducted by Jiuru et al. (1992), revealed the critical role of the joint stirrup ratio. The experimental results indicated that an optimized stirrup ratio improves the seismic performance and joint shear strength, and the incorporation of steel-fiber reinforced concrete can even enhance this effect.

2.3.3.2 Composite Compressive Strength

The compressive strength of FRCC plays a vital role in determining the seismic behavior of beam-to-column connections similar to that of reinforced concrete. Not only does a higher compressive strength enhance the bond and shear strength of the material, preventing the longitudinal bar slippage, but it also improves its ability to withstand seismic activity, enhancing the load carrying capacity (Sachdeva et al., 2021). Consequently, the compressive strength stands out as a significant parameter that shapes the behavior of FRCC beam-to-column connections. Therefore, it should be carefully considered among other crucial factors when evaluating the performance of beam-to-column joints (Unal, 2010).

The compressive stress-strain behavior of FRCCs exhibits ductility characteristics that are influenced by the volume fraction and aspect ratio of the fibers (Fanella & Naaman, 1985). This can be seen in Figure 2.10 and Figure 2.11 where both factors enhance the material's ability to withstand axial compressive strain, resulting in a more ductile behavior. Also, the difference in compressive strength between FRCC

and conventional concrete is not substantial, particularly in relation to the enhancement in strain capacity.

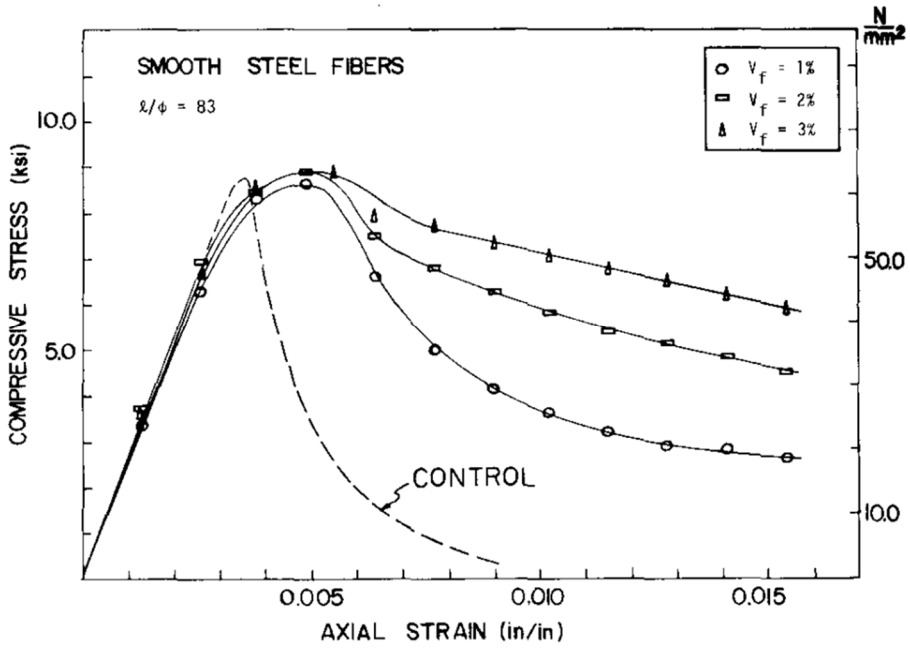

Figure 2.10. Effect of volume fraction on compressive stress strain behavior of FRCC (Fanella & Naaman, 1985).

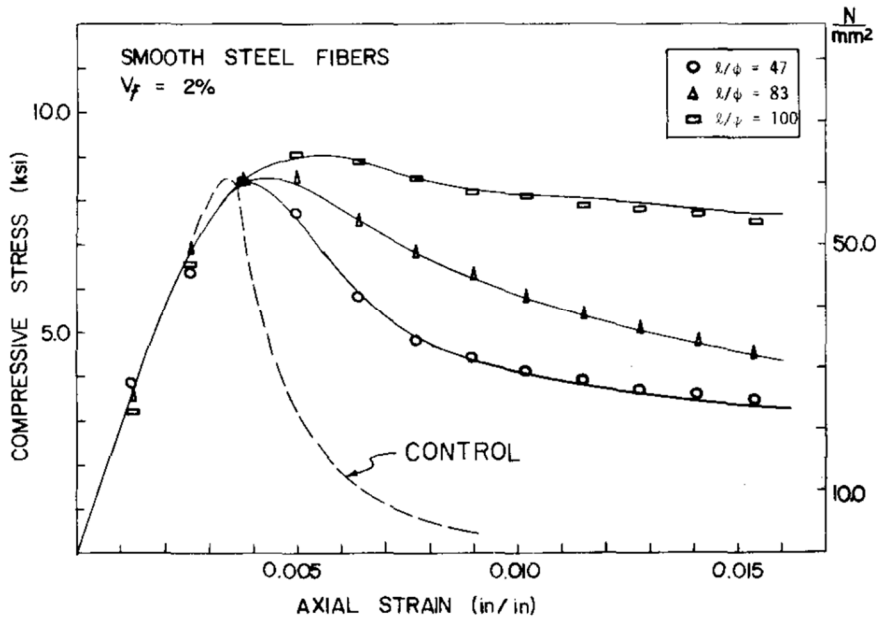

Figure 2.11. Effect of aspect ratio on compressive stress strain behavior of FRCC (Fanella & Naaman, 1985).

In the code provisions, the shear strength is commonly expressed as a constant multiplied by the square root of the compressive strength, representing the tensile strength of the material. This underlines the critical nature of accurately determining the compressive strength of the composite material.

Compressive strength may be obtained from standard cylinder and cube tests. These tests commonly involve using cylinders with dimensions of either 100mm x 200mm or 150mm x 300mm, and cubes with 150mm sides. For different shapes and sizes of specimens, conversion factors or equations must be utilized to conservatively use these values in design. Furthermore, designers may also have to convert the compressive strength of plain concrete (PC) to that of fiber-reinforced concrete (FRC) based on the volume fraction and reinforcing index of fibers incorporated in the mix.

There are different approaches that establish the relationships required to convert the compressive strength of plain concrete to that of fiber-reinforced concrete based on the volume fraction and reinforcing index of fibers used in the mix. This section compiles and presents the equations for various fiber types in Table 2.4. Some of these equations have limitations, such as strength intervals or volume fraction restrictions that need to be taken into account. Additionally, it is noteworthy that in certain research studies, the authors stated that there is no observed change in the compressive strength after adding fibers. In order to accurately represent this finding, a conversion factor of 1.0 is used in Table 2.4.

While some researchers have reported significant changes in compressive strength with the addition of fibers, many others have concluded that the addition of fibers has little or no effect on the compressive strength. Some researchers believe that the influence of fibers on compressive strength depends on the fiber type. For instance, addition of polypropylene fibers may not affect the compressive strength while steel fiber inclusion may considerably alter it (Ghosni et al., 2016). All in all, it was concluded in the ACI 544.4-18 Code that adding fibers into the matrix does not have a significant effect on its compressive strength (ACI 544.4-18, 2018).

Table 2.4 Compressive strength conversions.

Fiber	Source	Reference		Target		Conversion Rule
		Material	Dim (mm)	Material	Dim (mm)	
HESF	(Fang et al., 2022)	FRC	100x200	FRC	150x300	$f_{cy150} = (1.00)f_{cu150}$
		FRC	100x200	FRC	70x70x70	$f_{cu70} = (1.09)f_{cu150}$
		FRC	100x200	FRC	100x100x100	$f_{cu100} = (1.00)_{fcu150}$
		FRC	100x200	FRC	150x150x150	$f_{cu150} = (0.91)f_{cu150}$
	(Thomas & Ramaswamy, 2007)	PC	150x150x150	FRC	150x150x150	$f_{cuF} = f_{cu} + 0.014f_{cu}RI + 1.09RI$
		PC	150x150x150	FRC	150x300	$f_{cyF} = 0.84f_{cu} + 0.046f_{cu}RI + 1.02RI$
	(Gao et al., 2023)	PC	150x150x150	FRC	150x150x150	$f_{fcu} = f_{ocu}\,(1 - 0.19RI^2 + 0.34RI)$
	(Song & Hwang, 2004)	PC	150x300	FRC	150x300	$f'_{cf} = 85 + 15.12V_f - 4.71V_f^2$
	(Abbass et al., 2018)	PC	100x200	FRC	100x200	$f_{cf} = f_{cp} + 5.59RI$
	(Ou et al., 2012)	PC	150x300	FRC	150x300	$f_{cyF} = f_{cy} + 2.35RI$
	(Ezeldin & Balaguru, 1992)	PC	100x200	FRC	150x300	$f_{cyF} = f_{cy} + 3.51RI$
	(Mansur et al., 1999)	FRC	100x100x100	FRC	100x200	$f_{cyF} = (0.93)\ f_{cuF}$
		PC	100x100x100	FRC	100x100x100	$f_{cuF} = (1.05)\ f_{cu}$
	(Zhu et al., 2019)	FRC	150x150x150	FRC	100x200	$f_{cy150} = (0.738)f_{cu150}$
Straight Steel	(Graybeal & Davis, 2008)	FRC	100x100x100	FRC	75x150	$f_{cy75} = (1.0)\ f_{cu100}$
		FRC	100x100x100	FRC	100x200	$f_{cy100} = (1.0)\ f_{cu100}$
		FRC	70x70x70	FRC	75x150	$f_{cy75} = (0.94)\ f_{cu70}$
		FRC	70x70x70	FRC	100x200	$f_{cy100} = (0.93)\ f_{cu70}$
		FRC	50x50x50	FRC	75x150	$f_{cy75} = (0.96)\ f_{cu50}$
		FRC	50x50x50	FRC	100x200	$f_{cy100} = (0.96)\ f_{cu50}$
		FRC	100x200	FRC	75x150	$f_{cy75} = (1.01)\ f_{cy100}$
		FRC	75x150	FRC	100x200	$f_{cy100} = (0.99)\ f_{cy75}$
		FRC	50x100	FRC	75x150	$f_{cy75} = (1.08)\ f_{cy50}$
		FRC	50x100	FRC	100x200	$f_{cy100} = (1.07)\ f_{cy50}$
	(Yuliarti et al., 2015)	FRC	100x100x100	FRC	100x200	$f_{cy100} = (0.94)\ f_{cu100}$
	(Wille et al., 2011)	FRC	100x200	FRC	100x100x100	$f_{cy100} = (0.98)\ f_{cu100}$
		FRC	150x300	FRC	100x200	$f_{cy150} = (0.96)\ f_{cy100}$
		FRC	150x150x150	FRC	100x100x100	$f_{cu150} = (1.05)\ f_{cu100}$
	(Nataraja et al., 1999)	PC	150x300	FRC	150x300	$f_{cf}' = f_c + 2.1604(RI)$
	(Bhargava et al., 2006)	PC	100x200	FRC	100x200	$f_{cf100} = f_{c100} + 0.45 + 8.89RI_{short} + 2.47RI_{long}$

Table 2.4 (Cont'd)

Fiber	Source	Reference		Target		Rule
		Material	Dim (mm)	Material	Dim (mm)	
PVA	(Chung et al., 2018)	FRC	100x200	FRC	100x100x100	$f_{cu} = 2.128f_{cy} - 28.9$ $40Mpa \leq fcy < 58Mpa$
	(Sagar & Sivakumar, 2021)	PC	100x200	FRC	100x200	$f_{cf} = -368.14RI^2 + 74.383RI + f_{cp}$ for fc≈30Mpa
		PC	100x200	FRC	100x200	$f_{cf} = -377.92RI^2 + 74.589RI + f_{cp}$ for fc≈50Mpa
		PC	100x200	FRC	100x200	$f_{cf} = -449.21RI^2 + 81.896RI + f_{cp}$ for fc≈70Mpa
	(Nuruddin et al., 2015)	PC	100x100x100	FRC	100x100x100	$f_{cuf} = 1.03f_{cup} - 0.03055f_{cup}RI + 17.98x\sqrt{CRM}$
		PC	100x100x100	FRC	100x200	$f_{cyf} = 0.846f_{cup} - 0.0311f_{cup}RI + 13.575x\sqrt{CRM}$
	(Ayub et al., 2019)	PC	100x200	FRC	100x200	$f_{cf100} = f_{c100} + 0.0425RI$ for $V_f = 1\%$
		PC	100x200	FRC	100x200	$f_{cf100} = f_{c100} + 0.1213RI$ for $V_f = 2\%$
		PC	100x200	FRC	100x200	$f_{cf100} = f_{c100} + 0.0962RI$ for $V_f = 3\%$
Glass	(Krishna et al., 2011)	FRC	150x150x150	FRC	150x300	$f_{cy150} = (0.81)\ f_{cu150}$
		FRC	100x100x100	FRC	100x200	$f_{cy100} = (0.96)\ f_{cu100}$
Basalt	(Krishna et al., 2011)	FRC	150x150x150	FRC	150x300	$f_{cy150} = (0.79)\ f_{cu150}$ for $V_f = 0\%$
		FRC	150x150x150	FRC	150x300	$f_{cy150} = (0.77)\ f_{cu150}$ for $V_f = 0.5\%$
		FRC	150x150x150	FRC	150x300	$f_{cy150} = (0.74)\ f_{cu150}$ for $V_f = 1\%$
		FRC	150x150x150	FRC	150x300	$f_{cy150} = (0.72)\ f_{cu150}$ for $V_f = 1.5\%$
		FRC	150x150x150	FRC	150x300	$f_{cy150} = (0.72)\ f_{cu150}$ for $V_f = 2\%$
	(Jalasutram et al., 2017; Jiang et al., 2014)	FRC	100x200	PC	100x200	$f_{cyf} = (1.00)\ f_{cyp}$
	(Ayub et al., 2014)	FRC	100x200	PC	100x200	$f_{cyf} = (1.00)\ f_{cyp}$
	(Branston et al., 2016)	FRC	100x200	PC	100x200	$f_{cyf} = (1.00)\ f_{cyp}$

Table 2.4 (Cont'd)

Fiber	Source	Reference		Target		Rule
		Material	Dim (mm)	Material	Dim (mm)	
HESF + Micro Steel	(Chasioti & Vecchio, 2017)	FRC	150x150x150	FRC	100x200	$f_{cy100} = (0.93)\ f_{cu150}$
PE	(Said & Razak, 2015)	PC	100x100x100	FRC	100x100x100	$f_{cuf} = f_{cu} - 0.0143RI$
	(Y. Wang et al., 2020)	PC	50x100	FRC	50x100	$f_{cyf} = (0.84)f_{cy}$ $V_f = 1\%$
		PC	50x100	FRC	50x100	$f_{cyf} = (0.85)f_{cy}$ $V_f = 1.5\%$
		PC	50x100	FRC	50x100	$f_{cyf} = (0.81)f_{cy}$ $V_f = 2\%$
	(Y. Wang et al., 2020)	FRC	50x50x50	FRC	100x200	$f_{cy100} = (0.94)\ f_{cu}$
		FRC	70x70x70	FRC	100x200	$f_{cy100} = (0.96)\ f_{cu}$
		FRC	100x100x100	FRC	100x200	$f_{cy100} = (0.97)\ f_{cu}$
		FRC	150x150x150	FRC	100x200	$f_{cy100} = (0.98)\ f_{cu}$
Recycled HDPE	(Pešić et al., 2016)	PC	100x200	FRC	100x200	$f_{cyf} = (1.00)f_{cy}$
Aramid (Bundle)	(Y.-F. Li et al., 2022)	PC	100x200	FRC	100x200	$f_{cyf} = (1.23)f_{cy}$ $V_f = 0.5\%$, L = 12mm
		PC	100x200	FRC	100x200	$f_{cyf} = (1.14)f_{cy}$ $V_f = 1\%$, L = 12mm
		PC	100x200	FRC	100x200	$f_{cyf} = (1.14)f_{cy}$ $V_f = 1.5\%$, L = 12mm
		PC	100x200	FRC	100x200	$f_{cyf} = (1.24)f_{cy}$ $V_f = 0.5\%$, L = 24mm
		PC	100x200	FRC	100x200	$f_{cyf} = (1.15)f_{cy}$ $V_f = 1\%$, L = 24mm
		PC	100x200	FRC	100x200	$f_{cyf} = (1.14)f_{cy}$ $V_f = 1.5\%$, L = 24mm
Aramid	(Jongvivatsakul et al., 2020)	PC	150x300	FRC	150x300	$f_{cyf} = (1.04)f_{cy}$
	(Y.-F. Li et al., 2021)	PC	100x200	FRC	100x200	$f_{cyf} = (1.32)f_{cy}$
PET	(Nibudey et al., 2013a)	FRC	150x150x150	FRC	150x300	$f_{cy150} = (0.80)\ f_{cu150}$
	(Kim et al., 2010)	PC	100x200	FRC	100x200	$f_{cyf} = (0.99)f_{cy}$
	(Nibudey et al., 2013b)	PC	150x150x150	FRC	150x150x150	$f_{cuf} = (0.99)f_{cu}$
	(Sharma et al., 2014)	PC	150x150x150	FRC	150x150x150	$f_{cuf} = (1.00)f_{cu}$ L = 30mm
		PC	150x150x150	FRC	150x150x150	$f_{cuf} = (1.00)f_{cu}$ L = 60mm

Table 2.4 (Cont'd)

Fiber	Source	Reference		Target		Rule
		Material	Dim (mm)	Material	Dim (mm)	
PP	(Ahmad et al., 2021)	PC	150x300	FRC	150x300	$f_{cyf} = (1.05)f_{cy}$ $V_f = 1\%$
		PC	150x300	FRC	150x300	$f_{cyf} = (1.12)f_{cy}$ $V_f = 2\%$
		PC	150x300	FRC	150x300	$f_{cyf} = (0.95)f_{cy}$ $V_f = 3\%$
		PC	150x300	FRC	150x300	$f_{cyf} = (0.87)f_{cy}$ $V_f = 4\%$
	(Al-Lebban et al., 2021)	PC	150x300	FRC	150x300	$f_{cyf} = (1.16)f_{cy}$ $V_f = 1\%$
		PC	150x300	FRC	150x300	$f_{cyf} = (1.30)f_{cy}$ $V_f = 2\%$
	(Alsadey, 2016)	PC	50x50x50	FRC	50x50x50	$f_{cuf} = (1.31)f_{cu}$
		PC	150x150x150	FRC	150x150x150	$f_{cuf} = (1.04)f_{cu}$ $V_f = 1\%$
		PC	150x150x150	FRC	150x150x150	$f_{cuf} = (1.12)f_{cu}$ $V_f = 2\%$
	(Sharan & Lal, 2016)	PC	150x150x150	FRC	150x150x150	$f_{cuf} = (1.16)f_{cu}$ $V_f = 1\%$
		PC	150x150x150	FRC	150x150x150	$f_{cuf} = (1.08)f_{cu}$ $V_f = 2\%$

2.3.3.3 Slab Participation

In recent years, researchers have increasingly focused on the impact of slab contribution on the behavior of FRC beam-to-column connections. Slabs are essential components in these connections that exert a crucial role in enhancing the seismic performance by confining the joint.

The presence of slab significantly enhances the joint confinement, thereby increasing its shear resistance and overall stiffness. This confinement effect arises due to the interaction between the slab and the joint, effectively reducing the deformation and damage sustained by the joint during seismic loading. Additionally, the slab contribution leads to a more uniform distribution of forces throughout the joint, which reduces localized stresses that could cause premature failure.

Furthermore, the slab can be considered to provide confinement, similar to the joint stirrups, fibers within the joint, and transverse beams confining the joint in the direction perpendicular to the applied load. A joint with superior confinement can achieve a higher shear strength.

Akin (2011) reported that a more comprehensive understanding of the behavior of the entire structure under seismic loading can be achieved by taking into account the contribution of the slab. Therefore, there has been an increasing trend in the literature regarding tests that aim to comprehend the behavior of FRCC beam-to-column joints under earthquake loading while considering the slab effect. It should be noted that testing such connections without considering the slab would be unconservative, as the moment capacity of the beams would be higher with flanged sections compared to rectangular sections, which would enlarge the force demand on the joint (Han & Lee, 2022). Moreover, the load-displacement behavior exhibits an asymmetric nature due to the flange contribution by the slab, which should not be neglected in the tests.

Tingting et al. (2022) conducted a study, where they subjected beam-to-column connection specimens including slabs to reversed cyclic loading. The study

emphasized the impact of slabs on the mechanical characteristics of the joint, and the outcomes revealed a considerable improvement in the joint stiffness and strength. By acting as a form of confinement to the joint, the slabs or the effective flange width successfully decreased the level of deformation and damage caused during loading. Liang & Lu (2018) also observed that the incorporation of transverse beams and slabs in the experimental setup increases the shear resistance of the beam-to-column joints.

The cyclic behavior of high-performance fiber-reinforced cementitious composite corner joints was investigated in a recent study, conducted by Han & Lee (2022), with specific emphasis on the influence of slabs. The study revealed that the inclusion of slabs in the test setup significantly increased overall stiffness, strength, and energy dissipation capacity of the joints. The slabs acted as a confining member, effectively reducing deformation and damage during cyclic loading. The results of the study indicate that the use of slabs in the design of these joints is crucial for ensuring their overall stability and safety, particularly under seismic loading. As such, the inclusion of slabs should be considered as an essential aspect in the design of FRC beam-to-column connections, in order to achieve satisfactory performance during seismic events.

Lu & Liang (2020) investigated the influence of high-performance fiber reinforced composites (HPFRCC) on the seismic performance of beam-column-slab subassemblies while taking the slab effect into account. The study concluded that the inclusion of HPFRCC significantly improved the seismic performance of the subassemblies, particularly in terms of stiffness, strength, and energy dissipation capacity. The presence of slabs further enhanced these benefits by acting as a form of confinement on the joints, reducing deformation and damage during loading. It is noteworthy that the placement of HPFRCC surrounding the longitudinal bars of the slab can delay their yielding and serve as an additional load-carrying mechanism that enhances the ductility. This, in turn, may potentially induce strong column - weak beam failure mode.

2.3.3.4 Bond Behavior

The bond strength between fibers and the matrix is a crucial factor for the seismic performance of fiber-reinforced cementitious composite beam-to-column connections. It resembles the mortar in brick walls, holding the bricks firmly together, forming a stable and sturdy structure. Similarly, the bond between fibers and the matrix is crucial for creating a cohesive and resilient composite material. Regardless of the superior quality of fibers and matrix, a weak bond between them leads to inadequate performance, much like bricks without mortar, which would collapse and crumble.

Fibers serve as bridges that cross the cracks in the composite material, transferring tensile stresses and redistributing them across the crack surface. This effectively inhibits the formation and propagation of cracks, which is a well-established phenomenon. A fiber can function to its fullest potential without exhibiting any adverse behavior when it has a strong bond with the matrix. However, if the bond between the fiber and the matrix cannot be established, fibers start to pull-out instead of bridging the cracks ending up with tensile fracture of the matrix, which is represented in the Figure 2.12. Therefore, it can be concluded that proper bond between the fibers and the matrix is an essential prerequisite for achieving optimal performance of fiber-reinforced cementitious composites.

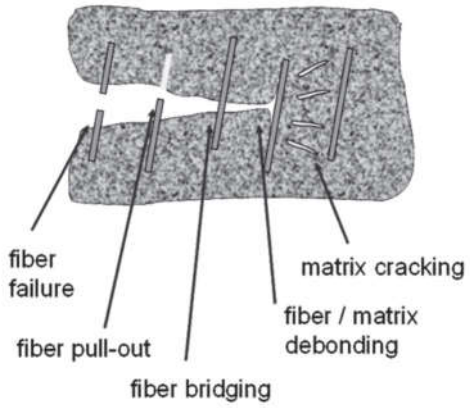

Figure 2.12. The mechanism by which fibers function. (ACI 544.4-18, 2018).

There are basically 3 types of bonding mechanisms, namely, electrostatic bonding, chemical bonding and mechanical bonding. The first type, electrostatic bonding, a bonding mechanism present in fiber-reinforced cementitious composites, arises from the opposing charges at the interface of the matrix and fibers. This phenomenon can be illustrated by taking the example of silane coating, which works well for particular fibers such as wood and glass, but not for magnesium (Lin et al., 2023). Secondly, the physicochemical properties of the interfacial zone between the matrix and fiber are associated with the chemical bond. This bond depends on the fiber type. For instance, the hydrophilic nature of PVA fiber grants it with a distinctive property of high chemical bond strength. This characteristic is attributed to a robust hydrogen intermolecular bond, which contributes to a sturdy bond between PVA fiber and cementitious materials (Suwannakarn, 2009). Lastly, mechanical bonding occurs when the fibers are physically interlocked with the matrix, creating a mechanical connection. To enhance the mechanical bond between the fiber and matrix, the fiber surface can be modified along its length by inducing mechanical deformations or roughening it. Consequently, various modifications such as indentation, deformation, crimping, coiling, twisting, and the addition of end hooks, paddles, buttons, or other anchorage systems can be employed to achieve this objective (Naaman, 2008).

Yagmur (2018) conducted an analytical investigation that involved modeling of fiber-reinforced cementitious composite deep beams and compiling a database of prior experimental data. As a result, Equation **(2.16)** was proposed to predict the bond strength.

$$\tau = \left(\frac{L_f}{D_f}\right)^{V_f} \sigma_{mu} \qquad \textbf{(2.16)}$$

In Equation **(2.16)**, L_f / D_f and V_f denote the aspect ratio and volume fraction of the fiber, while σ_{mu} represents the average splitting tensile strength, which is proposed to be found as addressed in **(2.17)**.

$$\sigma_{mu} = \begin{cases} 6.7\sqrt{f_c'} & \text{in psi} \\ 0.556\sqrt{f_c'} & \text{in MPa} \end{cases} \quad \textbf{(2.17)}$$

2.3.3.5 Flexural Strength Ratio

The flexural strength ratio is a parameter that denotes the flexural capacity of the columns compared to the beams in a beam-to-column connection (Liang & Lu, 2018; Tingting et al., 2022). It is determined by dividing the summation of flexural capacities of the columns by that of the beams framing into the joint as shown in Equation **(2.18)**.

$$M_r = \frac{\sum M_{r,cols}}{\sum M_{r,beams}} \quad \textbf{(2.18)}$$

In their experimental research, Tingting et al. (2022) tested six FRCC beam-to-column connection specimens with different flexural strength ratios, namely 1.1, 1.2, 1.4 and 1.6, having the same joint transverse reinforcement for all specimens. The authors concluded that as the ratio increases, joint shear strength negligibly increased, yet the shear distortion corresponding to the peak strength reduced considerably.

Liang and Lu (2018) tested 4 FRCC beam-to-column connection specimens, in order to observe the effect of flexural strength ratio on the overall behavior. The authors noted that as the flexural strength ratio increases from 1.1 to 1.2, 1.4 and 1.6, load bearing capacity increased by around 7%, 12% and 19%, respectively. Moreover, according to the test results, increasing flexural strength ratio resulted in considerable enhancement in the cumulative energy dissipation and stiffness.

Liang et al. (2016) conducted an experimental investigation on the effect of flexural strength ratio on the seismic behavior of beam-to-column joints in fiber-reinforced concrete structures. The study involved conducting reversed cyclic loading tests on four connection specimens. It was observed that the formation of plastic hinge on the

column next to the joint face occurs when the flexural strength ratio is less than 1.0. Conversely, the plastic hinge formation takes place on the beams when the flexural strength ratio is greater than 1.0. Additionally, it was stated that an increase in flexural strength ratio led to an increase in the area within the hysteresis curves, thereby enhancing the energy dissipation capacity of the subassembly. Another key finding was that increasing the flexural strength ratio reduces the pinching of the hysteresis curves, which is mainly caused by shear stresses and can result in shear failure of the joint. Hence, flexural strength ratio can be regarded as a significant parameter that reduces the risk of joint shear failure.

Design codes such as ACI 352-02, ACI 318-19 and TSC2018 have effectively addressed this issue by following the “strong column - weak beam" design principle. By adhering to this principle, plastic hinges are formed in beams instead of columns, which leads to a more ductile behavior. ACI 352-02, ACI 318-19, and TSC2018 require that the flexural strength ratio should not be less than 1.2, as presented in Equation **(2.19)**.

$$M_r = \frac{\sum M_{r,cols}}{\sum M_{r,beams}} \geq 1.2 \qquad \textbf{(2.19)}$$

2.3.3.6 Joint Type

As discussed in the section "Classification of Beam-to-Column Connections", joint type not only affects joint shear capacity but also joint shear demand. As such, the location of a joint, whether exterior or interior, is a crucial parameter that significantly influences its behavior.

Exterior connections are notably more susceptible to horizontal joint shear stresses when compared to interior joints. This is due to the fact that exterior connections only have one longitudinal beam in the direction of loading, while interior connections have two. This phenomenon is supported by the fact that connection failures predominantly occur at exterior connections following earthquakes.

Wang et al. (2018) discussed the effect of joint type on joint behavior based on the results of a test series of 9 FRCC joints. The study on beam-to-column joints in Ultra-High Performance Fiber-Reinforced Concrete (UHPFRC) highlights the noticeable role of joint type in modifying the shear carrying capacity of UHPFRC joints. The findings reveal that the shear strength of interior joints significantly surpassed their exterior counterparts due to variations in the UHPFRC diagonal strut. Specifically, the vertical anchoring portion of the beam bar in exterior joints led to a smaller cross-section and a larger inclination angle in the diagonal compression strut, which hindered the shear carrying capacity of such joints. By contrast, the diagonal compression strut in interior joints exhibited greater cross-sectional area and lower inclination angle, thus contributing to higher shear strength. Evidently, the shear strength ratio of exterior to interior joints was found to be approximately 80%. These results emphasize the importance of joint type in dictating the behavior and performance of UHPFRC beam-to-column joints.

2.3.3.7 Transverse Beams

In addition to the longitudinal beams, the number of transverse beams that frame into the joint is a crucial factor that influences its behavior. The ACI 318-19, ACI 352-02 and TSC2018 building codes require the transverse beams to have widths equal to at least 75% of the column width they frame into. The significance of both the presence and width of these transverse beams are highlighted as they confine the joint.

However, the scarcity of tests including transverse beams is a notable issue in the literature due to the complexities involved in forming and testing connections that incorporate these beams (Han & Lee, 2022).

As an output of their tests, Liang & Lu (2018) stated that the inclusion of transverse beams in beam-column-slab subassemblies has an apparent effect on their seismic

behavior, particularly in terms of joint damage. It was concluded that addition of the transverse beams resulted in a noticeable reduction in the joint distortion.

2.3.3.8 Axial Load Applied on the Column

Undoubtedly, reinforced concrete is a material much more widespread around the world than FRCC, which leads to the fact that there has been a significant academic research effort spent for RC over the last decades. However, even for reinforced concrete beam-to-column connections, the impact of axial load on the behavior of beam-to-column joints is a highly debated topic among researchers, and despite this, a conclusive agreement on the matter has not been established, with various conflicting findings reported in the literature (Akin, 2011; Unal, 2010).

According to Wang et al. (2018), the application of axial compression can have a positive reflection on the shear carrying capacity of specimens. This may be attributed to the extension of the compression zone caused by the increased column compression, resulting in the FRC diagonal strut's sectional area resisting the enlarged compression. Furthermore, appropriate compressive stresses can enhance the initial cracking strength of FRC, and cause crack closure as low magnitude axial loads will provide confinement to the joint. On the other hand, when the axial compression on a specimen surpasses a specific threshold, the compression zone is pushed beyond the joint boundaries, leading to a reduction in the slope of the compression strut and subsequently, its shear carrying capacity.

In the investigation by Liang et al. (2016), it was observed that increasing axial load on the column leads to higher load carrying and energy dissipation capacities, less pinched load displacement behavior, and reduced deformations.

Yuan et al. (2013) stated that increased axial load on the column fails to enhance the ultimate load capacity and ductility, specifically in the event of beam flexural failure. However, such an increase in axial load can potentially yield higher ductility due to its ability to constrain the propagation of cracks in the joint.

As a part of the same analogy with joint transverse reinforcement and the fibers themselves, column axial load also creates confinement effect within the joint, only up to a compression level. Shi et al. (2021) tested a series of FRC beam-to-column joints with axial compression levels of 0.2, 0.3 and 0.4. The authors concluded that load carrying capacity and ultimate displacement capacity were improved as the axial load level increased from 0.2 to 0.4.

2.3.3.9 Fiber Related Parameters

Various fiber-related parameters are known to have significant effects on the behavior of fiber-reinforced concrete beam-to-column joints. These parameters include but are not limited to the fiber type, aspect ratio, volume fraction, reinforcing index and tensile strength. It is worth mentioning that the effects of these parameters are not isolated, and they can interact with each other, leading to a complex behavior. For instance, the fiber aspect ratio can affect the fiber-matrix bond strength, which in turn can impact the joint shear strength (Yagmur, 2018). In return, bond strength can also influence the cracking and post-cracking tensile strengths of the composite, and consequently, the overall performance of the joint (Naaman, 2018). Therefore, a comprehensive understanding of the correlation between these fiber-related parameters is essential to optimize the design and performance of fiber-reinforced concrete beam-to-column joints.

2.3.3.9.1 Fiber Type

Fiber type is a vital parameter that exerts a significant influence on the mechanical behavior of fiber-reinforced cementitious composite beam-to-column connections. The diverse mechanical properties of different fiber types, such as steel, carbon and polymeric fibers, as presented in Figure 2.13, render them to interact distinctively with the cementitious matrix. Thus, choosing the appropriate fiber type is an

important step in attaining the intended mechanical performance of the composite (Parra-Montesinos, 2005).

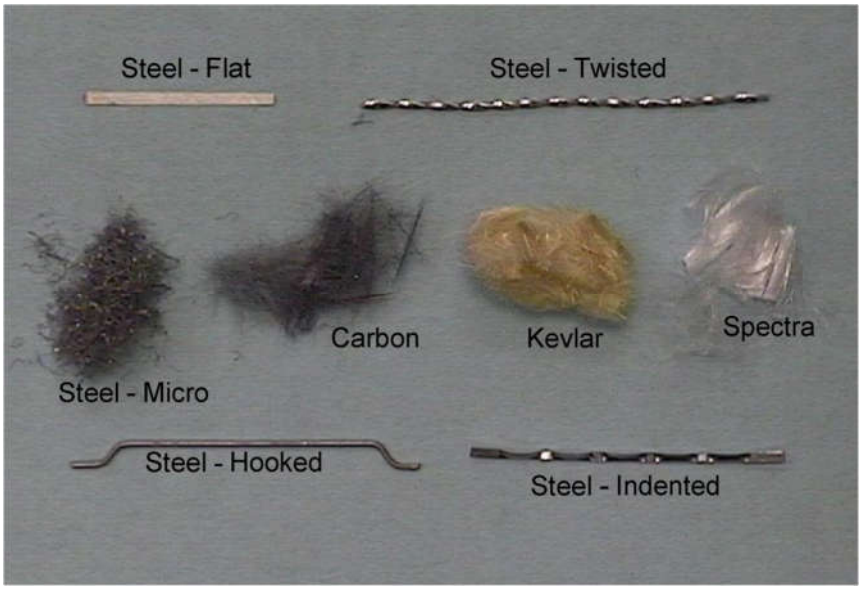

Figure 2.13. Typical fiber types utilized in FRCC. (Naaman, 2008).

The mechanical properties of the fibers, including stiffness, tensile strength, and elongation at break, play a pivotal role in determining the reinforcement efficiency of the composite. Notably, high-strength fibers, such as steel and glass fibers, exhibit superior reinforcement properties, leading to an improved mechanical performance of the composite. On the other hand, low-strength fibers, such as natural fibers, may not provide optimal reinforcement but instead offer desirable properties, such as low density and biodegradability (Sathishkumar et al., 2013).

Furthermore, the interaction between the fiber and the cementitious matrix also depends on the fiber type. Some fibers, such as polymeric fibers, exhibit a favorable ability to form a chemical bond with the matrix, leading to superior interfacial bond strength and enhanced mechanical properties (Kanda & Li, 1999). Conversely, other fibers, such as glass fibers, rely on mechanical interlocking and adhesion rather than forming a chemical bond with the matrix (Khabaz, 2014). Hence, understanding the impact of the fiber type on the mechanical behavior of the composite is important in selecting the appropriate fiber type and accomplishing the desired mechanical

performance of fiber-reinforced cementitious composite beam-to-column connections.

Considering the behavior of beam-to-column connections made of fiber reinforced cementitious composites, the type of fiber dispersed amongst the matrix is a key parameter as it drastically alters the way joint behaves.

2.3.3.9.2 Fiber Aspect Ratio

The fiber aspect ratio is an essential parameter that governs the mechanical behavior of fiber-reinforced cementitious composite beam-to-column connections (Filiatrault et al., 1994). Defined as the ratio of the fiber length to its diameter, it plays an important role in determining the fiber-matrix interaction and the resulting mechanical properties.

The fiber aspect ratio is a key parameter that significantly influences the bond strength of fiber-reinforced cementitious composites (FRCC). The bond strength is related to the surface area or embedment length of the fiber. As the aspect ratio increases, there is a corresponding increase in the surface area of the fiber. This results in superior bonding behavior between the fiber and matrix, which creates an environment that promotes an improved crack-bridging ability of the fibers. Therefore, it can be concluded that the fiber aspect ratio increases the interfacial area between the fiber and matrix, leading to an enhanced bond strength and improved crack-bridging ability of the fibers in FRCC members (Ranade, 2014; Ranade et al., 2013). When the fibers fail to bridge the cracks, a pull-out type of failure may occur, which is an undesired and brittle mode of failure. This is precisely why it is challenging to achieve tensile strain-hardening behavior, exhibit multi-cracking, particularly when short fibers with low aspect ratios are utilized (Li & Wu, 1992).

Moreover, the increased interfacial area resulting from the higher fiber aspect ratio reduces the localized stresses on each individual fiber, promoting a more uniform stress distribution throughout the fibers. This leads to higher load carrying capacity

for the fibers. As a result, fracturing the fibers becomes harder, requiring an increased fracture energy that is proportional to the higher fiber aspect ratio (Li, 1992).

The primary advantage HPFRCC lies in its tensile behavior that highly depends on the aspect ratio of the fibers embedded in the matrix. This holds true not only for beam-to-column connections, but also for all other structural members or structures constructed with this material. The values of cracking and post-cracking strengths are of critical significance since they dictate the overall behavior of the structure under diverse loading conditions. It is therefore imperative to understand that both the cracking and post-cracking strengths are highly reliant on the aspect ratio of the fibers (Naaman, 2008; Naaman & Reinhardt, 1996). Furthermore, the aspect ratio of fibers exerts a considerable influence on the minimum volume fraction necessary to achieve strain hardening behavior under tension. As the aspect ratio of fibers increases, the critical volume fraction decreases, as illustrated in Figure 2.14. As such, the importance of selecting a suitable aspect ratio in the joint design process becomes apparent regarding attaining optimal tensile behavior of the composite.

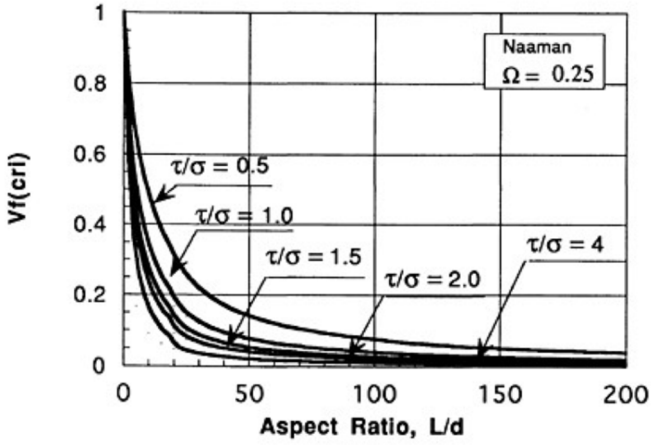

Figure 2.14. Relationship between aspect ratio and critical volume fraction. (Naaman & Reinhardt, 1996)

Nevertheless, excessively high aspect ratios can present challenges during mixing, placing, and compacting the material. The longer fibers are more susceptible to becoming entangled, potentially resulting in a reduction in the homogeneity and durability of the material (Wu, 2001).

2.3.3.9.3 Fiber Volume Fraction

The incorporation of additional fibers into the cementitious matrix generally leads to an improvement in the flexural and shear strength of the connection, primarily due to the resulting increase in the fiber bridging effect. Additionally, the increased fiber volume fraction can enhance the connection ductility by delaying the initiation of cracking and reducing the crack width. The fiber volume fraction represents a vital parameter that exerts a profound influence on the mechanical behavior of fiber-reinforced cementitious composite beam-to-column connections, encompassing their strength, ductility, and energy dissipation capacity (Filiatrault et al., 1994; Gencoglu, 2007; Li et al., 2022; Pekgokgoz & Avcil, 2022; Rajkumar et al., 2021; Chidambaram & Agarwal, 2018).

The main source of the improvement in the flexural and the shear behavior of FRC with the increase of fiber volume fraction is the enhancement of the bridging capability, ending up with a rise in both cracking and post-cracking strengths. It is worth emphasizing that one of the most salient factors to take into account is the fiber volume fraction, which serves as a confining media within the joint, exerting a significant impact on the cracking and post-cracking responses of the composite, similar to the influence of the fiber aspect ratio (Choi & Bae, 2019; Naaman, 2008; Naaman & Reinhardt, 1996).

There are numerous studies examining the influence of fiber volume fraction on the behavior of FRC beam-to-column connections. Sarmah et al. (2018a) proved that the increasing fiber volume fraction improves the ductility in case of both steel FRC and basalt FRC. It is noteworthy that the increased volume fraction results in a decrease in the ultimate load capacity of Basalt FRC; conversely, for Steel FRC, the load carrying capacity, as well as initial stiffness, is enhanced directly proportional to the increase in the volume fraction. Moreover, the degradation of concrete was notably more noticeable in samples with a higher fiber volume fraction, due to the de-bonding phenomenon. For this reason, Basalt FRC with a higher volume fraction

demonstrated a significant reduction in the initial stiffness, as well as energy dissipation capacity.

Shi et al. (2021) stated that the increase in volume fraction of steel fibers resulted in an enhancement of ductility and energy dissipation capacity of SFRC beam-to-column connections. Thus, the force-displacement hysteresis curves for higher volume fractions are expected to be wider. It is worth noting that such enhancements become particularly evident following the yielding of the longitudinal bars in the beam, which marks the onset of inelastic behavior.

The investigation carried out by Sachdeva et al. (2021) involved testing six beam-to-column joints, which featured headed bars, four of which were reinforced with steel fibers. The primary objective of the study was to analyze the behavior of these connections, both with and without headed bars, under varying fiber volume fractions. The authors determined that the specimen with the highest volume fraction of fibers exhibited the most ductile behavior.

Chidambaram & Agarwal (2018) evaluated the performance of metallic and synthetic fiber hybridization on the cyclic behavior of exterior beam-to-column joints. The study involved testing specimens that have varying fiber volume fractions. The study proved that a significant rise in steel fiber volume considerably enhances both the aggregate interlocking capacity and bond strength, resulting in a significant reduction of the pullout failure mechanism. Moreover, increasing the fiber volume fraction may alter the failure mode from joint shear failure to beam flexural failure, which represents a more desirable, ductile mode of failure.

Excessive addition of fibers to the cementitious matrix can have a detrimental effect on the performance of fiber-reinforced cementitious composite beam-to-column connections. When the fiber volume fraction exceeds the optimal range, the fibers tend to agglomerate and form lumps, leading to an uneven distribution of fibers within the matrix, which also reduces the workability (Gencoglu & Eren, 2002). These fiber lumps create localized areas of high stress concentration and weak points in the material, which can ultimately result in significant strength loss and reduced

ductility of the connection (Chidambaram & Agarwal, 2018). The lumped fibers can also cause cracking to occur prematurely, leading to further degradation of the material's mechanical performance. Therefore, the optimum fiber volume fraction must be carefully determined to ensure that the fibers are uniformly dispersed within the matrix, thereby avoiding the formation of fiber lumps, and enhancing overall strength and durability of the material.

Supporting this phenomenon, Wille et al., (2014) conducted research to observe the effect of increase in the volume fraction of added steel fibers into the composite on the cracking and post cracking behavior. The results proved that they both increase with increasing fiber volume fraction, yet the rate of increase reduces. This means that at some volume fraction, a peak will be reached and then the excessive amount of fibers will start to harm the structure by degrading its behavior (Wille et al., 2011)

2.3.3.9.4 Fiber Reinforcing Index

The fiber reinforcing index, which is the product of the aspect ratio and fiber volume fraction, is a key parameter affecting the mechanical performance of fiber-reinforced cementitious composites. As illustrated in different sections of this thesis, this dimensionless parameter has a substantial influence on various characteristics, including the cracking and post-cracking tensile strengths (Naaman, 2008; Naaman & Reinhardt, 1996), as well as modulus of rupture and modulus of elasticity (Yang, 2011).

The computation of the reinforcing index for fiber reinforced cementitious composites that has a single fiber type is relatively simple. However, when hybrid fiber reinforced cementitious composites (HFRCC), which involve at least two types of fibers, are considered, the calculation becomes somewhat complicated.

The reinforcing index for such composites may be obtained by employing the expression given in Equation **(2.20)**, where the contribution of non-steel fibers is taken into account considering their tensile strength (Almusallam et al., 2016).

$$RI_v = \sum_{i=1}^{n} k_i V_{fi} \left(\frac{L}{D}\right)_i \left(\frac{f_{ti}}{f_{ts}}\right)^a \quad \textbf{(2.20)}$$

In Equation **(2.20)**, the symbol, V_{fi}, represents the volume fraction of the i^{th} fiber type, while $(L/D)_i$ signifies the aspect ratio of the i^{th} fiber type. The tensile strength of the i^{th} fiber type is denoted by f_{ti}, whereas f_{ts} refers to the tensile strength of steel fiber. The bond factor for the i^{th} fiber type is given by k_i. Furthermore, the tension stiffness parameter 'a' is proposed to be taken as 0.5.

The bond factor, denoted by k, is regarded as an essential parameter that signifies the mechanical anchorage of a fiber to the matrix through the surface shape of the fiber. In the existing literature, the value of the constant 'a' is often adopted as 1.0 for rough-surfaced fibers that exhibit remarkable anchorage, such as crimped fibers, hooked-end steel fibers, and corrugated fibers. Conversely, smooth-surfaced fibers, such as straight polyethylene, polypropylene fibers, and PVA fibers, are assigned a lower value of 0.1. This value is typically considered due to the reduced frictional forces between the smooth fiber surface and the matrix.

There are deviations in the numerical values reported for the bond factor, particularly with respect to different types of fibers, whereas the term 'a' remains the same. Equation **(2.20)** employs a fixed value of 0.5 for the term 'a' (Cui et al., 2022; Gao et al., 2022; Ibrahim et al., 2016; Liu et al., 2023). However, discrepancies are observed in the bond factor term 'k' for various fiber types, where Cui et al. (2022) proposed a value of 0.1 for micro steel fibers, Ibrahim et al. (2016) recommend a value of 1.0 for hooked end steel fibers and crimped polypropylene fibers, and Liu et al. (2023) suggested a value of 0.8 for plain Kevlar.

An alternative method to determine the reinforcing index of High-Performance Fiber Reinforced Cementitious Composite (HFRCC) is to incorporate the non-steel fibers and compare their elastic moduli with that of the steel fiber, as described in Equation **(2.21)** (Cao & Li, 2018).

$$RI_v = \sum_{i=1}^{n} V_{fi} \left(\frac{L}{D}\right)_i \left(\frac{E_i}{E_s}\right)^{\eta} \quad \textbf{(2.21)}$$

The term η in Equation **(2.21)** is set at 1.5 or 2 in the case of PVA fiber, and it is assigned a value of 2 for whisker fibers (Cao & Li, 2018).

Abbas et al. (2022) proposed Equation **(2.22)** for obtaining the reinforcing index of the Hybrid steel-PVA HPFRCC. In Equation **(2.22)**, different from Equation **(2.21)**, η term is taken as unity. The subscripts 's' and 'p' stand for steel and PVA, respectively.

$$RI_v = k_s V_s \left(\frac{L_s}{D_s}\right) + k_p V_p \left(\frac{L_p}{D_p}\right)\left(\frac{E_p}{E_s}\right) \quad \textbf{(2.22)}$$

Abadel et al. (2016) proposed Equations **(2.23)** and **(2.24)** to determine the reinforcing index of HFRCC. The value of k is taken as 1 for both hooked end steel fibers and crimped polypropylene, while for plain Kevlar fibers it is set at 0.8.

$$RI_v = \sum_{i=1}^{n} RI_{vi} \quad \textbf{(2.23)}$$

$$RI_{vi} = k_i V_{fi} \left(\frac{L}{D}\right)_i \left(\frac{E_i}{E_s}\right) \quad \textbf{(2.24)}$$

Another way of calculating the fiber reinforcing index is neglecting both the relative tensile strength and modulus of elasticity. In this method, Equation **(2.25)** is utilized to obtain the reinforcing index of HFRCC, which includes steel and synthetic fibers (Guler et al., 2019). This approach fails to account for the diverse bonding abilities of different fibers, and in its most basic form, the reinforcing index of hybrid fibers is calculated by only considering the contributions of individual fibers, without taking into account their relative bond properties.

$$RI_v = \sum_{i=1}^{n} V_{fi} \left(\frac{L}{D}\right)_i \quad \textbf{(2.25)}$$

Finally, Khan et al. (2020) stated that the bonding capacity of fibers is affected by various factors, including their chemical nature. Polypropylene fibers, for example, have a hydrophobic characteristic, which makes them less adhesive to the surrounding matrix. Therefore, an additional term k_a, adhesion coefficient, was introduced to the reinforcing index equation as illustrated in Equation **(2.26)**. The values of 2, 1, and 0.5 are assigned as the adhesion coefficients of steel fiber, basalt fiber, and CaCO3 whisker, respectively, which were determined from pull-out tests.

$$MRI_v = \sum_{i=1}^{n} k_i k_a V_{fi} \left(\frac{L}{D}\right)_i \left(\frac{f_{ti}}{f_{ts}}\right)^{\eta} \quad \textbf{(2.26)}$$

2.4 Analytical Modeling of Beam-to-Column Connections

Despite the common approach of modeling joint regions as rigid and elastic, they undergo substantial inelastic deformations that result in nonlinearity (Akin, 2011). Employing rigid modeling, results in unrealistically rigid regions, leading to an erroneous structural response characterized by increased forces, reduced deformations, and inaccurate hinge mechanisms (Unal & Burak, 2013). Thus, it is crucial to utilize a reasonably accurate yet practical model during nonlinear analysis.

In light of experimental outcomes, numerous analytical investigations have been undertaken to investigate the influence of different parameters on the seismic response of the connection region and estimate the load-deformation relationships. Consequently, analytical models that capture the joint shear stress vs. distortion response have been recommended.

Unal & Burak (2013) proposed a joint model for reinforced concrete beam-to-column joints that incorporates a joint moment versus joint distortion interaction,

obtained by a statistical correlation technique. This model assigns the parametric moment-distortion model to the panel zone, and nonlinear hinges at the plastic hinge regions of the beams and columns, enabling the observation of nonlinear joint response during seismic analysis.

Burak & Wight (2005) proposed a joint model to predict the shear behavior of reinforced concrete beam-to-column joints by incorporating experimental data. The model was used to analyze subassemblies, yielding consistent results, while a comparison between a five-story building analyzed using rigid connections and those with the joint model indicated that neglecting the model could result in an underestimation of roof drifts of up to 35%. These findings emphasize the necessity of utilizing accurate and comprehensive models in structural analyses.

While there are numerous studies on reinforced concrete, the number of models proposed for fiber-reinforced cementitious composite (FRCC) beam-to-column joints is relatively limited.

With regard to FRCC joint shear behavior, more recently, Tingting et al. (2022) studied the relationship between shear force and distortion. The Bayesian parameter estimation method was utilized to establish the model reflecting the shear behavior of HPFRCC joints. As shown in Figure 2.15, the model is made of four characteristic points, including points A_j, B_j, C_j and D_j, which refer to the cracking point, yield point, peak point and limit point, respectively. Joint shear strength prediction equation, incorporating the parameters that exert the greatest influence on joint behavior at the peak characteristic point is provided in Equation **(4.2)**.

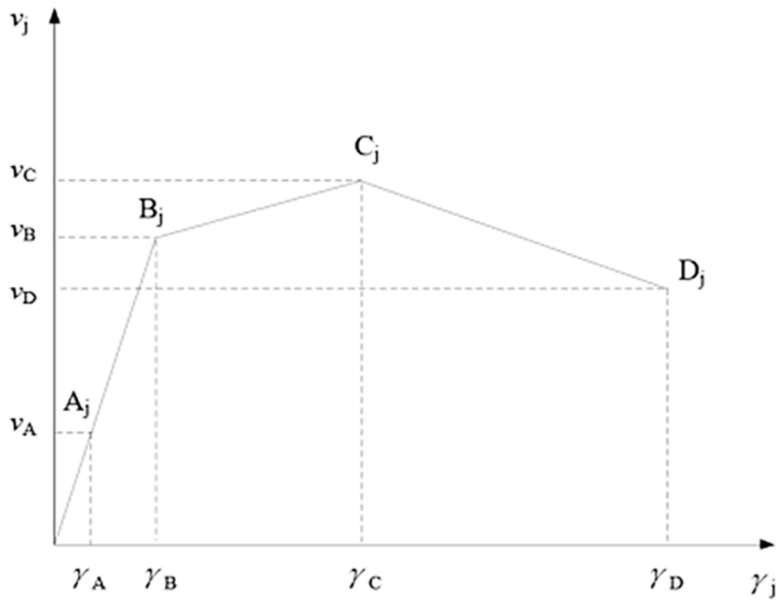

Figure 2.15. Joint shear stress vs. strain model developed by Tingting et al. (2022).

The authors proposed Equation **(2.27)** to predict the shear strain at the peak point. The terms used in this equation are explained in Section 4.1.2.

$$\gamma_j \text{ (rad)} = \text{BI}.(\text{TB})^{5.101}.\left(\frac{A_{sh,pro}}{A_{sh,req}}\right)^{-1.472}.\left(\frac{S_{pro}}{S_{req}}\right)^{1.378}.\left(\frac{b_b}{b_c}\right)^{-2.865}.\left(\frac{h_b}{h_c}\right)^{-0.578}(\varepsilon_t)^{0.074}.(\text{CI})^{-0.304}.(\text{JI})^{2.503}.\left(\frac{v_j}{f_c}\right)^{-1.913} \quad \textbf{(2.27)}$$

The model acknowledges the utilization of specific coefficients to represent the stresses experienced at points A, B, and D, with values of 0.44, 0.89, and 0.90, respectively, relative to the joint shear stress observed at point C. Similarly, corresponding coefficients of 0.0198, 0.3610, and 2.2 are proposed to characterize the strains occurring at these aforementioned points in relation to the strain measured at point C.

CHAPTER 3

DATABASE COLLECTION

3.1 Overview

A comprehensive database has been constructed based on the collection of experimental data documented in the literature pertaining to the seismic behavior of beam-to-column connections. The database encompasses a thorough compilation of all available data, to the knowledge of the author, pertaining to specimen dimensions, details of fibers utilized, material properties, loading protocols, reinforcement detailing, and experimental outcomes. The main goals for the construction of this database are to furnish a valuable resource for researchers working in the field of structural engineering and to come up with a shear strength prediction equation, as well as a shear stress vs. shear strain model that reflects the behavior of FRCC beam-to-column connections under seismic activity.

Construction of such a comprehensive database presents formidable challenges, the most prominent of which is the lack of test data, especially those containing shear distortion instrumentation. Moreover, the search for data related to the tests conducted on beam-to-column connections can prove more challenging when compared to those on other structural elements such as beams and columns, due to the intricate and variable nature of connection behavior under seismic loading.

By incorporating the entirety of the existing data, the database can effectively identify gaps in available information and steer the development of novel experimental programs. In summary, the establishment of this database stands as a crucial contribution to the field of structural engineering, significantly advancing the comprehension of the seismic response of FRCC beam-to-column connections.

It is noteworthy to highlight that two different databases were constructed, in the scope of this study. The first database is the comprehensive one, which encompasses a vast array of 212 diverse specimens. Inclusive of an assortment of failure modes, such as beam and column flexural failures, as well as joint shear failures, this database provides a comprehensive overview of the specimens tested. On the other hand, the secondary database, known as the joint failure database, is a subordinate part of the first database, and comprises a total of 117 specimens, which have joint failure.

The reduction in the number of specimens from the overall database to the joint failure database can be attributed to the researchers' focus on exploring the application of FRCC, particularly HPFRCC, in the joint region to facilitate a shift in failure mechanism from joint shear failure to beam flexural failure. As a consequence, almost 50% of the tests in the overall database resulted in the desired beam flexural failure, leading to the reduction in the number of specimens in the joint failure database.

3.2 Selection Criteria for Specimens

Within this section, the criteria on selection of the specimens that are included in the database will be outlined. The selection criteria are categorized into several distinct groups, including member geometry, eccentricity, failure mode, longitudinal beam reinforcement detailing, loading type, inclusion of slabs or wide beams, and type of casting.

3.2.1 Fiber Type

This investigation is differentiated from the prior studies by its extensive inclusion of a variety of fiber types. These fibers consist of Aramid, Basalt, Hooked End Steel, Straight Steel, Polyethylene, Polyethylene Terephthalate, Polypropylene, Poly-vinyl Alcohol, and Glass fibers. In addition, this study goes further than previous research

by analyzing test results not only on single fiber inclusions but also on hybrid fiber reinforced concrete which integrates at least two different fiber types. As a result of these unique attributes, this study can be viewed as pioneering, as it is the first one to undertake the task of predicting joint shear strength and creating a shear stress-shear strain model that incorporates such a diverse range of fiber types and hybrid fiber reinforced composite specimens.

3.2.2 Specimen Geometry Selection Criteria

The literature contains numerous experimental results on the behavior of FRCC beam to column connections with varying geometrical properties. These can be differentiated based on whether the connection region is a part of a subassembly or a frame and can be further distinguished by the number of beams and columns that are connected at the joint, as well as the span lengths and cross-sectional dimensions of these structural elements. Consequently, it is imperative to establish a set of conditions to determine which specimens will be included in the database. By doing so, it will be possible to create a database that is both reliable and accurate.

3.2.2.1 Selection Among Subassemblies and Frames

The specimens that have been tested previously can be broadly classified into two categories: frame structures and sub-assemblies. The tested frames are generally simple structures consisting of a single bay and one story, making them easy to classify. However, sub-assemblies may vary in terms of type and dimensions, as discussed in the literature review chapter, and depicted in Figure 2.2. In order to ensure consistency, limitations are set on the criteria for specimens that will be included in the database, which will be explained in this section.

3.2.2.2 Selection based on Joint Type

The number of tests performed on the seismic behavior of FRCC beam-to-column connections is notably lower than that conducted on conventional reinforced concrete. Consequently, it is not easy to find tests for all of the connection geometries depicted in Figure 2.2, even though it would be ideal. Hence, although the number of tests obtained from the literature is adequate for the objectives of the present study, the range of specimen geometry is restricted. To be precise, this study solely encompasses specimens classified as E0, E1, I0, I1, I2, and RE0.

3.2.2.3 Selection based on the Point of Inflection

Only the specimens in which the points of inflection of the members occurred at the mid-height of the columns and mid-span of the beams were included in the database. Any other specimens that were tested in the literature were disregarded and not included in the database.

3.2.2.4 Selection based on the Member Dimensions or Scale

The selection criteria for the database prioritize reliability of the data by taking into account several factors, among them the scale of the test specimens. Due to the increased likelihood of fiber lumping caused by higher volume fractions or longer fiber lengths, small-scale specimens are excluded from the database. Nevertheless, there may be some exceptions, such as in the case of small-scale specimens derived from real bridge beam to column connections with significantly large beam and column cross sections.

3.2.3 Eccentricity Selection Criteria

Eccentric beam-to-column connections are connections where the beam centerline does not coincide with the column centerline, resulting in eccentricity in the load transfer mechanism. However, these types of connections are not considered in the database because of the lack of available test data.

3.2.4 Wide Beam Selection Criteria

A wide beam-to-column connection pertains to a scenario where the width of the beam surpasses that of the column framing into the joint, along the direction of loading. Such connections behave quite differently than regular connections as some of the longitudinal beam reinforcement remains outside the column core and pass through the transverse beams (Burak, 2005). However, despite their relevance in the behavior of beam-to-column connections, wide beams are not included in the database due to the absence of any available test data.

3.2.5 Beam Longitudinal Bar Detailing Selection Criteria

This research study employs beam reinforcement layout as one of the criteria for selecting test specimens. In particular, specimens where the longitudinal bars of the beam are placed diagonally in the joint, which is regarded as a special reinforcement type, are excluded from the database. In contrast, specimens featuring headed but straight bars are included in the database.

3.2.6 Loading Type Selection Criteria

Monotonically loaded specimens are excluded from the database, and only those under reversed cyclic loading are included. This selection criterion is motivated by the fact that reversed cyclic loading represents the dynamic nature of seismic

activity, which is characterized by reversible loads. Therefore, the use of reversed cyclic loading provides a more accurate and reliable representation of the behavior of beam-to-column connections under seismic loading.

Furthermore, bidirectionally loaded specimens are not included in the database, in order to maintain a dataset that is not affected by prior loading, since the number of tests conducted under such loading conditions was found to be significantly lower.

3.2.7 Slab Inclusion Selection Criteria

Besides the aforementioned parameters, specimens cast with slabs are also taken into account during the database collection process. This is simply due to the fact that the existence of a slab in a beam-to-column connection may affect the degree of confinement of the joint, which is a decisive element for the seismic response of the joint. Furthermore, the contribution of the slab to the stiffness and strength of the joint could significantly influence the behavior of the connection region under seismic loading. Therefore, the inclusion of specimens featuring slabs in the database leads to a more thorough comprehension of the behavior of the beam-to-column connections with slabs.

3.2.8 Casting Type Selection Criteria

Owing to the primary research objective of examining moment and shear transfer along the joint between columns and beams, the precast beam-to-column connections are deliberately omitted from the database. Accordingly, the tests conducted on precast beam-to-column connections are not included in the database.

3.2.9 Failure Mode Selection Criteria

The optimal failure mode for beam-to-column connections is the initiation of a beam plastic hinge in the vicinity of the joint face, which leads to a ductile mode-of-failure.

This scenario, also known as beam flexural failure, is preferable as it allows for significant energy absorption and excessive plasticization before ultimate failure. However, this ideal outcome is not always achieved, and in some instances, column flexural failure may occur instead. When column flexural failure occurs, the column exceeds its capacity and undergoes free rotation while carrying a constant sustained moment. This mode-of-failure is undesirable, as the sequence of column hinges may result in a mechanism leading to collapse of entire structure. Moreover, joint shear failure, where diagonal cracks are formed in the joint, is the most undesirable mode of failure. This brittle failure type may be catastrophic, resulting in significant stiffness loss in the story, ultimately causing the building to collapse.

In addition to the failure modes previously mentioned, interface failure is another possible mode of failure that can occur due to the combined effect of shear and bending. This type of failure typically occurs at the intersection of the beam and the joint face. If the cracks propagate into the panel zone, it is classified as a joint shear failure; whereas, if the crack is parallel to the joint face, it is classified as an interface failure. Table 3.1 provides an overview of the possible failure modes of a beam-to-column connection, which includes a combination of the aforementioned failure modes.

Table 3.1 Probable failure modes of beam-to-column connections.

Failure Mode	**Explanation**
B	Beam Flexural Failure
C	Column Flexural Failure
J	Joint Shear Failure
BJ	Beam Flexural Failure Prior to Joint Shear Failure
CJ	Column Flexural Failure Prior to Joint Shear Failure
I	Interface Failure
IJ	Interface Failure Prior to Joint Shear Failure

The database compiled in the present study encompasses all potential failure modes outlined in Table 3.1. However, it is important to note that the shear strength prediction equation and the shear stress versus shear strain model are established solely on the basis of three failure modes, namely, J, CJ, and BJ. The rationale behind this selection is that only these failure modes lead to a brittle shear failure, where the joint reaches its shear strength. Consequently, only specimens that experienced one of these three failure modes were deemed eligible for inclusion in the final database.

3.2.10 Axial Load on the Column

The application of a constant axial load on the column during testing can be attributed to two primary reasons. Firstly, this technique is utilized by researchers to stabilize the system for ease of testing, and secondly, to simulate the axial load on the column during seismic activity. Therefore, it is common practice to apply an axial load on the column during testing.

It should be noted that there is an alternative method where the axial load is applied on the column in an alternating manner, which better represents the modification of the axial load on the column. However, this approach has been sparsely used in the literature and thus, such tests have not been included in the database. Therefore, only specimens under a constant axial load or under no axial load have been included in the database.

3.3 Range of Specimen Properties

In this section, the range of key specimen properties present in the database will be outlined. Distinct ranges are assigned to each database, one including all the failure modes and the other that consists of only the specimens with joint failure.

Table 3.2 Range of Key Parameters in both Databases

Parameter	Unit	Overall Database		Joint Shear Database	
		Min	Max	Min	Max
f_c'	MPa	16.93	107.00	16.93	107.00
n	%	0	50	0	50
V_f	%	0.5	5.0	0.5	3.5
$(L/D)_f$	-	25	1083	25	1000
RI_f	-	0.22	21.67	0.22	15.00
b_b/b_c	-	0.43	1.00	0.43	1.00
ρ_{gross}	%	0.00	1.32	0.00	1.32

Table 3.2 provides a summary of the key variables utilized in this study. The compressive strength is denoted by f_c', while 'n' represents the axial load ratio, which is calculated as $N/(f_c'A_g)$, where 'N' denotes the constant axial force applied on the column and A_g denotes the gross column cross-sectional area. Additionally, $(L/D)_f$ accounts for the fibers' aspect ratio, which is the fiber length divided by the fiber diameter and RI_f represents the reinforcing index of the fibers, as explained by Almusallam et al. (2016). The ratio of beam width to column width is denoted by b_b/b_c, while ρ_{gross} is the volumetric ratio of joint transverse reinforcements, calculated based on the gross joint area. A detailed explanation of the joint transverse reinforcement ratio calculation will be provided in the following chapter.

3.4 Selected Specimens

This section provides an overview of the experiments included in the database, highlighting the general properties of the specimens and the key parameters considered in each research study.

Qudah & Maalej (2014) investigated the assessment of the feasibility of utilizing Engineered Cementitious Composites (ECC) with PE fibers for improving beam-to-

column connection behavior. Nine interior connection specimens, labeled S1 to S9, were tested, with only the first one serving as the reinforced concrete control specimen. While the joints of the specimens had regular geometrical properties, the study focused on exploring the amount and detailing of transverse reinforcement, as well as the material used within the plastic hinging regions of the connection and the joint itself. To evaluate the advantages of using ECC in this type of application, the performance of the ECC interior connection specimens was compared to that of the control reinforced concrete specimen, using load-displacement responses, energy absorption capacities, and cracking responses.

Parra-Montesinos et al. (2005) explored the possibility of using High-Performance Fiber-Reinforced Cementitious Composites (HPFRCC) as a replacement for traditional joint transverse reinforcement. To this end, the researchers conducted tests on two specimens, each containing varying amounts of longitudinal reinforcement in the beams. Notably, the HPFRCC material was employed both in the panel zone and the beams that are framed into the joint. The specimens were subjected to maximum shear stresses of around 1.2 and 1.4 times the square root of the composite's compressive strength, respectively, with no special transverse reinforcement detailing provided in the beam plastic hinge regions. In light of their findings, the authors investigated the potential of HPFRCC in eliminating the need for traditional transverse reinforcement in the plastic hinge regions of beams.

The objective of the investigation conducted by Sachdeva et al. (2021) was to assess the performance of steel FRCC exterior beam-to-column connections in which headed bars are utilized. In order to make a comparative analysis, the authors assessed the headed bar specimens against conventionally hooked bars designed as per ACI 318-19 (ACI 318-19, 2019) and ACI 352-02 (ACI 352-02, 2002). Furthermore, the researchers examined the influence of different compressive strength values (C20 and C40) and varying amounts of fibers (1.0% and 1.5% volume fractions) on the behavior of hysteresis response, energy absorption capacity, the stiffness and ductility characteristics of the specimens.

In their investigation, Van & Trung (2019) conducted tests on three steel fiber-reinforced cementitious composite (SFRCC) specimens. The first specimen was the control specimen, designed in accordance with Eurocode 8 (Eurocode 8, 2004) with a high degree of plasticity. For the second and third specimens, stirrups were not employed in the joint or the beam plastic hinge region. However, the beam stirrup spacings varied slightly between the second and third specimens.

In the investigation carried out by Tingting et al. (2022) the primary objective was to interpret the influence of High-Performance Fiber-Reinforced Cementitious Composites (HPFRCC) on the mechanical response of beam-to-column subassemblies. The study placed particular emphasis on the impact of the flexural strength ratio, ranging from 1.1 to 1.6, while simultaneously examining the influence of flange width on the joint behavior of such subassemblies.

Kang et al. (2019) executed comprehensive full-scale experiments on a conventional reinforced concrete roof specimen and two HPFRCC specimens, one roof and one exterior specimen. The authors further explored the hypothesis that the inclusion of steel fibers in a volume fraction of 1% could potentially result in a reduction in the requirement for transverse reinforcement within the joint.

Lu & Liang (2020) focused on the effect of substituting reinforced concrete with High-Performance Fiber-Reinforced Cementitious Composites (HPFRCC) on the seismic behavior and damage pattern of interior beam-to-column subassemblies, which included slabs and transverse beams as the confining floor system. The authors conducted experiments on three specimens, wherein one was a conventional reinforced concrete control specimen, while the other two were constructed using HPFRCC, and varied in terms of column longitudinal reinforcements and slab flange widths.

In their investigation, Han & Lee (2022) conducted a series of unidirectional and bidirectional loading tests on a total of seven full-scale beam-to-column connection specimens that included slabs. Despite the similarity in dimensions and configurations across all specimens, the authors deliberately incorporated variations

in the joint's transverse reinforcement detailing and the application of HPFRCC. Notably, the researchers accounted for the presence of slabs and its impact on the mechanical behavior of the joint.

Wang et al. (2018) examined the seismic behavior and shear bearing capacity of beam-to-column joints constructed using Ultra-High Performance Fiber-Reinforced Concrete. The authors tested a total of nine specimens, comprising five exterior and four interior joints and analyzed the specimens' behavior in terms of failure modes, load bearing patterns, shear distortions, and load carrying capacity. The study further examined the impact of joint types, axial load levels, and joint reinforcement ratios on the joint failure modes and shear strength.

The seismic performance of interior beam-to-column joints with high-strength steel rebars and the impact of combined use of High-Strength Steel Fiber Reinforced Concrete and diagonally placed X-shaped reinforcement, were explored in a study conducted by Zhang et al. (2022). To examine the seismic behavior of the joints, eight full-scale interior connections were tested, evaluating the influence of the combined use of specially detailed reinforcement with SFRCC on cracking patterns, load carrying and energy absorption capacities, and ductility.

The effectiveness of using HPFRCC, enriched with the hybridization of steel microfibers and double hooked-end steel fibers, was proposed by Saghafi et al. (2021). To investigate the efficiency of this approach, four half scale external beam-to-column joints were cast and tested. Specimens comprised a conventional reinforced concrete specimen, serving as the control, which complies with ACI 318-14 requirements, and three HPFRCC specimens with reduced transverse reinforcement in the beam and column plastic hinge regions. Subsequently, this study aims to compare the load vs. displacement and shear stress vs. shear distortion behaviors, load bearing and energy absorption capacities, and cracking patterns for each specimen.

Zhang et al. (2015) put forward the proposal of using Polypropylene Fiber Reinforced Engineered Cementitious Composites (PP-ECC) as a means of

addressing congestion problems in joints within rigid-framed railway bridges. To ascertain the viability of this strategy, cyclic loading tests were conducted on three one-sixth scale beam-to-column connections. The specimens included a control specimen designed in accordance with the structural standards of existing railway bridges in Japan, but lacking transverse reinforcements in the joint, in addition to two more specimens with reduced stirrups in beams and columns.

In the experimental investigation conducted by Jiuru et al. (1992), 12 beam-to-column connections, comprising of five exterior and seven interior joints, made of steel FRCC, were tested. The researchers explored the impacts of the beam and joint reinforcement ratios and the beam development length of the beam longitudinal reinforcement.

Choi & Bae (2019) executed an experimental investigation to investigate the seismic impact of steel fibers on beam-to-column joint subassemblies. In total, seven specimens were tested, four of which are SFRCC. The parameters evaluated in the study were fiber volume fraction, 1% or 2%, the presence of joint stirrups, and the spacing of beam stirrups.

Banu et al. (2023) conducted an investigation to evaluate the behavior of beam-to-column joints reinforced with steel fibers (SFRCC). The specimens were classified into three categories, Type A, B, and C, each with different reinforcement detailing. Type A, a reinforced concrete control specimen, was designed to behave in a ductile manner in accordance with IS 13920-2016 requirements. Type B and C were SFRCC specimens, in which the SFRCC was applied in the joints and the plastic hinge regions of beams and columns. The difference between Type B and C was the spacing of stirrups in the plastic hinge regions of beams and columns.

In an effort to examine the seismic performance of beam-to-column connections, Li et al. (2022) conducted a study that involved five half-scale specimens made of various materials, including conventional reinforced concrete, conventional steel fiber-reinforced cementitious composites (SFRCC), and three types of recycled steel FRCC, each having a varying fiber content within the joint core area.

In their experimental study, Said & Razak (2015) investigated the performance of an exterior beam-to-column connection reinforced with polyvinyl alcohol (PVA) fiber-reinforced cementitious composite, as compared to a conventional reinforced concrete one. The FRCC was applied in the joint, as well as the plastic hinge regions of the beam and column.

Said (2016a) conducted a study examining the seismic behavior of exterior beam-to-column joints under cyclic loading. Two full-scale specimens without transverse reinforcement were tested, one made of conventional reinforced concrete as a control and the other consisting of FRCC incorporating polyethylene fibers. The investigation aimed to evaluate the failure type, cracking pattern, hysteresis behavior, and energy dissipation capacity.

In a comparative study conducted by Said (2017), the seismic behavior of two exterior beam-to-column connection specimens was examined. The first specimen was a regular reinforced concrete specimen designed following ACI 352-02 (ACI 352-02, 2002) requirements, conforming to Type-2 joint definition. Meanwhile, the second specimen was a PVA-FRCC exterior beam-to-column connection, in which both the conventional reinforced concrete and transverse reinforcement in the joint were replaced with Engineered Cementitious Composite containing PVA fibers at a 2.5% volume fraction, as well as the beam and column plastic hinge regions. The study aimed to compare the seismic performance of these two specimens under cyclic loading.

Saghafi & Shariatmadar (2018) conducted an experimental investigation on six half-scale exterior beam-to-column connections to address the joint reinforcement congestion problems in conventional reinforced concrete beam-to-column connections. The researchers employed HPFRCC containing a hybrid combination of a total 2% volume fraction of hooked end steel fibers and macro synthetic fibers. The study aimed to examine the effects of utilizing these fibers on the energy dissipation capacity, load-displacement relationships, and ductility characteristics of the beam-to-column connections.

Nouri et al. (2019) conducted research on the effectiveness of using HPFRCC so as to enhance the behavior of exterior beam-to-column joints under seismic loading. The study involved testing four specimens of regular reinforced concrete connections designed following the requirements of ACI 318-14 Code, as well as three specimens of HPFRCC connections with different stirrup spacings in the beams and columns. No transverse reinforcement was used in the joint for these specimens.

In a study conducted by Saghafi et al. (2019), the feasibility of utilizing HPFRCC to eliminate the need for transverse reinforcement in beam-to-column joints under seismic loading was investigated. The researchers tested four half scale exterior beam-to-column connection specimens, consisting of two reinforced concrete and two HPFRCC specimens, with varying compressive strength values. The HPFRCC specimens had no transverse reinforcement in the joint. The study focused on comparing the mechanical behavior of the reinforced concrete and HPFRCC specimens.

Saghafi et al. (2020) executed an experimental study on four half scale exterior beam-to-column connection specimens, comprising two conventional reinforced concrete specimens, one with and one without seismic detailing, and two HPFRCC specimens. The aim of this research study was to investigate the effect of transverse reinforcement on the seismic behavior of the joint region and the feasibility of utilizing HPFRCC in the joint area.

Gencoglu (2000) conducted experiments on eight steel FRCC exterior beam-to-column connection specimens and two reinforced concrete specimens. The steel FRCC specimens were categorized into two groups. In the first group, five specimens had a single transverse reinforcement in the joint core, whereas the second group had no transverse reinforcement in the joint for the remaining three specimens. It is worth mentioning that a few specimens encountered technical problems during the testing procedure. Hence, not all eight specimens were included in the constructed database for this study.

Zainal et al. (2021) utilized a hybrid FRCC, in which PE and PP synthetic fibers are combined, in six knee joint specimens. These specimens were subjected to lateral cyclic loading to evaluate their performance relative to a reinforced concrete control specimen.

Sarmah et al. (2018b) executed experiments on five 1/3 scale exterior beam-to-column connection specimens, with four of them using FRCC and one using conventional reinforced concrete. Two specimens were made with steel fibers, while the other two were made with basalt fibers, with fiber volume fractions of 1% and 2% for each fiber type. The study aimed to compare the efficiency of basalt fibers with regular reinforced concrete and steel FRCC.

In the study by Yuan et al. (2013), six exterior beam-to-column connections were tested. 2 specimens were reinforced concrete control specimens while the other 4 specimens were made of PVA-HPFRCCs. The authors investigated the parameters such as joint stirrup ratio, column axial load and utilization of HPFRCC in the connection region.

Ismail et al. (2018) investigated the effects of various fiber types on the behavior of beam-to-column joints made of HPFRCC. The fiber types included 8 mm and 12 mm polyvinyl alcohol fibers, 13 mm polypropylene fibers, and 13 mm steel fibers. In addition, a conventional reinforced concrete specimen was included to compare the load deformation characteristics, cracking pattern, ductility, and energy absorption capacity of HPFRCC specimens to that of conventional reinforced concrete.

Liang & Lu (2018) conducted an experimental investigation that involved testing five beam-to-column specimens that featured different flexural strength ratios. Four of these specimens were cast with HPFRCC in the critical zones of the beams, columns, and the joint. Additionally, the study considered the effect of presence of the slab on the behavior of the specimens.

Röhm et al. (2012) executed an experimental investigation on three distinct types of beam-to-column specimens. The first type, labeled as A, was constructed employing conventional reinforced concrete and was designed in accordance with the Indian Standard reference and Eurocode reference, with particular attention paid to the stirrup detailing of the joint. The second type, B, was constructed utilizing fiber reinforced cementitious composite (FRCC) with steel fibers and featured a modified rebar detailing. The third and final type, C, was engineered to exhibit a flexural failure mode.

In their investigation, Chidambaram & Agarwal, (2015) examined the seismic behavior of six exterior beam-to-column connection specimens. The specimens were composed of various composites employing HPFRCC featuring polypropylene FRCC and hybrid FRCC consisting of three fiber types, namely, hooked end steel fiber (HESF), brass coated steel, and polypropylene (PP) fibers.

Liang et al. (2016) conducted an experimental study on 8 interior beam-to-column connection specimens, including 7 PVA FRCC specimens and a conventional reinforced concrete. The authors focused on the impacts of column axial load, joint transverse reinforcement ratio, and flexural strength ratio on the seismic behavior of the joints.

Kheni et al. (2015) undertook an experimental study to investigate the behavior of four beam-to-column connections under cyclic loading. The specimens utilized in the study included: Specimen 1, serving as a control with no fibers; Specimen 2, comprising of 0.5% SF1, 0.5% SF2, and 0.15% PP fibers, combining steel and polypropylene; Specimen 3, consisting of 0.5% SF1, 0.5% SF2, and 0.15% PE fibers, combining steel and polyester; and Specimen 4, incorporating 0.5% SF1 and 0.5% SF2 steel fibers.

Shakya et al. (2012) performed a study to investigate the impact of using steel fiber reinforced concrete (SFRC) in the vicinity of beam-to-column connections. In addition to a reinforced concrete control specimen, three specimens were cast with

reduced steel reinforcement in columns. They examined the effect of using different steel fiber volume fractions on the behavior of these three specimens.

In the study carried out by Niwa et al. (2012) eight 1/6 scale specimens were subjected to testing, four being T-joint specimens and the other four being knee-joint specimens. In addition to the control specimens, FRCC specimens were also tested, incorporating up to 1.5% steel fibers by volume.

AbdelAleem et al. (2020) undertook an experimental study on eight exterior beam-to-column connection specimens, including one control specimen and seven specimens incorporating HPFRCC with 2% volume fraction of PVA fibers. The study investigated the effects of using different supplementary cementitious materials on the mechanical behavior of the connections.

In the study conducted by Bayasi & Gebman (2002), six half-sized exterior beam-to-column connection specimens were tested, where two were reinforced concrete while the other four were made of steel FRCC. The authors aimed to examine the potential of utilizing FRCC with fibers placed in the joint region to reduce the required amount of transverse reinforcement (Gebman, 2001).

In a recent study by Shi et al., (2021), the seismic behavior of beam-to-column joints in steel fiber reinforced concrete (SFRCC) was investigated through a series of experiments involving seven specimens. The influence of multiple variables was examined, including the volume fraction of fibers, compressive strength of the composite, joint transverse reinforcement ratio, and column axial load, on the seismic performance of the connection regions.

Tsonos et al. (2021) executed experiments on seven exterior beam-to-column connection specimens, which were divided into three distinct groups. The first group comprised of three specimens cast with conventional reinforced concrete, design per Eurocode (Eurocode 8, 2004), for medium ductility class. The second group also consisted of three specimens constructed with conventional reinforced concrete, but

with no special consideration given to seismic detailing. The final group had a single specimen made of steel FRCC, with no seismic detailing incorporated.

Filiatrault et al. (1995) conducted an experimental investigation on three 1:1 scale interior beam-to-column connection specimens, as part of their study. The first specimen was constructed using conventional reinforced concrete, without considering any seismic detailing. In contrast, the second specimen, also a control specimen made of conventional reinforced concrete, was designed by considering all seismic detailing requirements of the National Building Code of Canada. Notably, the third specimen was constructed with hooked end steel fibers, despite the absence of any seismic detailing considerations in its design.

In an experimental investigation conducted by Filiatrault et al. (1994), four 1:1 scale exterior beam-to-column connection specimens were subjected to reversed cyclic loading, revealing valuable insights into the seismic behavior of reinforced concrete structures. The first two specimens comprised conventional reinforced concrete, with the first specimen lacking special seismic lateral reinforcement detailing, while the second specimen incorporated seismic detailing. The third and fourth specimens, on the other hand, featured steel fiber reinforced concrete, using hooked end steel fibers, with and without special seismic detailing, respectively.

In a recent experimental investigation, Suryanto et al. (2022) examined the seismic performance of four full-scale exterior beam-to-column connection specimens. The first specimen was constructed with conventional reinforced concrete, while the second and third specimens were built with HPFRCC incorporating PVA fibers at a volume fraction of 2%, but with different joint stirrup ratios. The final specimen was cast using steel fiber-reinforced cementitious composites (SFRCC) with a volume fraction of 1.8%. The study aimed to explore the influence of using different types of fibers and composites on the seismic behavior of exterior beam-to-column connections.

Sano et al. (2015) performed an experimental study on the behavior of two precast interior beam-to-column connection specimens. The first one served as the control

specimen, while the second was an FRCC specimen with a 1% PVA fiber admixture. Subsequently, Yamada et al. (2016) expanded upon this research by testing four additional precast specimens. These specimens, with identical geometries as their predecessors, explored the effects of fiber type and volume fraction of the composite in the joint, employing 1% and 2% volume fractions of steel and PVA fibers to facilitate comparison of their respective mechanical responses. Hanif & Kanakubo (2017) continued this line of research by testing two more specimens, which retained the same geometry and loading pattern as the previous studies. However, 1% volume fraction of Aramid fiber and PP fiber were utilized for these two specimens, respectively. Finally, Mu et al. (2018) tested two more specimens, utilizing PVA fiber. The key difference between these two specimens was the utilization of a vibrator during casting.

In their research study, Gefken & Ramey (1989) tested 10 exterior beam-to-column connection specimens to examine the possibility of replacing the joint transverse reinforcement with steel fibers. To investigate the intricate interaction between the joint stirrup spacing and the steel fiber contribution on the seismic behavior, varying number of joint stirrups are used in their specimens. Their aim was assessing the potential of steel fiber use in reducing the need for transverse reinforcement and, consequently, simplifying the construction process.

Chidambaram & Agarwal (2018) carried out an experimental study on three distinctive groups of beam-to-column connection specimens. The initial group, referred to as Type 1, consisted of two ordinary reinforced concrete specimens. The subsequent group, designated as Type 2, comprised of five FRCC specimens, while the last group, referred to as Type 3, consisted of three specimens of hybrid FRCC. Despite the fact that all specimens featured identical rebar configurations, each specimen was designed and formulated to serve a specific purpose. The Type 1 specimens were compared based on their confinement levels, while the Type 2 specimens were differentiated based on fiber type (Crimpled Steel Fiber and Hooked-End Steel Fiber) and volume fraction (1% and 2%). Lastly, the final group of specimens had varying amounts of PP fibers and macro synthetic fibers, providing

a more nuanced perspective on the impact of different fiber types and volume fractions on the behavior of beam-to-column connections.

In a series of experiments, Hosseini et al. (2018) investigated the behavior of eight beam-to-column connection specimens, comprising four corner and four exterior connections. Their study accounted for transverse beams and involved bidirectional loading, as well as torsional forces on some specimens. Furthermore, the impact of inclusion and exclusion of joint transverse reinforcement was explored.

In their study, Marthong & Marthong (2016) examined the effect of incorporating PET fibers on the seismic performance of exterior beam-to-column connections. Their experimental program involved three 1/3-scale specimens with distinct failure modes, namely beam flexural failure, beam shear failure, and column shear failure. Furthermore, the consequences of completely eliminating stirrups in the plastic hinge regions of both beams and columns were investigated.

Muthuswamy & Thirugnanam (2014) carried out an experimental study on exterior beam-to-column connection specimens, consisting of three specimens including a control, a steel fiber reinforced cementitious composite (SFRCC), and a hybrid FRCC specimen. The hybrid FRCC specimen was cast with both glass and steel fibers. A comparative analysis of the mechanical performance of these specimens was conducted, evaluating their energy dissipation capacity, hysteresis behavior, and ductility.

In their study, Rajkumar et al. (2021) conducted tests on six exterior beam-to-column connection specimens to explore the effect of utilizing a hybrid Fiber Reinforced Cementitious Composite (FRCC) consisting of polypropylene (PP) and crimped steel fibers. Both types of fibers were used at identical volume fractions for each specimen, ranging from 0% to 2.5% at 0.5% intervals, to examine the influence of different combinations of fiber volume fractions. The authors investigated the impact of varying volume fractions, ranging from 0% to 5%, in the tested specimens.

In a recent study, Pekgokgoz & Avcil (2022) investigated the behavior of six beam-to-column connection specimens, consisting of three conventional reinforced concrete specimens and three fiber reinforced self-compacting concrete specimens. The study aimed to investigate the improvement in behavior due to the use of different fiber volume fractions, ranging from 0.5% to 1%, compared with conventional reinforced concrete. Notably, no joint transverse reinforcement was used in any specimen.

Patel et al. (2013) conducted a study to investigate the possibility of utilizing steel FRCC for improving the ductility of exterior beam-to-column connections. Six specimens were tested, some of which incorporated 1.5% volume fraction of steel fibers. Furthermore, the study took into account both ductile and non-ductile connection designs as variables.

Liu (2006) examined seven exterior beam-to-column connection specimens, which demonstrated substantial variations in terms of the investigated parameters, which include the effect of using steel FRCC in the connection region, varying stirrup spacing in the beam plastic hinge region, incorporating fibrous concrete in the column plastic hinge region, and reducing the spacing of stirrups in the column plastic hinge region.

Said (2016b) undertook an experimental study, in which 14 full scale exterior beam-to-column connection specimens were tested. The specimens included control specimens of reinforced concrete, as well as FRCC specimens with PVA and PE fibers. Primary research parameters were the fiber type and reinforcing index of the fibers. The research outcomes included the comparison of joint shear strength among the fibrous and non-fibrous concrete specimens, as well as among different fiber types.

3.5 Resulting Database

A comprehensive database has been assembled from 57 distinct experimental studies, featuring a total of 212 specimens. Table 3.3 presents key information on the specimens integrated into the database, encompassing the authors, specimens, beam and column dimensions, joint type, compressive strength of the composite placed in the joint, fiber type and reinforcing index and the presence or absence of joint transverse reinforcement.

Table 3.3 Overall Database Including All Failure Modes

Specimen General Information					Fibers		Member Dimensions mm				Joint Stirrup
Researcher	**Specimen**	**Type**	**Failure Mode**	**f_c' MPa**	**Type**	**Vf %**	**h_b**	**b_b**	**h_c**	**b_c**	
Qudah & Maalej	S2	I0	B	57.0	PE	2.00	200	150	185	185	+
	S3	I0	B	60.0	PE	2.00	200	150	185	185	+
	S4	I0	B	60.0	PE	2.00	200	150	185	185	+
	S5	I0	B	57.0	PE	2.00	200	150	185	185	-
	S6	I0	B	69.0	PE	2.00	200	150	185	185	-
	S7	I0	B	69.0	PE	2.00	200	150	185	185	-
	S8	I0	B	71.0	PE	2.00	200	150	185	185	-
	S9	I0	B	71.0	PE	2.00	200	150	185	185	-
Han & Lee	HC-JO-U	E1	BJ	33.9	PVA	2.12	500	250	330	330	+
	HC-JX-U	E1	BJ	33.9	PVA	2.12	500	250	330	330	-
	HC-JO-B	E1	BJ	33.9	PVA	2.12	500	250	330	330	+
	HC-JX-B	E1	BJ	33.9	PVA	2.12	500	250	330	330	-
Wang et al.	EJ-1	E0	B	85.4	SF	1.30	250	150	200	200	-
	EJ-2	E0	J	96.7	SF	1.30	250	150	200	200	+
	EJ-3	E0	J	91.6	SF	1.30	250	150	200	200	+
	EJ-4	E0	BJ	83.6	SF	1.30	250	150	200	200	-
	EJ-5	E0	J	90.8	SF	1.30	250	150	200	200	+
	J-1	I0	J	104.4	SF	1.30	250	150	200	200	-
	J-2	I0	J	96.8	SF	1.30	250	150	200	200	-
	J-3	I0	J	98.4	SF	1.30	250	150	200	200	+
	J-4	I0	J	91.6	SF	1.30	250	150	200	200	+
Zhang et al.	IS1	I0	BJ	53.3	HESF	1.20	400	250	350	350	+
	IS2	I0	BJ	53.3	HESF	1.20	400	250	350	350	+
Saghafi et al.	BCJ2-HPC	E0	IJ	54.0	Hybrid	2.00	250	220	250	250	-
	BCJ3-HPC	E0	IJ	54.0	Hybrid	2.00	250	220	250	250	-
	BCJ4-HPC	E0	IJ	54.0	Hybrid	2.00	250	220	250	250	-
Zhang et al.	TJ-1	E0	I	48.2	PP	3.00	200	170	250	250	-
	TJ-2	E0	I	33.6	PP	3.00	200	170	250	250	-
	TJ-3	E0	B	33.6	PP	3.00	200	170	250	250	-

Table 3.3 (Cont'd)

Specimen General Information					Fibers		Member Dimensions mm				Joint Stirrup
Researcher	**Specimen**	**Type**	**Failure Mode**	**f_c' MPa**	**Type**	**Vf %**	**h_b**	**b_b**	**h_c**	**b_c**	
Jiuru et al.	SF1	E0	J	19.8	SF	1.20	350	200	350	250	-
	SF2	E0	BJ	29.9	SF	1.50	350	200	350	250	+
	SF3	E0	B	29.9	SF	1.50	350	200	350	250	+
	SF5	E0	B	19.8	SF	1.50	350	200	350	250	-
	SF6	I0	J	16.9	SF	1.50	350	200	350	250	-
	SF7	I0	J	16.9	SF	1.50	350	200	350	250	+
	SF8	I0	J	35.2	SF	1.50	350	200	350	250	+
	SF9	I0	BJ	16.9	SF	1.50	350	200	350	250	-
Saghafi & Shariatmadar	J1-C1-HPFRCC	E0	BI	41.5	Hybrid	2.00	250	220	250	250	+
	J1-C2-HPFRCC	E0	B	41.5	Hybrid	2.00	250	220	250	250	+
	J2-C1-HPFRCC	E0	IJ	41.5	Hybrid	2.00	250	220	250	250	-
	J2-C2-HPFRCC	E0	BI	41.5	Hybrid	2.00	250	220	250	250	-
Nouri et al.	SJ2-HPC	E0	BI	49.6	HESF	2.00	250	220	250	250	-
	SJ3-HPC	E0	BI	49.6	HESF	2.00	250	220	250	250	-
	SJ4-HPC	E0	B	49.6	HESF	2.00	250	220	250	250	-
Parra-Montesinos et al.	1	I0	BJ	39.3	PE	1.50	350	150	350	350	-
	2	I0	BJ	42.7	PE	1.50	350	150	350	350	-
Saghafi et al.	SC2-A	E0	B	41.5	Hybrid	2.00	250	220	250	250	-
	SC2-B	E0	IJ	50.6	HESF	2.00	250	220	250	250	-
Saghafi et al.	J2HP1	E0	BI	49.9	HESF	2.00	250	220	250	250	-
	J2HP2	E0	BI	49.9	HESF	2.00	250	220	250	250	-
Sarmah et al.	SF1	E0	J	20.2	HESF	1.00	150	120	150	120	+
	SF2	E0	J	20.2	HESF	2.00	150	120	150	120	+
	BF1	E0	J	20.2	Basalt	1.00	150	120	150	120	+
Yuan et al.	S3	E0	BJ	39.7	PVA	2.00	400	200	350	250	-
	S4	E0	BI	39.7	PVA	2.00	400	200	350	250	+
	S5	E0	B	39.7	PVA	2.00	400	200	350	250	+
	S6	E0	B	39.7	PVA	2.00	400	200	350	250	+

Table 3.3 (Cont'd)

Specimen General Information					Fibers		Member Dimensions mm				Joint Stirrup
Researcher	**Specimen**	**Type**	**Failure Mode**	**f_c' MPa**	**Type**	**Vf %**	**h_b**	**b_b**	**h_c**	**b_c**	
Ismail et al.	ECC-PVA8	E0	I	49.0	PVA	2.00	250	250	250	250	+
	ECC-PVA12	E0	BI	48.0	PVA	2.00	250	250	250	250	+
	ECC-PP13	E0	BI	46.0	PP	2.00	250	250	250	250	+
	ECC-SF13	E0	I	52.0	SF	2.00	250	250	250	250	+
Liang & Lu	ECCBCS-1	I2	CJ	33.9	PVA	2.00	300	150	250	250	+
	ECCBCS-2	I2	BJ	33.9	PVA	2.00	300	150	250	250	+
	ECCBCS-3	I2	BJ	33.9	PVA	2.00	300	150	250	250	+
	ECCBCS-4	I2	BJ	33.9	PVA	2.00	300	150	250	250	+
Röhm et al.	SP-6a	E0	J	38.7	HESF	1.00	400	300	300	300	+
	SP-6a-2	E0	CJ	50.5	Hybrid	1.50	400	300	300	300	+
	SP-6-3	E0	J	72.0	Hybrid	1.50	400	300	300	300	-
Chidambaram & Agarwal	SJ3	E0	BJ	35.0	HESF	2.00	150	130	150	150	+
	SJ5	E0	BJ	39.0	Hybrid	3.50	150	130	150	150	+
	SJ6	E0	BJ	33.0	Hybrid	3.50	150	130	150	150	+
Liang et al.	FRCJ1	I0	BJ	45.3	PVA	2.00	300	150	250	250	+
	FRCJ2	I0	CJ	45.3	PVA	2.00	300	150	250	250	+
	FRCJ3	I0	CJ	45.3	PVA	2.00	300	150	250	250	+
	FRCJ4	I0	BJ	45.3	PVA	2.00	300	150	250	250	+
	FRCJ5	I0	BJ	45.3	PVA	2.00	300	150	250	250	+
	FRCJ6	I0	BJ	45.3	PVA	2.00	300	150	250	250	+
	FRCJ7	I0	BJ	45.3	PVA	2.00	300	150	250	250	+
Kheni et al.	2	E0	BJ	24.8	Hybrid	1.15	240	200	200	200	+
	3	E0	BJ	27.0	Hybrid	1.15	240	200	200	200	+
	4	E0	BJ	27.3	Hybrid	1.00	240	200	200	200	+
Shakya et al.	BCJ-1.0	E0	B	23.3	HESF	1.00	200	168	250	250	+
	BCJ-1.5	E0	B	30.0	HESF	1.50	200	168	250	250	+
Niwa et al.	KJ-1.0	RE0	C	28.9	HESF	1.00	330	250	250	250	+
	KJ-1.5	RE0	C	30.1	HESF	1.50	330	250	250	250	+

Table 3.3 (Cont'd)

Specimen General Information					Fibers		Member Dimensions mm				Joint Stirrup
Researcher	**Specimen**	**Type**	**Failure Mode**	**f_c' MPa**	**Type**	**Vf %**	**h_b**	**b_b**	**h_c**	**b_c**	
AbdelAleem et al.	ECC-FA	E0	I	49.0	PVA	2.00	250	250	250	250	+
	ECC-FA-5CR	E0	BI	45.6	PVA	2.00	250	250	250	250	+
	ECC-FA-10CR	E0	I	39.7	PVA	2.00	250	250	250	250	+
	ECC-FA-15CR	E0	BI	35.2	PVA	2.00	250	250	250	250	+
	ECC-MK	E0	BI	63.3	PVA	2.00	250	250	250	250	+
	ECC-SLF	E0	BI	54.8	PVA	2.00	250	250	250	250	+
	ECC-FA-NS	E0	BI	48.5	PVA	2.00	250	250	250	250	+
Bayasi & Gebman	Joint #1	E0	BJ	22.3	HESF	2.00	305	254	254	254	+
	Joint #2	E0	BJ	22.3	HESF	2.00	305	254	254	254	+
	Joint #4	E0	BJ	22.3	HESF	2.00	305	254	254	254	+
	Joint #5	E0	BJ	22.3	HESF	2.00	305	254	254	254	+
Shi et al.	BCJ1	I0	BJ	74.5	HESF	1.00	250	150	200	200	+
	BCJ2	I0	BJ	76.4	HESF	0.50	250	150	200	200	+
	BCJ3	I0	BJ	83.2	HESF	1.00	250	150	200	200	+
	BCJ4	I0	BJ	73.6	HESF	1.00	250	150	200	200	-
	BCJ5	I0	BJ	76.0	HESF	1.00	250	150	200	200	-
	BCJ6	I0	BJ	72.6	HESF	1.00	250	150	200	200	-
Tsonos et al.	SFJ1	E0	BJ	20.0	SF	1.50	300	200	200	200	+
Filiatrault et al.	S3	I0	J	46.0	HESF	1.60	500	400	400	400	+
	S3	E0	BJ	45.0	HESF	1.00	450	350	350	350	-
	S4	E0	BJ	43.0	HESF	1.60	450	350	350	350	-
Sachdeva et al.	HS_2	E0	BJ	28.2	HESF	1.00	200	150	200	150	+
	HS_3	E0	BJ	28.9	HESF	1.50	200	150	200	150	+
	HS_5	E0	BJ	46.7	HESF	1.00	200	150	200	150	+
	HS_6	E0	BJ	47.2	HESF	1.50	200	150	200	150	+
Suryanto et al.	ECC-050d	E0	I	24.8	PVA	2.00	200	200	200	200	+
	ECC-075d	E0	BI	29.4	PVA	2.00	200	200	200	200	+
	SFRC-075d	E0	I	35.2	HESF	1.80	200	200	200	200	+

Table 3.3 (Cont'd)

Specimen General Information					Fibers		Member Dimensions mm				Joint Stirrup
Researcher	**Specimen**	**Type**	**Failure Mode**	**f_c' MPa**	**Type**	**Vf %**	**h_b**	**b_b**	**h_c**	**b_c**	
Sano et al.	No. 25	I0	CJ	52.5	PVA	1.00	420	380	500	500	-
Yamada et al.	No. 26	I0	CJ	52.9	PVA	1.00	420	380	500	500	+
	No. 27	I0	CJ	50.0	PVA	2.00	420	380	500	500	-
	No. 28	I0	J	56.8	SF	1.00	420	380	500	500	-
	No. 29	I0	J	59.2	SF	2.00	420	380	500	500	-
Hanif & Kanakubo	No. 30	I0	J	51.3	Aramid	1.00	420	380	500	500	-
	No. 31	I0	J	51.5	PP	1.00	420	380	500	500	-
Mu et al.	No. 32	I0	J	49.1	PVA	1.00	420	380	500	500	-
	No. 33	I0	CJ	48.0	PVA	1.00	420	380	500	500	-
Gefken & Ramey	JB1	E0	J	18.8	SF	2.00	254	203	305	203	+
	JC1	E0	J	18.8	SF	2.00	254	203	305	203	+
	JD1	E0	J	32.7	SF	2.00	254	203	305	203	+
	JE1	E0	J	32.7	SF	2.00	254	203	305	203	-
Chidambaram & Agarwal	HYJ 3	E0	I	50.6	SF	1.00	225	150	225	150	+
	HYJ 4	E0	I	48.0	SF	2.00	225	150	225	150	+
	HYJ 5	E0	BI	48.1	HESF	1.00	225	150	225	150	+
	HYJ 6	E0	I	54.3	HESF	2.00	225	150	225	150	+
	HYJ 7	E0	I	35.8	PP	1.00	225	150	225	150	+
	HYJ 8	E0	I	35.8	Hybrid	1.50	225	150	225	150	+
	HYJ 9	E0	BI	42.2	Hybrid	1.50	225	150	225	150	+
	HYJ 10	E0	I	51.6	Hybrid	1.50	225	150	225	150	+
Gencoglu	3	E0	BJ	25.0	HESF	1.00	600	250	400	250	-
	5	E0	BJ	26.2	HESF	1.00	600	250	400	250	+
	6	E0	BJ	32.0	HESF	1.00	600	250	400	250	+
	8	E0	BJ	32.0	HESF	1.00	600	250	400	250	+
	9	E0	BJ	22.0	HESF	3.00	600	250	400	250	-
	10	E0	BJ	22.0	HESF	1.00	600	250	400	250	+
Van & Trung	S2	E0	BJ	107.0	SF	2.00	450	350	350	350	-
	S3	E0	BJ	107.0	SF	2.00	450	350	350	350	-

Table 3.3 (Cont'd)

Specimen General Information					Fibers		Member Dimensions mm				Joint Stirrup
Researcher	**Specimen**	**Type**	**Failure Mode**	**f_c' MPa**	**Type**	**Vf %**	**h_b**	**b_b**	**h_c**	**b_c**	
Zainal et al.	FFC	RE0	C	31.6	Hybrid	1.20	400	280	400	400	+
	F6U3	RE0	I	27.0	Hybrid	1.50	400	280	400	400	+
	F6S3	RE0	I	23.9	Hybrid	1.50	400	280	400	400	+
	F6E3	RE0	I	26.9	Hybrid	1.50	400	280	400	400	+
	F6N3	RE0	I	25.6	Hybrid	1.50	400	280	400	400	+
Hosseini et al.	C/RECC/ABB/RS	E1	BJ	17.4	PVA	2.00	203	203	203	203	+
	C/RECC/ABB/NS	E1	B	29.9	PVA	2.00	203	203	203	203	-
	E/RECC/ABB/RS	I1	BJ	36.8	PVA	2.00	203	203	203	203	+
	E/RECC/ABB/NS	I1	B	49.7	PVA	2.00	203	203	203	203	-
Marthong & Marthong	BWFSF	E0	BJ	30.0	PET	0.87	120	100	100	100	+
	BWSSF	E0	BJ	30.0	PET	0.87	120	100	100	100	+
	CWSSF	E0	J	30.0	PET	0.87	150	80	100	80	+
Muthuswamy & Thirugnanam	SRFC	E0	I	36.2	SF	1.00	170	120	230	120	+
	HFRC	E0	I	36.2	Hybrid	1.03	170	120	230	120	+
Rajkumar et al.	1% HSHFRC	E0	I	64.7	Hybrid	1.00	200	150	200	150	+
	2% HSHFRC	E0	I	66.0	Hybrid	2.00	200	150	200	150	+
	3% HSHFRC	E0	I	67.1	Hybrid	3.00	200	150	200	150	+
	4% HSHFRC	E0	I	56.6	Hybrid	4.00	200	150	200	150	+
	5% HSHFRC	E0	I	50.1	Hybrid	5.00	200	150	200	150	+
Pekgokgoz & Avcil	NC0.5	E0	I	37.2	SF	0.50	300	300	400	300	-
	NC1	E0	I	37.2	SF	1.00	300	300	400	300	-
	SCC0.5	E0	I	37.2	SF	0.50	300	300	400	300	-
	SSC1	E0	I	37.2	SF	1.00	300	300	400	300	-
Tingting et al.	F-1	I0	BJ	38.3	PVA	2.00	300	150	250	250	+
	F-2	I0	BJ	38.3	PVA	2.00	300	150	250	250	+
	F-3	I0	BJ	38.3	PVA	2.00	300	150	250	250	+
	F-4	I0	BJ	38.3	PVA	2.00	300	150	250	250	+
	F-5	I0	BJ	38.3	PVA	2.00	300	150	250	250	+
	F-6	I0	BJ	38.3	PVA	2.00	300	150	250	250	+
Patel et al.	NDS2	E0	J	34.9	HESF	1.50	200	125	200	200	+
	DS1S2	E0	BI	34.9	HESF	1.50	200	125	200	200	+
	DS2S2	E0	BI	34.9	HESF	1.50	200	125	200	200	+
	DS3S2	E0	BJ	34.9	HESF	1.50	200	125	200	200	+

Table 3.3 (Cont'd)

Specimen General Information					Fibers		Member Dimensions mm				Joint Stirrup
Researcher	Specimen	Type	Failure Mode	f_c' MPa	Type	Vf %	h_b	b_b	h_c	b_c	
Gao et al.	JDZ0.3-0.5-0.6	I0	J	76.4	SF	0.50	250	150	200	200	+
	JDZ0.3-1.0-0	I0	J	76.0	SF	1.00	250	150	200	200	-
	JDZ0.2-1.0-0	I0	J	73.6	SF	1.00	250	150	200	200	-
	JDZ0.4-1.0-0	I0	J	72.6	SF	1.00	250	150	200	200	-
Kang et al.	R-HPFRC	RE0	B	100.3	HESF	1.00	560	400	500	750	+
	E-HPFRC	E0	B	102.8	HESF	1.00	650	400	500	500	+
Lu & Liang	BC-2	I2	CJ	36.1	PVA	2.00	300	150	250	250	+
	BC-3	I2	BJ	36.1	PVA	2.00	300	150	250	250	+
Choi & Bae	JNR-1-BTR	E0	BJ	54.1	HESF	1.00	375	250	300	300	-
	JNR-2-BTR	E0	BJ	54.7	HESF	2.00	375	250	300	300	-
	JTR-1-BNR	E0	BJ	54.1	HESF	1.00	375	250	300	300	+
	JTR-2-BNR	E0	BJ	54.7	HESF	2.00	375	250	300	300	+
Banu et al.	Type B	E0	J	39.9	HESF	1.50	150	100	100	200	+
	Type C	E0	J	39.9	HESF	1.50	150	100	100	200	+
Li et al.	SJ-2	I0	BJ	42.2	SF	0.50	400	250	300	300	+
	SJ-3	I0	BJ	43.2	SF	1.00	400	250	300	300	+
	SJ-4	I0	CJ	45.4	SF	1.50	400	250	300	300	+
	SJ-5	I0	CJ	40.6	SF	0.50	400	250	300	300	+
Said & Razak	ECC	E0	BJ	60.2	PVA	2.00	250	170	250	170	-
Said	ECC	E0	BJ	64.6	PE	1.50	250	170	250	170	-
Said	ECC	E0	BJ	57.4	PVA	2.50	250	170	250	170	-
Liu	SF-2	E0	CJ	23.2	HESF	1.00	330	200	230	230	-
	SF-3	E0	J	28.1	HESF	2.00	330	200	230	230	-
	SF-4	E0	CJ	27.5	HESF	1.00	330	250	250	250	+
	SF-5	E0	BJ	28.1	HESF	1.00	330	250	250	250	+

Table 3.3 (Cont'd)

Specimen General Information					Fibers		Member Dimensions mm				Joint Stirrup
Researcher	Specimen	Type	Failure Mode	f_c' MPa	Type	Vf %	h_b	b_b	h_c	b_c	
Said	PVA_1	E0	BJ	61.1	PVA	2.50	250	170	250	170	-
	PE_4	E0	BJ	61.3	PE	2.00	250	170	250	170	-
	PE_5	E0	BJ	62.7	PE	2.00	250	170	250	170	+
	PE_6	E0	BJ	58.8	PE	2.00	250	170	250	170	+
	PVA_2	E0	BJ	60.2	PVA	2.00	250	170	250	170	-
	PVA_3	E0	BJ	57.4	PVA	2.50	250	170	250	170	-
	PVA_4	E0	BJ	55.6	PVA	3.00	250	170	250	170	-
	PVA_5	E0	BJ	58.2	PVA	2.00	250	170	250	170	+
	PVA_6	E0	BJ	62.0	PVA	2.00	250	170	250	170	+
	PE_1	E0	BJ	64.6	PE	1.50	250	170	250	170	-
	PE_2	E0	BJ	63.9	PE	2.00	250	170	250	170	-
	PE_3	E0	BJ	60.7	PE	2.50	250	170	250	170	-

Furthermore, Table 3.4 shows the key parameters of the conducted tests along with the corresponding number of specimens that adhere to each parameter.

Table 3.4 Classification of the specimens in the overall database

Specimen Properties	**Interior**	**Exterior**	**Total**
Have axial load on column	48	106	154
No axial load on column	17	41	58
Have transverse beams	8	6	14
No transverse beams	57	141	198
Have slab	10	4	14
No slab	55	143	198
Have joint stirrups	39	97	136
No joint stirrups	26	50	76
Joint shear failure	51	66	117
Other failure modes	14	81	95
TOTAL	**65**	**147**	**212**

An intriguing point is that the overall database is comprised of a significantly higher number of exterior connection specimens when compared to interior connection specimens, which may be attributed to two fundamental reasons. Firstly, the seismic behavior of exterior connections is of greater concern from structural engineering point of view. Unlike interior conn exterior connections have a lower degree of confinement provided by the adjoining beams. As a result, the shear carrying capacity of an exterior joint that has the same reinforcement detailing as an interior one is lower, causing more vulnerability to seismic loading. Consequently, researchers devote significant attention to the examination of exterior connections, aiming to gain deeper insight into their behavior and devise efficient design approaches that can optimize their seismic performance.

Secondly, conducting tests on exterior connections is more practical and requires less effort as well as lower capacity actuators when compared to interior connections. The accessibility and simplicity of instrumenting exterior joints make them more feasible for experimental investigations. This ease of testing contributes to a larger number of experiments being conducted on exterior connections, providing a more comprehensive understanding of their behavior.

A notable finding from Table 3.4 reveals that there is a considerably low number of specimens that include slab and transverse beams in the literature. This can be attributed to the complexity of testing these subassemblies due to the need for enhanced laboratory conditions and more robust machinery. Therefore, most specimens in the study did not include these structural members. As a result, the influence of transverse beams and slab on the behavior of beam-to-column connections was not extensively accounted for in the collected specimens.

CHAPTER 4

SHEAR STRENGTH PREDICTION

4.1 Overview

The strength and integrity of beam-to-column connections under significant horizontal shear forces is of paramount importance. Therefore, it is crucial to conduct a comprehensive analysis of their capacity to withstand such forces. This chapter is dedicated to the development of an innovative prediction equation specifically designed to estimate the joint shear strength of Fiber Reinforced Cementitious Composite (FRCC) beam-to-column connections. The chapter provides a comprehensive interpretation of joint shear strength, drawing upon relevant scholarly investigations, identifying key research gaps, and outlining the primary objective of the current study.

4.1.1 Aim of the Study

The primary aim of this investigation is to develop an inclusive and reliable prediction equation that accurately estimates the shear strength of beam-to-column joints constructed using FRCCs. Emphasizing the importance of accuracy and practical implementation, the equation is designed to provide engineers and designers with a dependable tool for optimizing structural design. Furthermore, this study distinguishes itself by its aim of encompassing all possible fiber types in the proposed shear strength prediction equation.

4.1.2 Existing Prediction Equations

Jiuru et al. (1992) stated that the overall shear capacity of the joint is a result of the combined effects of the composite, fibers, and stirrups, emphasizing their respective contributions to the overall strength. The authors provide Equation **(4.1)** to determine the overall shear carrying capacity.

$$V_j = 0.1(1+n)f_c b_j h_j + 2\frac{L_f}{D_f}V_f b_j h_j + f_y\frac{A_{sv}}{s}(h_0 - a'_s) \quad \textbf{(4.1)}$$

In Equation **(4.1)**, the term n represents the axial load ratio on the column, which is obtained as $N/f_c b_c h_c$, where the term N stands for the axial force applied to the column. The effective joint width, denoted as 'b_j', was adopted from the GBJ 10-89 (GBJ 10-89, 1989) Code.

In their work, Tingting et al. (2022) introduced Equation **(4.2)** as a mathematical expression aimed at estimating the shear strength of PVA-HPFRCC beam-to-column joints.

$$v_j\ (\text{MPa}) = (\text{TB})^{1.103}.\left(\frac{A_{sh,pro}}{A_{sh,req}}\right)^{0.159}.\left(\frac{S_{pro}}{S_{req}}\right)^{0.346}.\left(\frac{b_b}{b_c}\right)^{0.501}.\left(\frac{h_b}{h_c}\right)^{0.348}.(\varepsilon_t)^{0.011}.(\text{CI})^{0.04}.(\text{BI})^{0.662}.(\text{JI})^{0.115}.(f_c)^{0.947} \quad \textbf{(4.2)}$$

According to the authors, TB is a geometric parameter that takes into account the confinement effect of slab and transverse beams, while ε_t is tensile strain capacity of the composite. A_{sh} is the parameter reflecting the effect of joint stirrups and S denotes the joint stirrup spacing. The terms b_b, h_b, b_c, h_c stand for beam width, beam depth, column width and column depth, respectively. The subscripts "pro" and "req" indicate whether the values are provided in the specimen or required by the design codes. Furthermore, the terms CI and BI represent the column and beam reinforcing indices, respectively. CI is obtained by Equation **(4.3)**, while beam index is given in Equation **(4.4)**. Finally, the term JI stands for the joint stirrup index and is defined by Equation **(4.5)**.

$$CI = \frac{\rho_c f_{yc}}{f_c} \quad \textbf{(4.3)}$$

$$BI = \frac{\rho_b f_{yb}}{f_c} \quad \textbf{(4.4)}$$

$$JI = \frac{\rho_j f_{yj}}{f_c} \quad \textbf{(4.5)}$$

In Equations **(4.3), (4.4)** and **(4.5)**, the term ρ stands for the reinforcement ratio, while f_y is the yield strength of the corresponding reinforcement and f_c stands for the compressive strength of the composite.

Wang et al. (2018) examined the joint shear capacity of an FRCC joint by dividing it into three components: the contribution from the composite, the fibers, and the stirrups. They put forth an equation, denoted as Equation **(4.6)**, which expresses this relationship.

$$V_j = V_c + V_f + V_{sv} \quad \textbf{(4.6)}$$

Equation **(4.6)** introduces the variables V_c, V_f, and V_{sv}, representing the concrete contribution, fiber contribution, and stirrup contribution, respectively. Firstly, the concrete contribution, denoted by V_c, is given in Equation **(4.7)**.

$$V_c = 3.35\sqrt{f_c'}A_{str}\cos\left(\operatorname{atan}\left(\frac{h_b''}{h_c''}\right)\right) \quad \textbf{(4.7)}$$

In this equation, h_b'' and h_c'' represent the distance between the centerlines of outermost compression and outermost tension steel rebars for beams and columns, respectively. Furthermore, f_c' represents the compressive strength of the composite, and A_{str} denotes the effective diagonal strut area. A_{str} is obtained by using Equation **(4.8)**.

$$A_{str} = b_s \,.\, a_s \quad \textbf{(4.8)}$$

As proposed by the authors, the symbol b_s represents the width of the diagonal strut. It is suggested to be set equal to the joint width, b_j, which can be determined using Equation **(4.9)**.

$$b_s \approx b_j = \min\left(\frac{b_b + b_c}{2}; b_b + 0.5h_c; b_c\right) \quad \textbf{(4.9)}$$

Moreover, the term 'a_s' in Equation **(4.8)** is determined by employing Equation **(4.10)**.

$$a_s = \sqrt{a_b^2 + a_c^2} \quad \textbf{(4.10)}$$

The computation of a_s in Equation **(4.10)** necessitates the incorporation of two essential parameters, namely a_b and a_c, which correspond to the beam strut height and column strut height, respectively. According to the authors, in the event that a prominent bending plastic hinge emerges and significant FRCC spalling occurs, the value of a_b is stipulated as zero. Conversely, in cases where these conditions are not observed, a_b may be taken as approximately $h_b/5$. The term a_c, on the other hand, is obtained by using Equation **(4.11)**.

$$a_c = (0.25 + 0.85N/f_c'b_ch_c)h_c \quad \textbf{(4.11)}$$

Secondly, the authors proposed an equation to determine the contribution of fibers to the joint shear strength, as presented in Equation **(4.12)**.

$$V_f = \left(16.447 - 14.30\lambda_f^{0.061}\right)\lambda_f h_b b_c \quad \textbf{(4.12)}$$

In this equation, λ_f is the reinforcing index, which is obtained by the multiplication of fiber volume fraction and aspect ratio.

Lastly, the authors provide an equation to quantify the contribution of stirrups to the overall joint shear strength, as depicted in Equation **(4.13)**.

$$V_{sv} = \psi f_{yv} A_{sv} \frac{h_0 - a_s'}{s} \quad \textbf{(4.13)}$$

In this equation, the yield strength of the stirrups is denoted by f_{yv}, while the total cross-sectional area of the stirrups is A_{sv}. The effective depth of the beam reveals itself as h_0, and the stirrup spacing is expressed as s. Moreover, the distance from the compression rebars' axis to the outermost fiber of the beam is designated as a_s'. Lastly, the coefficient ψ, a coefficient standing for stirrup non-uniformity, is included in the equation, varying between the value of 0.85 and 1.00 based on the stirrup characteristic value, which is defined as $\rho_{sv} f_{yv} / f_c'$.

Gao et al. (2014) employed a similar approach in their investigation to determine the ultimate shear carrying capacity of steel FRCC beam-to-column joints and came up with Equation **(4.14)**.

$$V_j = \gamma \left[0.1(1 + 0.38n) \left(1 + 1.08 V_f \frac{L_f}{D_f} \right) f_c b_j h_j + 0.96 f_y \frac{A_{sv}}{s} (h_0 - a_s') \right] \quad \textbf{(4.14)}$$

Li et al. (2022) directed their attention towards predicting the shear strength of recycled steel FRCC beam-to-column joints. In their study, they derived Equation **(4.15)** to estimate the shear strength.

$$V_j = 0.4 f_c k b_s h_c + \frac{2}{3} f_{yv} \frac{A_{sv}}{S} (h_0 - a_s') + \mu \eta_b \lambda_f (1 + 1.177 \lambda_f) b_j h_j \quad \textbf{(4.15)}$$

In Equation **(4.15)**, λ_f corresponds to the reinforcing index of fibers, while the definition of effective joint width is adopted based on the approach outlined in ACI 352-02 (ACI 352-02, 2002) Code. η_b is a coefficient for representing the interfacial bond. μ is computed as the product of η_b and α_1, which is assigned a value of 0.41 for the recycled steel fibers. Lastly, the coefficient k is determined utilizing Equation **(4.16)**.

$$k = 0.168(1 + 0.263n)(1 + 0.492\lambda_f)(1 + 6.054\lambda_s) \quad \textbf{(4.16)}$$

In Equation **(4.16)**, the parameter λ_s is assigned a value 0.08, representing a characteristic value for stirrups.

Zhang et al. (2022) introduced an iterative methodology aimed at determining the shear strength of beam-to-column joints constructed using steel Fiber Reinforced Concrete (SFRCC). In their study, the researchers employed a modified compression filed theory to derive a comprehensive flowchart for the calculation of joint shear strength. This flowchart, given as Figure 4.1, outlines the step-by-step process involved in determining the shear strength of these joints, providing a systematic approach for prediction.

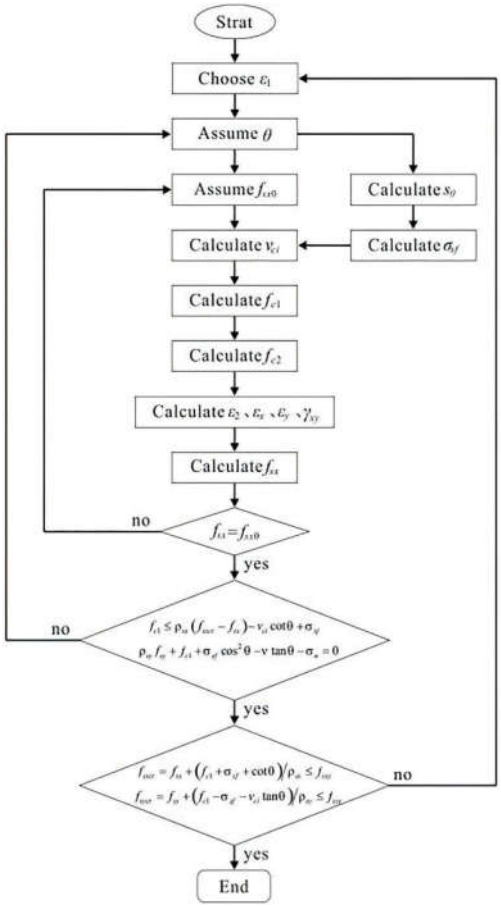

Figure 4.1. Determination of shear strength for steel FRCC beam-to-column joints. (Zhang et al., 2022).

4.1.3 Literature Gap

The available literature on shear strength prediction equations for FRCC beam-to-column joints is notably limited, exacerbated by the scarcity of tests conducted on such joints. Furthermore, the existing equations are specific to certain fiber types employed in the joints, mainly steel fibers. Consequently, this research addresses a crucial gap in the current body of knowledge by incorporating a wide range of fiber types. By doing so, it establishes itself as a pioneering and innovative contribution in the field of FRCC beam-to-column joint analysis. The comprehensive nature of the proposed equation ensures its potential applicability to diverse FRCC structures, further enhancing the significance and originality of this study.

4.2 Methodology

Within this methodology section, readers will be provided with a comprehensive understanding of the calculation methodology employed for determining the joint shear strength of the specimens compiled from the literature. Subsequently, an elucidation of the software employed to derive a precise and dependable shear strength prediction equation will be presented. Moreover, detailed explanation will be provided regarding the selection process for the parameters incorporated within the prediction equation. Finally, a comprehensive account of the limitations imposed, and assumptions made during the research endeavor will be expounded upon.

4.2.1 Determination of the Joint Shear Strength

In the available literature, reversed cyclic loading is applied to beam-to-column connection specimens, both interior and exterior, using two separate methods. The first method involves applying the load directly on top of the column, while the second method entails applying the load on the beam end.

Within the scope of the present study, a total of 212 specimens were collected from the literature, while only 87 of these specimens were specifically examined and numerically presented their joint shear strength. This subset constitutes less than half of the total number of specimens. As for the remaining 125 specimens, the primary focus was investigating the advantages of employing FRCC and/or HPFRCC materials near the joint region. These investigations primarily centered on evaluating behavioral changes, such as ultimate failure mode, energy dissipation capacity, ductility, and hysteresis curve characteristics, rather than the specific examination of joint shear behavior.

The joint shear strength of the remaining 125 specimens was determined by three different approaches. These approaches include the force equilibrium approach, the strain gauge data approach, and the beam moment capacity approach. Each of these methods provides a unique perspective and methodology for calculating the joint shear strength in the specimens under investigation.

The force equilibrium approach has been widely adopted by researchers in their investigations. Parra-Montesinos et al. (2005), Tingting et al. (2022), Lu and Liang (2020), and Wang et al. (2018) utilized the beam moment capacity as a starting point to derive the joint shear strength. Similarly, Zhang et al. (2015), Choi and Bae (2019), and Gencoglu (2007) employed the force equilibrium approach, while Unal (2010) utilized the strain gauge data approach. By utilizing this approach, these researchers have been able to effectively calculate the joint shear strength of various beam-to-column joints. The widespread adoption of these approaches by researchers highlights their reliability and effectiveness in obtaining the shear behavior of such connections.

It is noteworthy to mention that the force equilibrium approach was not considered as the primary method when the explicit joint strength information was not provided in the respective studies. Instead, it was regarded as the last resort, despite its simplicity. This is primarily attributed to the fact that the strain gauge data approach and the beam flexural strength approach are more reliant on test-specific data,

considering all nonlinear activity that the specimen underwent, and therefore deemed more reliable and accurate in such cases.

In conclusion, in the absence of available joint shear strength data, beam flexural strength approach and strain gauge approach are utilized to estimate the joint shear strength. If these approaches are also not feasible, the force equilibrium approach is employed as an alternative method.

4.2.1.1 Force Equilibrium Approach

In this approach, the calculation of joint shear strength is accomplished through the force equilibrium, which involves solving three different equations simultaneously. Firstly, the moment equilibrium equation at the joint face of the beam is considered, ensuring that the moments exerted on the joint are in balance. Secondly, the horizontal force equilibrium at the mid-depth of the joint is taken into account, satisfying the equilibrium of forces acting on the joint. Lastly, the overall moment equilibrium within the connection is analyzed, ensuring the balance of moments exerted on the connection. By solving these three equations concurrently, the joint shear strength can be accurately determined, providing a comprehensive understanding of the structural behavior and integrity of the beam-to-column connections.

It is of utmost importance to highlight that this approach focuses on the evaluation of the demand for any given applied load level, rather than assessing the capacity of the joint. Yet, in cases where the joint undergoes shear failure, it is recognized that the ultimate load capacity has already been achieved. In such instances, the derived expression based on the ultimate applied load serves as a dependable estimate of the joint shear capacity. This approach proves to be a valuable means of assessing the joint performance and predicting its load-carrying capacity.

4.2.1.1.1 Exterior Beam-to-Column Specimens

4.2.1.1.1.1 Load-on-Beam Case

For exterior beam-to-column connection specimens, the load may be applied vertically at the beam end. In this configuration, depicted in Figure 4.2, the column is restrained by two pin supports located at the top and bottom, which act as points of inflection.

Figure 4.2. Exterior beam-to-column connection loaded at the beam end.

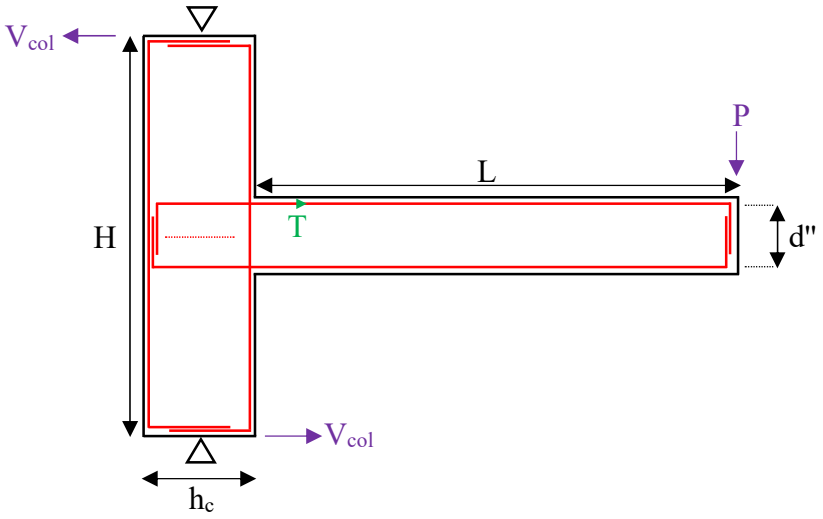

In Figure 4.2, P represents the load, while V_{col} represents the column shear force. T denotes the tensile force exerted on the longitudinal bars of the beam. And d" represents the distance between the outermost longitudinal bars of the beam. H is the length of the column between the pin supports and h_c is the column depth.

Using the principle of moment equilibrium, it is feasible to take moments about the geometrical centroid of the joint, yielding Equation **(4.17)**.

$$P \cdot \left(L + \frac{h_c}{2}\right) = V_{col} \cdot H \qquad \textbf{(4.17)}$$

One may take a moment at the interface of the beam and column as a subsequent step, leading to the formulation of Equation **(4.18)**.

$$T \cdot d'' = P \cdot L \quad \textbf{(4.18)}$$

Lastly, in accordance with the recommendations outlined in ACI 352-02 (ACI 352-02, 2002) code for exterior beam-to-column joints, the horizontal joint shear force can be computed by using Equation **(4.19)**.

$$V_{jh} = T - V_{col} \quad \textbf{(4.19)}$$

By combining these three equations, the resultant joint shear strength equation is obtained, as provided in Equation **(4.20)**.

$$V_{jh} = P \cdot \left(\frac{L}{d''} - \frac{L + 0.5h_c}{H}\right) \quad \textbf{(4.20)}$$

Due to the identical derivation procedures, the horizontal joint shear strength for other types of joints will be directly presented without additional derivation.

4.2.1.1.1.2 Load-on-Column Case

For exterior beam-to-column connection specimens, it is common practice to apply the load horizontally at the top of the top column. This loading arrangement, shown in Figure 4.3, effectively represents the lateral forces that the connection would experience under earthquake loading.

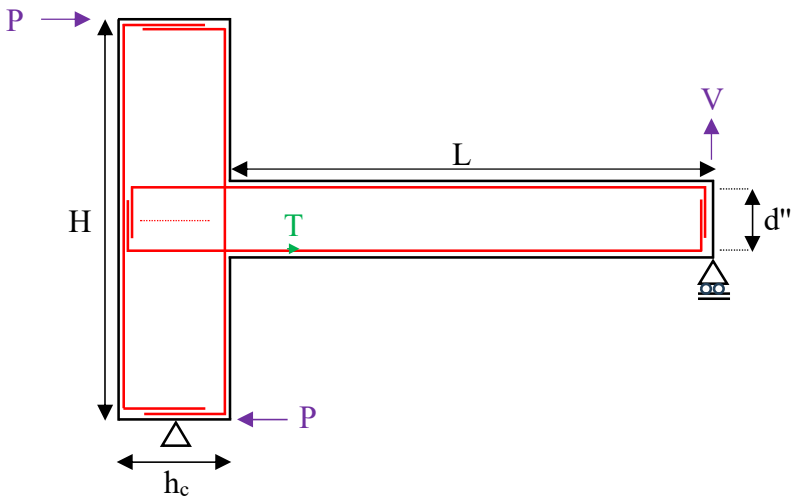

Figure 4.3. Exterior beam-to-column connection loaded at the column top.

For this loading type, the joint shear strength can be obtained from Equation **(4.21)**.

$$V_{jh} = P \cdot \left(\frac{H.L}{d''.(L + 0.5h_c)} - 1 \right) \qquad \textbf{(4.21)}$$

4.2.1.1.2 Interior Beam-to-Column Specimens

4.2.1.1.2.1 Load-on-Beam Case

For interior beam-to-column joints reversed cyclic loading may be applied to the beam ends, where the two ends of the beam are simultaneously loaded in reverse directions as illustrated in Figure 4.4. The shear strength of such joints is obtained by Equation **(4.22)**.

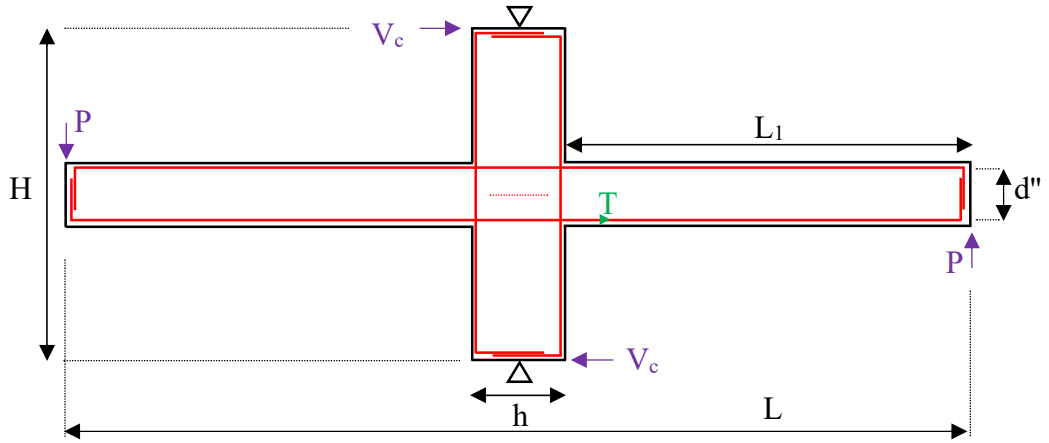

Figure 4.4. Interior beam-to-column connection loaded at beam ends.

$$V_{jh} = P \cdot \left(\frac{2L_1}{d''} - \frac{L}{H}\right) \quad \textbf{(4.22)}$$

4.2.1.1.2.2 Load-on-Column Case

For interior beam-to-column connection specimens, shown in Figure 4.5, Equation **(4.23)** can be used to obtain the joint shear strength.

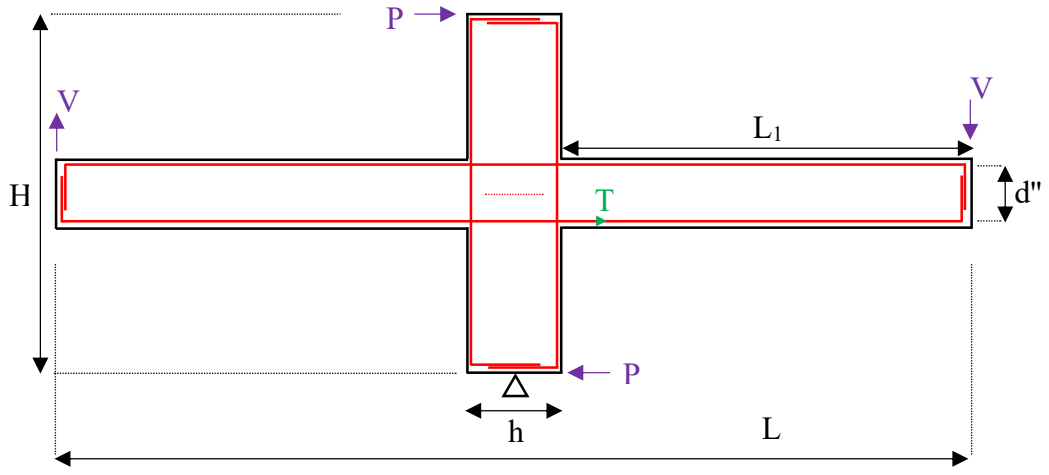

Figure 4.5. Interior beam-to-column connection loaded at the column top.

$$V_{jh} = P \cdot \left(2 \cdot \left(\frac{H}{d''}\right) \cdot \left(\frac{L_1}{L}\right) - 1\right) \quad \textbf{(4.23)}$$

4.2.1.2 Strain Gauge Data Approach

Strain gauges on steel reinforcing bars are utilized to monitor the inelastic deformations in the subassembly. If the strain gauge data for both the top and bottom longitudinal reinforcement of the beam is provided, the moment capacity of the beam can be obtained. The joint shear strength is directly correlated to the internal forces on the reinforcement, as shown in Equations **(4.24)** (Unal & Burak, 2012) and **(4.25)**.

$$T = \begin{cases} 1.25. A_s. f_y & \text{if } \varepsilon \geq \varepsilon_y \\ A_s. \varepsilon. E & \text{if } \varepsilon < \varepsilon_y \end{cases} \quad \textbf{(4.24)}$$

When the tensile force on the reinforcement is obtained, Equation **(4.25)** can be utilized to obtain the joint shear strength. Note that the tensile force is increased by a factor of 1.25 to account for the strain hardening behavior.

$$V_j = \begin{cases} T - V_{col} & \text{for exterior joints} \\ T_1 + T_2 - V_{col} & \text{for interior joints} \end{cases} \quad \textbf{(4.25)}$$

4.2.1.3 Beam Moment Capacity Approach

In addition to previously explained approaches, if the experimental study provides the moment vs. rotation or moment vs. curvature response of the beams, the joint shear strength can be computed using the moment capacities of the beams framing into the joint. By using the maximum moment capacity of the beams, the tensile force on the beam longitudinal bars can be derived, subsequently allowing for the computation of the joint shear strength. The joint shear strength obtained from the flexural capacity on the beam is given in Equation **(4.26)**.

$$V_j = \sum \frac{M_r}{jd} - V_{col} \quad \textbf{(4.26)}$$

In Equation **(4.26)**, M_r denotes the flexural strength of the beam.

4.2.2 Effective Joint Width

Throughout the course of this investigation, the experimental joint shear strength has been assessed and quantified in units of force, denoted as kilonewtons (kN). To transform this force into a measure of stress, in terms of megapascals (MPa), a crucial step involves dividing the shear force by the effective joint area. The effective joint area is determined as the product of the effective joint width and the column depth.

In this study, the effective joint width of ACI 318-19 (ACI 318-19, 2019) was preferred due to the increased effective joint area when compared to ACI 352-02 (ACI 352-02, 2002) for all tests included in the database. The reason for choosing larger effective joint width for FRCC, particularly for HPFRCC specimens, is that due to effective confinement provided by the fibers and bridging stresses the forces will be effectively transferred across cracks. This phenomenon gives rise to a multi-cracking and micro-cracking behavior, resulting in a network of cracks leading to a larger effective joint area that carries the transmitted stresses.

4.2.3 Development of the Prediction Equation

In this study, IBM SPSS software was employed to perform a range of statistical analyses and model development tasks to produce a joint shear strength prediction equation for FRCC beam-to-column connections. The extensive capabilities of SPSS were utilized to analyze a database of experimental data collected from literature, extracting valuable insights in this process. Specifically, SPSS was employed to conduct nonlinear regression, curve fitting, and correlation analyses, aimed at

uncovering the relationships between key variables and parameters that influence joint shear strength.

Through the use of SPSS, a thorough examination of the relationship between the geometrical properties of the joint, joint transverse reinforcement ratio, composite compressive strength, fiber-related properties, and joint shear strength was obtained. Additionally, SPSS facilitated the correlation analysis, enabling the assessment of the joint shear strength and determination of the correlation between variables. The computation of correlation coefficients allowed for the evaluation of interdependencies among different factors and their impact on the joint shear strength. By performing statistical analyses in SPSS, a thorough comprehension of the underlying patterns and trends within the data was obtained, which aided in developing a robust prediction equation.

The development of a prediction equation that captures the complex relationships between the variables was accomplished through the application of nonlinear regression analysis. SPSS's advanced curve fitting capabilities assisted in identifying the most suitable mathematical function that represents the relationship between variables, enabling the estimation of joint shear strength.

In summary, the utilization of IBM SPSS software in this study played a critical role in analyzing the collected data, uncovering relationships, and developing a prediction equation for joint shear strength in FRCC beam-to-column connections. The sophisticated statistical techniques available in SPSS provided valuable insights and enhanced the reliability of the study's findings. However, it should be noted that the selection of the key parameters and the physical relationship between each parameter and the shear strength were meticulously studied, and several iterations were performed to obtain the most reliable and simplest form of the equation.

4.2.4 Parameters Included in the Equation

The identification of parameters to be included in the shear strength prediction equation for FRCC beam-to-column connections constitutes a crucial aspect of this study. The robustness, reliability, and simplicity of the equation depends on the proper selection of these parameters. To accomplish this, correlation coefficients between each parameter and the experimental joint shear strength were assessed by using IBM SPSS.

A common confidence level of 95% is utilized for the correlation coefficients, which means that there is a 95% likelihood that the true correlation coefficient in the sample falls within the calculated confidence interval. It should be noted that the subsequent analyses in this study were focused specifically on the joint shear failure database, rather than the entire database. Therefore, the analyses were performed exclusively on a subset of 117 specimens, which provided a more targeted and specific examination of the joint shear failure.

4.2.4.1 Composite Properties

The correlation coefficient was computed to evaluate the relationship between the joint shear strength and the parameters of composite compressive strength, bond strength, and cracking strength for the interior and exterior joints separately.

The cracking strength was determined based on ACI 318-19 Code requirements, as Equation **(4.27)**, while the bond strength was computed by Equations **(2.16)** and **(2.17)**.

$$\sigma_{cr} = 0.62\sqrt{f_c'} \quad \textbf{(4.27)}$$

Table 4.1 illustrates the correlation coefficients between the joint shear strength and the parameters of compressive strength, cracking strength, and bond strength.

Table 4.1 Correlation between the joint shear strength and composite strength parameters.

Parameter	Correlation with Joint Shear Strength, v_j (MPa)	
	Exterior Joints	**Interior Joints**
f_c' (MPa)	0.649	0.454
σ_{cr} (MPa)	0.686	0.511
τ (MPa)	0.755	0.578

Table 4.1 clearly demonstrates a strong correlation between the joint shear strength and the composite properties. The joint shear strength of exterior joints exhibits a greater dependence on the composite properties compared to interior joints. This observation can be attributed to the fact that exterior beam-to-column joints are confined from only one side of the joint by a single longitudinal beam. Consequently, considering that the composite itself acts as a form of confinement in addition to stirrups, the shear strength of exterior joints is significantly influenced by composite properties.

4.2.4.2 Axial Load Factor

Among the 117 specimens, which experienced joint shear failure, a subset of 99 specimens (comprising 42 interior and 57 exterior beam-to-column connections) were subjected to non-zero axial loads. When examining the correlation between the joint shear strength and axial load applied on these specimens, the correlation coefficient for interior joints yielded a value of 0.560, while for exterior joints it was 0.361. Note that these correlation coefficients were derived from the subset of specimens with axial loading.

4.2.4.3 Joint Reinforcement Ratio

In order to achieve the optimal correlation between the joint transverse reinforcement ratio and the joint shear strength, the approach proposed by Unal and Burak (2012) was employed in this study. Following their methodology, three separate definitions of the joint transverse reinforcement volumetric ratio were computed for each specimen, and the correlation between each of these ratios and the joint shear strength was assessed.

The simplest definition of the joint transverse reinforcement ratio is the volume of the joint stirrups divided by the gross volume of the joint as demonstrated in Equation **(4.28)**. In this approach, the gross joint volume is computed by multiplying the values of the column depth (h_c), column width (b_c), and beam depth (h_b), as shown in Figure 4.6. The total length of the transverse reinforcement in the loading direction, l_e, is then multiplied by the cross-sectional area of one reinforcement (A_0), along with the number of transverse reinforcement layers (n) present within the gross joint volume.

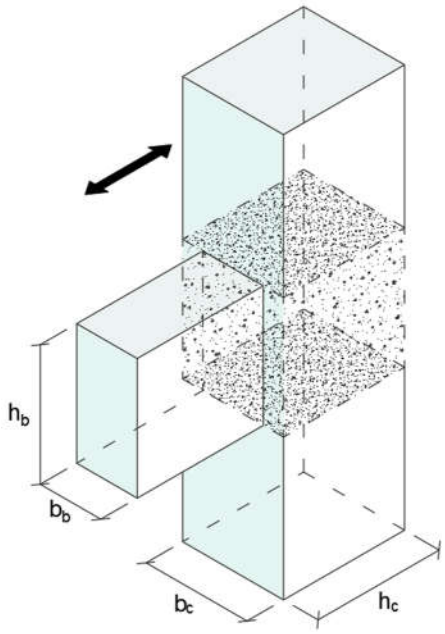

Figure 4.6. Gross joint volume, represented as the shaded region.

$$\rho_{gross} = \frac{n.A_0.l_e}{h_c.b_c.h_b} \quad \textbf{(4.28)}$$

The second definition takes into account the joint core volume, which is the volume enclosed by the outermost longitudinal rebars of the beam and the edges of the joint stirrups, as shown in Figure 4.7. The joint reinforcement ratio considering the joint core volume is computed using Equation **(4.29)**.

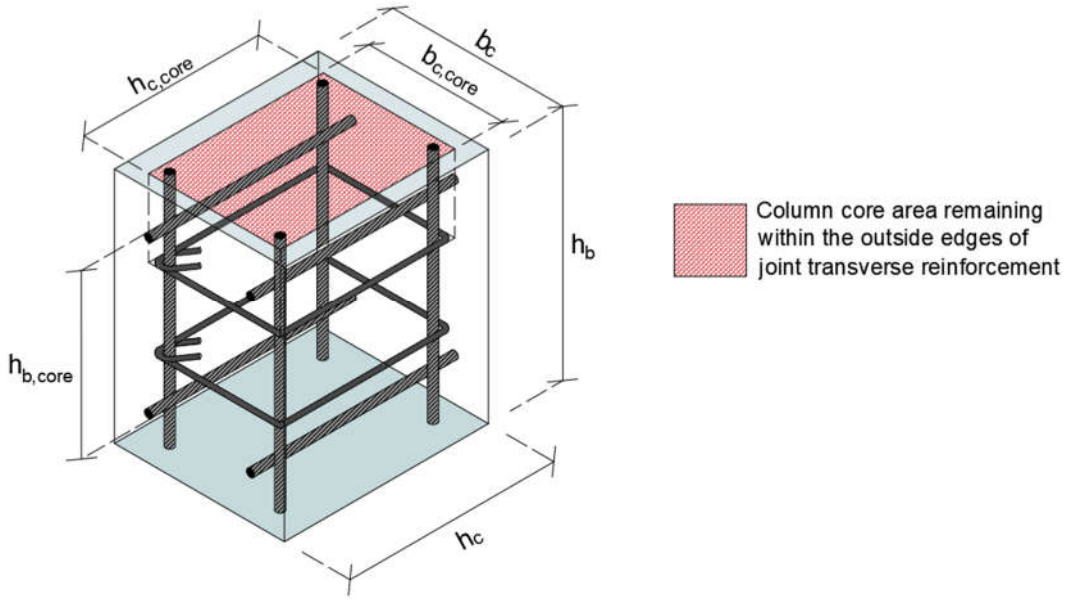

Figure 4.7. Column core area.

$$\rho_{core} = \frac{n.A_0.l_e}{h_{c,core}.b_{c,core}.h_{b,core}} \quad \textbf{(4.29)}$$

The single-layer volumetric reinforcement ratio, which is different from the first two approaches, considers a single layer of transverse reinforcement and its corresponding tributary area. The determination of the single-layer volumetric ratio of the joint reinforcement is expressed by Equation **(4.31)**, where the parameter "s" represents the stirrup spacing. When there is only one layer of transverse reinforcement in the joint, the spacing is determined as half the distance between the outermost longitudinal rebars of the beam. When multiple joint transverse reinforcement layers are present, the spacing is determined as the greater value

between the distance between the layers and the average distance of this distance and the maximum unconfined distance observed along the core depth of the beam. This configuration is visualized in Figure 4.8.

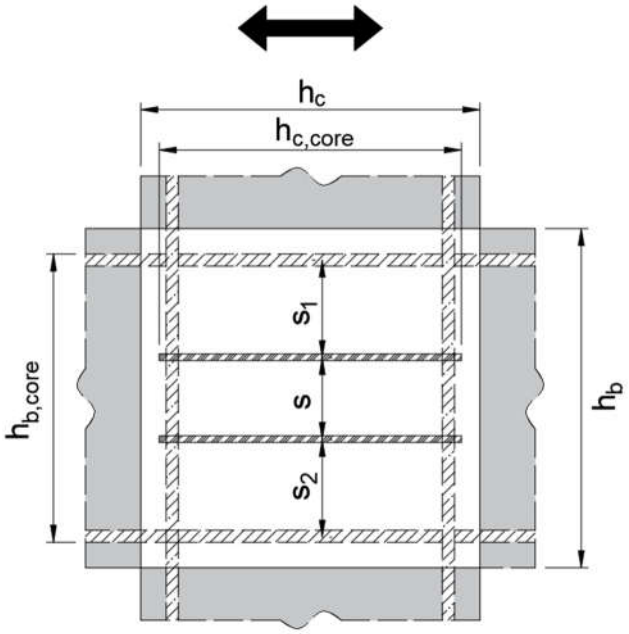

Figure 4.8. Joint hoop spacings

Equation **(4.30)** summarizes the determination of the spacing to be utilized in the joint transverse reinforcement ratio definition. It is essential to ensure that the spacing remains within the beam core depth, $h_{b,core}$.

$$s_{used} = \max\left(s, \frac{s+s_1}{2}, \frac{s+s_2}{2}\right) \quad \textbf{(4.30)}$$

Once the appropriate spacing has been determined, Equation **(4.31)** can be employed to calculate the single-layer joint reinforcement ratio.

$$\rho_{singlelayer} = \frac{A_0 . l_e}{h_{c,core} . b_{c,core} . s_{used}} \quad \textbf{(4.31)}$$

Considering all three joint reinforcement ratios, Table 4.2 presents a comprehensive summary of the correlation coefficients that were obtained.

Table 4.2 Correlation coefficients between the joint shear strength and the joint reinforcement ratios.

Volumetric Joint Stirrup Ratio Based on:	**Correlation with Joint Shear Strength, v_j (MPa)**	
	Exterior Joints	**Interior Joints**
Gross Volume	-0.103	0.386
Core Volume	0.148	0.365
Single-Layer Volume	0.493	0.408

As can be observed in Table 4.2, none of the joint reinforcement ratios exhibit a significantly higher correlation with the joint shear strength for interior joints. However, for exterior connections, the single-layer joint reinforcement ratio demonstrates a stronger correlation compared to the others.

While the single-layer definition yields higher correlation coefficients for both exterior and interior joints, it is worth noting that the gross volume definition offers the advantage of simplicity in shear strength prediction equations, owing to its straightforward calculation. A thorough examination of these two definitions, along with the resulting shear strength prediction equations derived from them, will be discussed in detail in Section 4.3.

4.2.4.4 Geometrical Dimensions

Beam and column dimensions are key factors in determining the joint shear strength. Apart from the important role of the beam depth and column width, the beam width and column depth, which are used to define the joint aspect ratio, also hold significant importance in obtaining the effective joint area. A larger joint area facilitates the transfer of horizontal shear forces, resulting in reduced stress concentrations and improved joint shear strength.

The present study extensively examined the geometric properties in terms of their correlation coefficients and demonstrated their interaction with the joint shear strength. The parameters investigated included the depth and width of beams and columns, as well as the aspect ratios of the members, namely beam aspect ratio (h_b/b_b) and column aspect ratio (h_c/b_c), and the ratio h_c/b_b, which assisted in normalizing the cross-sectional dimensions.

Figure 4.9 provides a clear representation of the cross-sectional area where these aspect ratios are calculated, using an illustrative sketch of a roof exterior beam-to-column connection labeled as RE0.

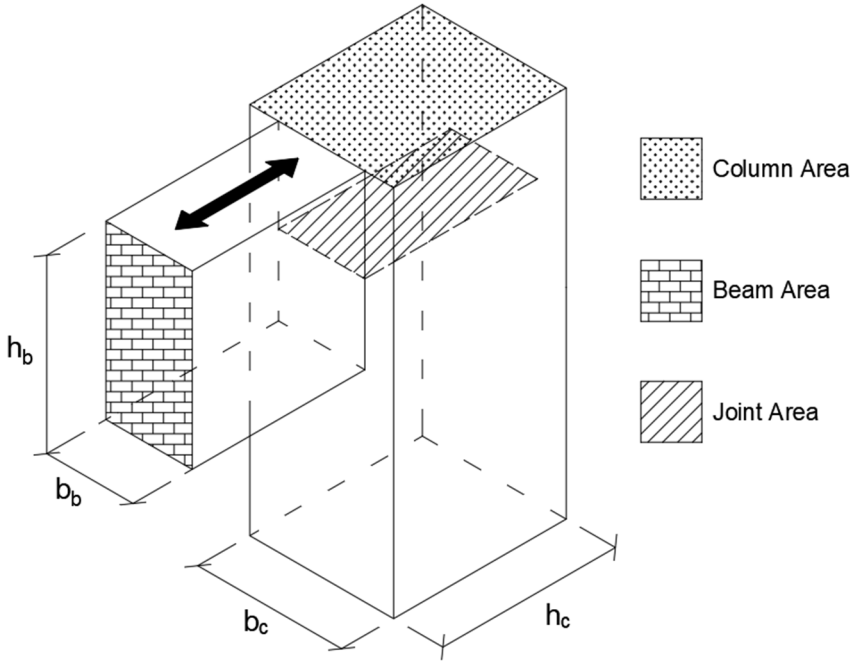

Figure 4.9. Column, beam and joint areas.

Table 4.3 summarizes the correlation coefficients obtained from the analysis of the geometric properties and their relationship with joint shear strength. While the width and depth dimensions of beams and columns exhibit a notable influence on the joint shear strength, it is the use of these dimensions in the form of aspect ratios that has higher correlation with the joint shear strength.

Table 4.3 Correlation factors for geometrical dimensions.

Geometrical Parameters	Correlation with Joint Shear Strength, v_j (MPa)	
	Exterior Joints	Interior Joints
Beam depth, h_b, (mm)	-0.330	0.111
Beam width, b_b, (mm)	-0.185	0.382
Column depth, h_c, (mm)	-0.086	0.194
Column width, b_c, (mm)	-0.244	0.371
h_b / b_b	-0.283	-0.491
h_c / b_c	0.303	-0.693
h_c / b_b	0.268	-0.578

4.2.4.5 Fiber Related Parameters

As discussed in the Literature Review Chapter, fiber-related parameters have a substantial impact on the shear carrying capacity of FRCC and HPFRCC beam-to-column joints. Therefore, it is crucial to analyze the experimental results in terms of the correlation between these parameters and the joint shear strength. The parameters considered for examination are the fiber volume fraction, aspect ratio, and reinforcing index. Table 4.4 provides the correlation coefficients associated with these parameters.

Table 4.4 Correlation between fiber related parameters and the joint shear strength.

Fiber Related Parameter	Correlation with Joint Shear Strength, v_j (MPa)	
	Exterior Joints	Interior Joints
Volume Fraction, (V_f)	0.488	-0.111
Aspect Ratio (L_f/D_f)	0.780	-0.269
Reinforcing Index V_f (L_f/D_f)	0.791	-0.247

Upon examining Table 4.4, it is evident that the fiber properties have substantial influence on the behavior of exterior joints. This can be attributed to the configuration of exterior joints, in which only a single longitudinal beam provides confinement to the joint. Due to the need for additional confinement, exterior joint behavior is affected more from the variations in fiber properties. As a result, even slight changes in the fiber related parameters can have a significant effect on the shear characteristics of exterior joints.

4.3 Development of the Proposed Joint Shear Strength Prediction Equation

Once the key factors have been identified, a joint shear strength prediction equation is developed with the help of IBM SPSS (reference) software. The methodology aims to keep a balance between simplicity, accuracy, and practicality. Consequently, the equation is designed to incorporate two main contributors, ensuring a concise yet effective representation of the joint shear strength.

The first component of the joint shear strength prediction equation is the composite contribution, incorporating both the matrix and the fiber properties. This term contains various factors, including the geometric dimensions such as beam aspect ratio, column aspect ratio, and joint aspect ratio, as well as the cracking strength of the composite, the reinforcing index of the fibers, referred to as fiber factor in ACI 544.9-17 (ACI 544.9-17, 2017) Code, and the axial load ratio on the column. This first component is strongly influenced by the joint type, interior or exterior. In order to address the variation in joint shear strength between interior and exterior joints, a shear strength factor denoted as γ is incorporated into the equation. This factor is similar to the term γ utilized in ACI 318-19 (ACI 318-19, 2019) and ACI 352-02 (ACI 352-02, 2002) codes, yet in a simplified form due to the additional confinement provided by the composite.

The second term in the joint shear strength prediction equation represents the joint transverse reinforcement contribution. Acknowledging the confining effects of both

the fibers and the joint reinforcement, this term compounds the impact of fibers on the confinement provided by the transverse reinforcement, in addition to the cracking tensile strength of the composite and the column axial load ratio.

Once the parameters and their influence on the joint shear strength were established, the considered equation was input into IBM SPSS. This enabled the software to perform a nonlinear regression analysis, facilitating a comprehensive evaluation of the chosen variables and their interrelationships in order to develop an effective model for predicting the joint shear strength. After numerous analyses, the one presented in Equation **(4.32)** is observed to yield the most accurate representation of the shear strength.

$$v_{jmax} = \sigma_{cc}\left[1 + \left(C1\frac{N}{f_c{}'A_g}\right)\right]\left[\gamma\left(\frac{h_b}{b_b}\right)^{C2}\left(\frac{h_c}{b_c}\right)^{C3}\left(\frac{b_b}{h_c}\right)^{C4} RI^{\alpha} + C5\left(\rho_{gross}\right)^{C6} RI^{\beta}\right] \qquad \textbf{(4.32)}$$

In Equation **(4.32)**, σ_{cc} denotes the cracking tensile strength of the composite. The term $\frac{N}{f_c' A_g}$ represents the column axial load ratio, which is obtained from division of the applied axial load by the cross-sectional area of the column. RI stands for the reinforcing index of the fibers, quantifying the presence and effectiveness of fibers used in the composite, further contributing to the overall joint shear strength.

There are mainly two groups of coefficients in Equation **(4.32)**, which were set utilizing the IBM SPSS. The first group, comprised of the joint type independent coefficients, from C1 to C6, and they are the same for both exterior and interior connections. On the other hand, the second group, including the joint type dependent terms α, β and γ, are selected separately for both joint types.

After performing the nonlinear regression analysis in IBM SPSS, the coefficients for the first group of variables were determined and recorded, as presented in Table 4.5.

Table 4.5 Nonlinear regression analysis results for the joint type independent coefficients.

Coefficient	Estimation	Std. Error	95% Confidence Interval	
			Lower Bound	Upper Bound
C1	0.214	0.098	0.019	0.409
C2	-1.069	0.087	-1.241	-0.896
C3	-0.077	0.059	-0.194	0.040
C4	-0.704	0.089	-0.881	-0.528
C5	2.458	1.617	-0.747	5.662
C6	0.526	0.115	0.298	0.753

It should be noted that the coefficients obtained from the regression analysis in Table 4.5 require further modification to facilitate their practical application in the equation. To address this, these estimations served as an initial reference point, and the data were subsequently reprocessed using MS Excel. This additional processing enables the refinement of the equation, taking into consideration the joint type dependent coefficients, thus enhancing the accuracy and simplicity of the equation. As a result of the data reprocessing, joint type dependent coefficients were selected as presented in Table 4.6. These coefficients incorporate the specific characteristics of each joint type, further improving the accuracy and applicability of the equation.

Table 4.6 Selected joint type dependent coefficients.

Coefficient	Estimation	
	Exterior Joints	Interior Joints
α	0.25	0.00
β	0.75	1.00
γ	1.50	2.10

In order to obtain the final form of the joint shear strength prediction equation, a subsequent iteration of nonlinear regression analysis is executed. Within this

iteration, the joint type dependent parameters assume the role of fixed constants and are directly integrated into IBM SPSS, while the primary emphasis lies on recalibrating the data for the joint type independent parameters. By this iterative methodology, the equation is refined, resulting in a higher precision and efficiency in predicting the joint shear strength.

The primary objective of employing IBM SPSS in the nonlinear regression analysis is to maximize the correlation between estimated values and actual values, resulting in an increased coefficient of determination (R^2) value and reduced error. However, it should be kept in mind that data scatter should be minimized. While minimizing absolute error, it is important to ensure that each individual estimation closely aligns with the experimental shear strength, preferably slightly underestimating it to be conservative. Merely achieving a high correlation does not guarantee a robust model. Instead, the model adopts a cautious approach by intentionally providing conservative estimations that prioritize safety considerations. This deliberate inclusion of a small percentage of underestimation error accounts for the uncertainties present in real-world scenarios. By generating slightly conservative estimations, the model enhances safety and addresses potential variations and uncertainties in the structural behavior. Figure 4.10 visually illustrates the ideal prediction model and the desired target prediction model, which intentionally exhibits a slight underestimation of the joint shear strength.

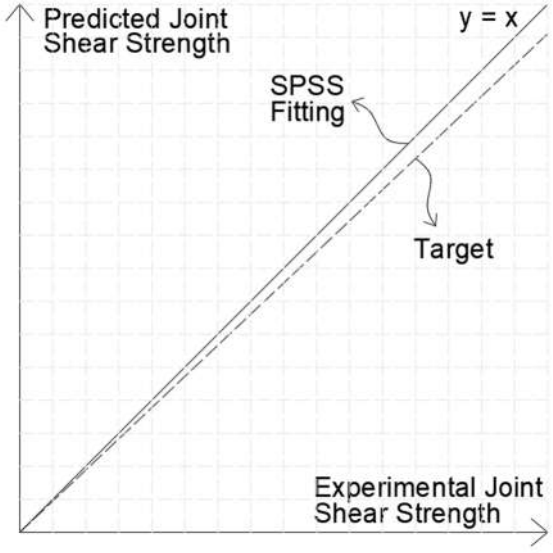

Figure 4.10. Target error for the shear strength predictions.

To satisfy these considerations, the final equation is refined in MS Excel, allowing for manual modification of the coefficients. The coefficients are adjusted in a way that the number of underestimations outweighs the number of overestimations, while still maintaining the overall integrity of the model. The final coefficients are presented in Table 4.7.

Table 4.7 Coefficients utilized in the joint shear strength prediction equation.

Coefficient	**Exterior Joints**	**Interior Joints**
C1	0.3	
C2	-1.1	
C3	-0.2	
C4	-0.7	
C5	2.0	
C6	0.5	
α	0.25	0,00
β	0.75	1.00
γ	1.50	2.10

The final joint shear strength prediction equation is provided in Equation **(4.33)**.

$$v_{jmax}\ (\text{MPa}) = \sigma_{cc}\left[1 + \left(0.30\frac{N}{f_c{}'A_g}\right)\right]\left[\gamma\left(\frac{b_b}{h_b}\right)^{1.1}\left(\frac{b_c}{h_c}\right)^{0.2}\left(\frac{h_c}{b_b}\right)^{0.7} RI^{\alpha} + 2(\rho_{gross})^{0.5} RI^{\beta}\right] \quad \textbf{(4.33)}$$

The values of α, β and γ are provided in Table 4.6. Figure 4.11 illustrates the comparison between the experimental and predicted joint shear strengths.

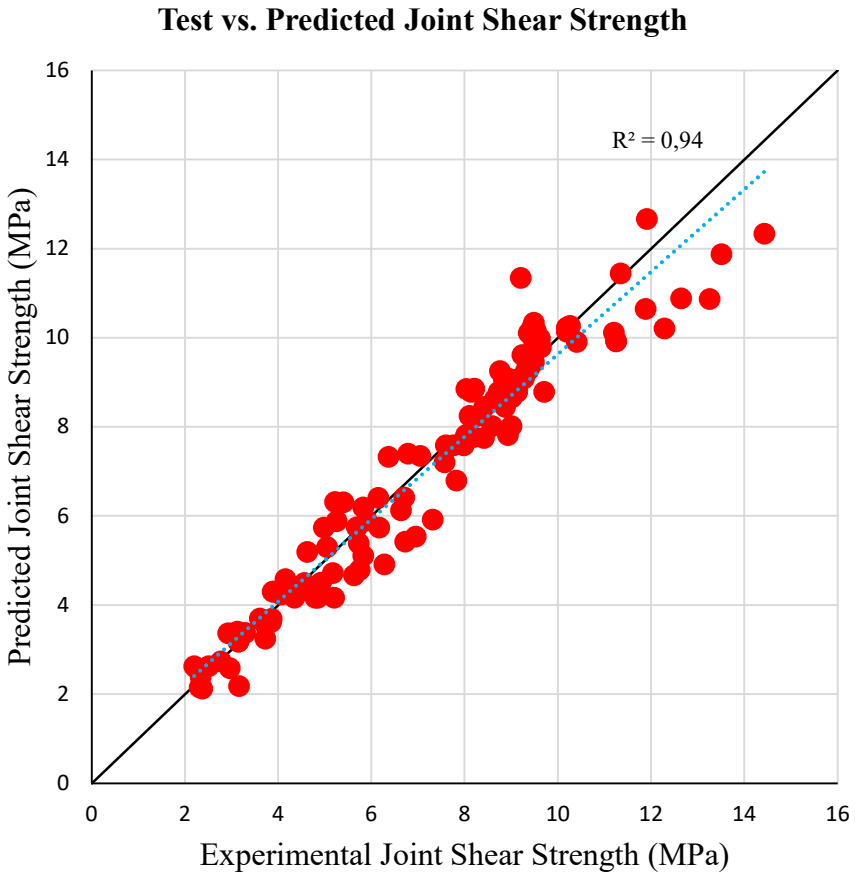

Figure 4.11. Comparison of experimental and predicted joint shear strengths.

The utilization of standardized residuals, which are derived by dividing the residuals by their standard deviation, provides a valuable means of evaluating the accuracy of the prediction equation. By plotting these standardized residuals against the corresponding test values, one can visually examine the presence of any noticeable patterns or trends. The emergence of such patterns may indicate the existence of

highly correlated parameters that were unintentionally not considered or not adequately accounted for in the prediction equation. Through the analysis of the standardized residuals plot, potential sources of error or parameters requiring further refinement in the prediction equation can be identified.

As can be observed from Figure 4.12, the standardized residuals mostly fall within the range of -2 to +2, indicating a satisfactory model. It is worth emphasizing that all data points, apart from one exception, are contained within the -3 to +3 range, which means that there is no considerable outlier within the data (Montgomery et al., 2012).

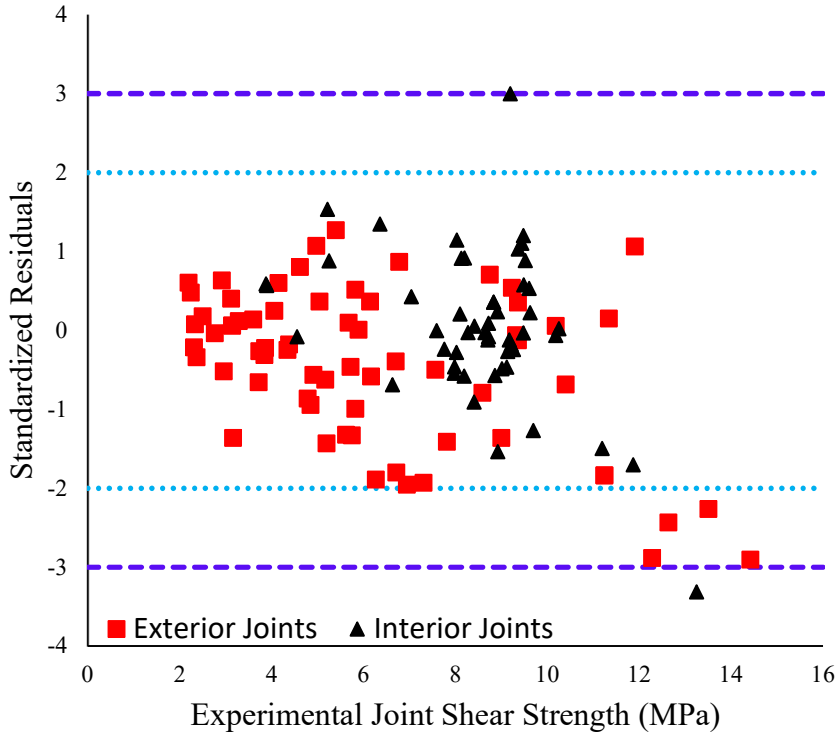

Figure 4.12. Standardized residuals for each experimental joint shear strength.

Figure 4.12 illustrates that the intentional decision to accept a higher error rate for increased joint shear strengths proved to be effective. Despite this observation, the standardized residuals exhibit no noticeable pattern overall, indicating that there is no significant parameter not accounted for in the prediction equation.

The average absolute error (AAE) is determined by Equation **(4.34)**, and Table 4.8 displays the coefficient of correlation, corresponding R^2 values, and average absolute errors for the proposed equation in relation to the test data. It can be observed from Table 4.8 that the number of underpredicted joint shear strength values surpass the number of overpredicted joint shear strength values, aligning with the intended objective of the prediction model.

$$\text{AAE between } v_{j,test} \text{ and } v_{j,predicted} = \frac{\left|v_{j,pred} - v_{j,test}\right|}{v_{j,test}} \text{ x } 100 \qquad \textbf{(4.34)}$$

Table 4.8 Average absolute Errors and correlation factors.

Parameters	Exterior Joints	Interior Joints	Overall
AAE (%)	9.18%	5.75%	7.69%
Coeff. of Correlation, R	0.98	0.92	0.97
Coeff. of Determination, R^2	0.95	0.84	0.94
#Overpredictions	27	24	51
#Underpredictions	39	27	66
#Total	66	51	117

As mentioned in Chapter 4.2.4.3, the single-layer joint reinforcement ratio was also used in the prediction equation due to its higher correlation with the joint shear strength. By following the same procedure employed for the gross volume definition, the equation for the single-layer joint reinforcement ratio is obtained as presented in Equation **(4.35)**.

$$\underset{(MPa)}{v_{jmax}} = \sigma_{cc}\left[1 + \left(0.30\frac{N}{f_c{}'A_g}\right)\right]\left[\gamma\left(\frac{b_b}{h_b}\right)^{1.1}\left(\frac{b_c}{h_c}\right)^{0.2}\left(\frac{h_c}{b_b}\right)^{0.7} RI^{\alpha} + \left(\rho_{singlelayer}\right)^{0.5} RI^{\beta}\right] \qquad \textbf{(4.35)}$$

Incorporating the single-layer joint reinforcement ratio in Equation **(4.33)**, primarily results in a change of the multipliers, C_5 and β, there are no other modifications to the other constants in the equation. The updated constants are provided in Table 4.9.

Table 4.9 Coefficients utilized in the joint shear strength prediction equation.

Coefficient	Exterior Joints	Interior Joints
C_5	1.0	
β	0.75	1.00

By using the equation with both the gross and the single-layer joint reinforcement ratio definitions, the resulting joint shear strength predictions are compared in the Figure 4.13, which illustrates the differences between the two definitions and their respective outcomes in terms of joint shear strength estimation.

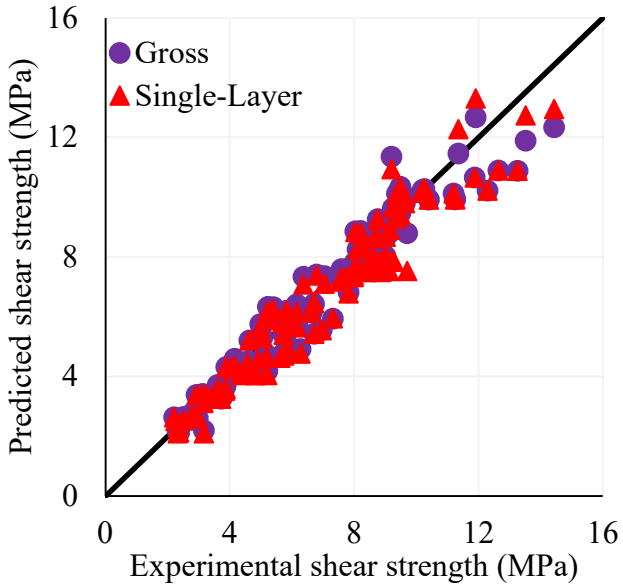

Figure 4.13. Comparison of joint shear strength prediction equations based on different joint reinforcement ratio definitions.

It can be observed from Figure 4.13 that there is no significant change in the scatter of the data after incorporating the single-layer joint reinforcement ratio. However, to make an informed decision on which equation to select, it is crucial to examine the error comparison and other relevant statistical parameters that provide a comprehensive understanding of the performance of the model. Table 4.10 presents

the errors, coefficients of determination (R), coefficients of correlation (R^2), and the number of overpredictions and underpredictions for both approaches.

Table 4.10 Comparison of key statistical parameters for based on different joint hoop ratio definitions.

Parameters	**Exterior Joints**		**Interior Joints**		**Overall**	
	Gross	**Single Layer**	**Gross**	**Single Layer**	**Gross**	**Single Layer**
AAE (%)	9.18%	9.44%	5.75%	8.44%	7.69%	9.00%
R	0.98	0.97	0.92	0.87	0.97	0.96
R^2	0.95	0.95	0.84	0.76	0.94	0.93
#Overpred.	27	22	24	18	51	40
#Underpred.	39	44	27	33	66	77
#Total	66	66	51	51	117	117

The statistical analysis reveals that the errors and coefficients of correlation exhibit minimal variation when incorporating the single-layer joint reinforcement ratio. Furthermore, there is a slight decrease observed in the count of overpredicted values. Considering the simplicity of obtaining the gross joint reinforcement ratio and the assumptions made during stirrup spacing computations, the use of single-layer joint reinforcement ratio is not practical. Due to achieving similar error margins using two different reinforcement ratios, the joint shear strength prediction equation based on the gross volume joint reinforcement ratio, as provided in Equation **(4.33)**, was selected for this study.

Table 4.11 summarizes the 'Joint Shear Failure Database', showing the specimens, experimental and predicted joint shear strengths, error and absolute error values and whether the strengths are over or under predicted.

Table 4.11 Joint Shear Failure Database Characteristics

Researcher	Specimen	$v_{j,exp}$ (MPa)	$v_{j,pred}$ (MPa)	Error	Abs. Error	Over / Under
Han & Lee (2022)	HC-JO-U	5.40	6.31	17%	17%	Over
	HC-JX-U	4.62	5.20	13%	13%	Over
Wang et al. (2018)	EJ-2	6.78	7.41	9%	9%	Over
	EJ-3	7.57	7.21	-5%	5%	Under
	EJ-4	5.82	6.20	6%	6%	Over
	EJ-5	7.82	6.80	-13%	13%	Under
	J-1	9.37	10.11	8%	8%	Over
	J-2	10.26	10.27	0%	0%	Over
	J-3	9.52	10.16	7%	7%	Over
	J-4	9.48	10.34	9%	9%	Over
Zhang et al. (2022)	IS1	8.93	7.82	-12%	12%	Under
	IS2	8.02	7.82	-2%	2%	Under
Jiuru et al. (1992)	SF1	3.72	3.25	-13%	13%	Under
	SF2	4.38	4.25	-3%	3%	Under
	SF6	3.90	4.31	10%	10%	Over
	SF7	4.56	4.50	-1%	1%	Under
	SF8	5.22	6.32	21%	21%	Over
	SF9	3.88	4.31	11%	11%	Over
Parra-Montesinos et al. (2005)	1	5.25	5.89	12%	12%	Over
	2	6.63	6.14	-7%	7%	Under
Sarmah et al. (2017)	SF1	3.60	3.70	3%	3%	Over
	SF2	4.15	4.59	10%	10%	Over
Liang & Lu (2017)	ECCBCS-1	8.13	8.79	8%	8%	Over
	ECCBCS-2	8.72	8.79	1%	1%	Over
	ECCBCS-3	9.12	8.79	-4%	4%	Under
	ECCBCS-4	9.70	8.79	-9%	9%	Under
Röhm et al. (2012)	SP-6-3	6.95	5.55	-20%	20%	Under

Table 4.11 (Cont'd)

Researcher	Specimen	$v_{j,exp}$ (MPa)	$v_{j,pred}$ (MPa)	Error	Abs. Error	Over / Under
Chidambaram & Agarwal (2015)	SJ3	5.68	5.75	1%	1%	Over
	SJ5	6.70	6.42	-4%	4%	Under
	SJ6	5.89	5.90	0%	0%	Over
Liang et al. (2016)	FRCJ1	7.98	7.59	-5%	5%	Under
	FRCJ2	6.36	7.33	15%	15%	Over
	FRCJ3	7.04	7.35	4%	4%	Over
	FRCJ4	7.98	7.65	-4%	4%	Under
	FRCJ5	8.41	7.76	-8%	8%	Under
	FRCJ6	7.59	7.59	0%	0%	Under
	FRCJ7	7.76	7.59	-2%	2%	Under
Kheni et al. (2015)	2	3.73	3.55	-5%	5%	Under
	3	3.86	3.70	-4%	4%	Under
	4	3.84	3.62	-6%	6%	Under
Bayasi & Gebman (2002)	Joint #1	5.20	4.17	-20%	20%	Under
	Joint #2	4.79	4.17	-13%	13%	Under
	Joint #4	4.85	4.17	-14%	14%	Under
	Joint #5	4.35	4.17	-4%	4%	Under
Shi et al. (2021)	BCJ1	9.14	8.95	-2%	2%	Under
	BCJ2	8.03	8.85	10%	10%	Over
	BCJ3	9.48	9.46	0%	0%	Under
	BCJ4	8.10	8.25	2%	2%	Over
	BCJ5	8.64	8.63	0%	0%	Under
	BCJ6	8.72	8.67	-1%	1%	Under
Tsonos et al. (2021)	SFJ1	2.77	2.74	-1%	1%	Under
Filiatrault et al. (1995)	S3	8.19	7.78	-5%	5%	Under
Filiatrault et al. (1994)	S3	4.06	4.24	4%	4%	Over
	S4	5.04	5.31	5%	5%	Over

Table 4.11 (Cont'd)

Researcher	Specimen	$v_{j,exp}$ (MPa)	$v_{j,pred}$ (MPa)	Error	Abs. Error	Over / Under
Sano et al. (2015)	No. 25	9.44	10.24	8%	8%	Over
Yamada et al. (2016)	No. 26	9.20	11.35	23%	23%	Over
	No. 27	9.61	9.99	4%	4%	Over
	No. 28	11.87	10.65	-10%	10%	Under
	No. 29	13.25	10.87	-18%	18%	Under
Hanif & Kanakubo (2017)	No. 30	11.19	10.12	-10%	10%	Under
	No. 31	10.19	10.14	0%	0%	Under
Mu et al. (2018)	No. 32	9.49	9.90	4%	4%	Over
	No. 33	9.63	9.79	2%	2%	Over
Gefken & Ramey (1989)	JB1	5.75	4.79	-17%	17%	Under
	JC1	5.62	4.67	-17%	17%	Under
	JD1	7.31	5.92	-19%	19%	Under
	JE1	6.72	5.43	-19%	19%	Under
Gencoglu (2000)	3	2.37	2.13	-10%	10%	Under
	5	2.33	2.39	3%	3%	Over
	6	2.50	2.63	5%	5%	Over
	8	2.24	2.59	15%	15%	Over
	9	2.20	2.63	20%	20%	Over
	10	2.31	2.16	-7%	7%	Under
Van & Trung (2019)	S2	8.59	8.02	-7%	7%	Under
	S3	9.00	8.02	-11%	11%	Under
Marthong & Marthong (2016)	BWFSF	3.14	3.18	1%	1%	Over
	BWSSF	3.14	3.18	1%	1%	Over
	CWSSF	3.16	2.19	-31%	31%	Under
Tingting et al. (2022)	F-1	8.92	9.09	2%	2%	Over
	F-2	8.83	9.09	3%	3%	Over
	F-3	9.22	9.09	-1%	1%	Under
	F-4	9.26	9.09	-2%	2%	Under
	F-5	8.83	9.09	3%	3%	Over
	F-6	9.18	9.09	-1%	1%	Under
Patel et al. (2013)	NDS2	4.97	5.74	15%	15%	Over
	DS3S2	6.16	5.74	-7%	7%	Under

Table 4.11 (Cont'd)

Researcher	Specimen	$v_{j,exp}$ (MPa)	$v_{j,pred}$ (MPa)	Error	Abs. Error	Over / Under
Gao et al. (2014)	JDZ0.3-0.5-0.6	8.20	8.86	8%	8%	Over
	JDZ0.3-1.0-0	8.71	8.63	-1%	1%	Under
	JDZ0.2-1.0-0	8.27	8.25	0%	0%	Under
	JDZ0.4-1.0-0	9.01	8.67	-4%	4%	Under
Lu & Liang (2020)	BC-2	8.86	8.46	-5%	5%	Under
	BC-3	8.42	8.46	0%	0%	Over
Choi & Bae (2019)	JNR-1-BTR	4.91	4.51	-8%	8%	Under
	JNR-2-BTR	5.72	5.39	-6%	6%	Under
	JTR-1-BNR	5.82	5.11	-12%	12%	Under
	JTR-2-BNR	6.14	6.41	4%	4%	Over
Banu et al. (2022)	Type B	5.17	4.72	-9%	9%	Under
	Type C	6.27	4.91	-22%	22%	Under
Said & Razak (2016)	ECC	9.23	9.62	4%	4%	Over
Said (2016)	ECC	9.36	9.28	-1%	1%	Under
Said (2017)	ECC	11.25	9.93	-12%	12%	Under
Liu (2006)	SF-2	2.96	2.59	-12%	12%	Under
	SF-3	2.92	3.38	16%	16%	Over
	SF-4	3.29	3.38	3%	3%	Over
	SF-5	3.12	3.41	9%	9%	Over
Said (2016)	PVA1	8.75	9.26	6%	6%	Over
	PVA2	9.36	9.62	3%	3%	Over
	PVA3	11.25	9.93	-12%	12%	Under
	PVA4	10.19	10.23	0%	0%	Over
	PVA5	11.34	11.45	1%	1%	Over
	PVA6	11.91	12.67	6%	6%	Over
	PE1	9.32	9.28	0%	0%	Under
	PE2	10.40	9.91	-5%	5%	Under
	PE3	12.28	10.21	-17%	17%	Under
	PE4	12.64	10.89	-14%	14%	Under
	PE5	13.51	11.88	-12%	12%	Under
	PE6	14.42	12.34	-14%	14%	Under

4.4 Comparison of the Proposed Equation with Previous Studies

The developed joint shear equation has a remarkably low average absolute error of 7.69%. To evaluate its effectiveness and accuracy, the results obtained from Equation 4.33 are compared with equations and code approaches found in the literature.

4.4.1 Comparison with Code Requirements

In the literature, there are currently no specific code requirements for determining the shear strength of FRCC beam-to-column joints. Although, the existing codes such as TSC2018 (TSC2018, 2018), ACI 318-19 (ACI 318-19, 2019) and ACI 352-02 (ACI 352-02, 2002) are applicable to reinforced concrete joints, their recommendations will be compared with the proposed equation using the composite strength. Since these codes do not consider the fiber contribution to the capacity, underestimation of the joint shear strength is expected.

The data presented in Table 4.12 summarizes the comparison of the proposed prediction equation and three building codes, namely TSC2018 (TSC2018, 2018), ACI 352-02 (ACI 352-02, 2002), and ACI 318-19 (ACI 318-19, 2019). The assessment is based on the average absolute error (AAE), which serves as a measure of accuracy.

Table 4.12 Comparison of proposed equation with building code requirements.

Parameters	Proposed	TSC2018	ACI 352-02	ACI 318-19
AAE	7.69%	29.16%	31.09%	29.16%
R	0.97	0.64	0.62	0.68
R^2	0.94	0.42	0.38	0.46
#Over	51	55	62	70
#Under	66	62	55	47
#Total	117	117	117	117

Figure 4.14 presents a comparison between the prediction equation and the code requirements, in addition to the comparison of code predictions within themselves.

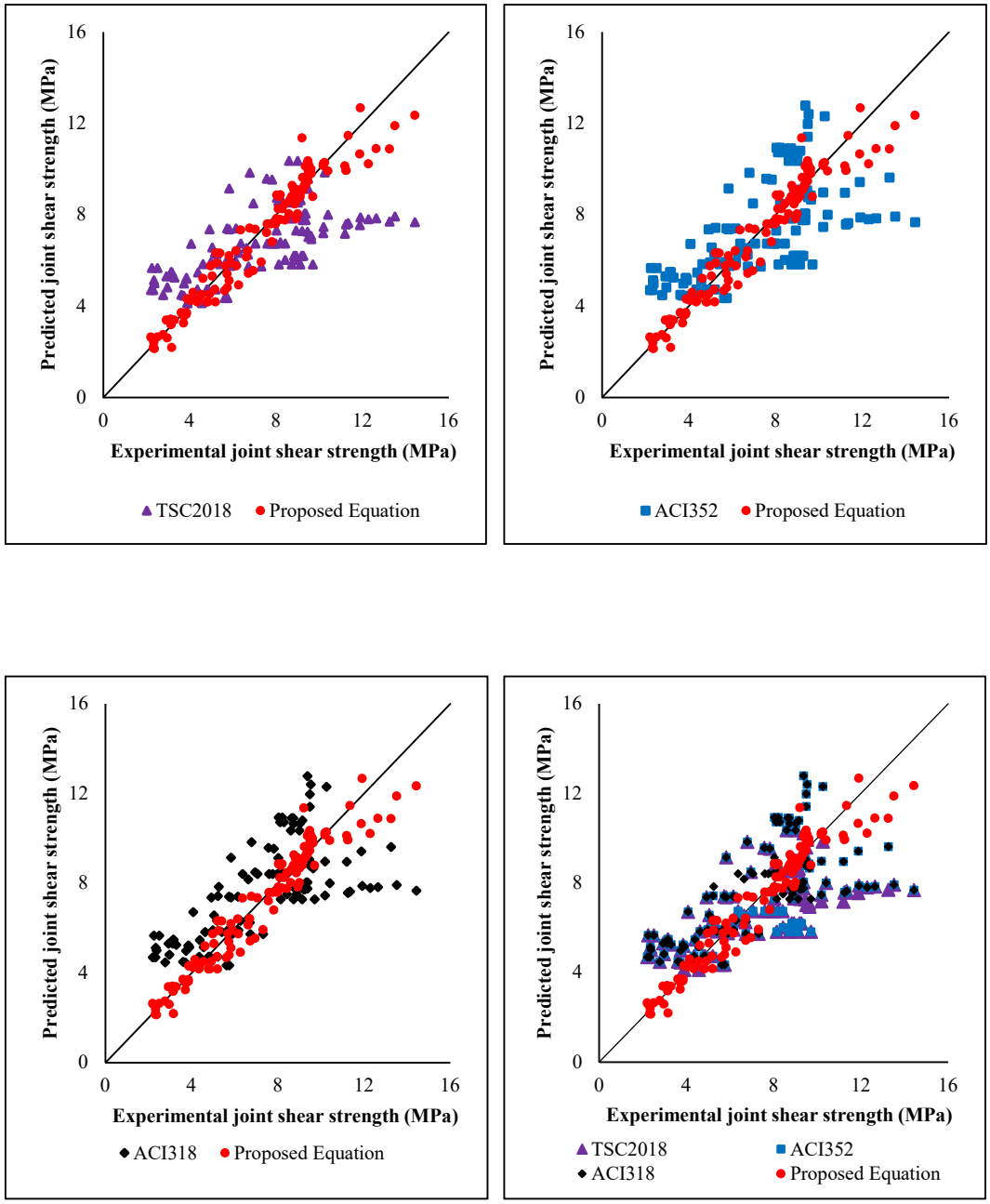

Figure 4.14. Comparison of predictions by proposed equation and design codes.

From Table 4.12 and Figure 4.14 it can be observed that the codes do not underestimate the joint shear strength. The error margins for the code predictions are high with a significant scatter of data, which reveals the need for new requirements adjusted to take into account the fiber contribution to the shear capacity.

Furthermore, the correlation coefficient (R) and coefficient of determination (R^2) are employed as indicators of the linear relationship between predicted and experimental values. Higher R and R^2 values represent a better fit to the experimental data. In this regard, the proposed equation demonstrates a higher R value of 0.97 and a higher R^2 value of 0.94, indicating a stronger correlation and a better overall fit in comparison to the code requirements.

Additionally, the table presents the number of overestimated and underestimated joint strength values by each method. Notably, the proposed equation exhibits the lowest number of overestimations (51) and the highest number of underestimations (66), signifying a tendency to slightly underestimate the joint shear strength as intended. This conservative approach enhances safety considerations by accounting for uncertainties and variations in real-world scenarios.

In conclusion, the results affirm that the building code requirements for reinforced concrete joints cannot directly be applied to FRCC beam-to-column joints, whereas the proposed equation provides significant accuracy, correlation and conservative estimations of the joint shear strength, which supports the need for building code requirements for predicting the joint shear strength.

4.4.2 Comparison with Other Prediction Equations

In this section, the proposed equation will be compared with other equations developed for predicting the joint shear strength of FRCC beam-to-column joints. Most of the existing joint shear strength prediction equations are developed solely for steel fiber reinforced composite (SFRC) joints. Figure 4.15 showcases the verification of steel SFRC specimens through a comparison of 63 specimens.

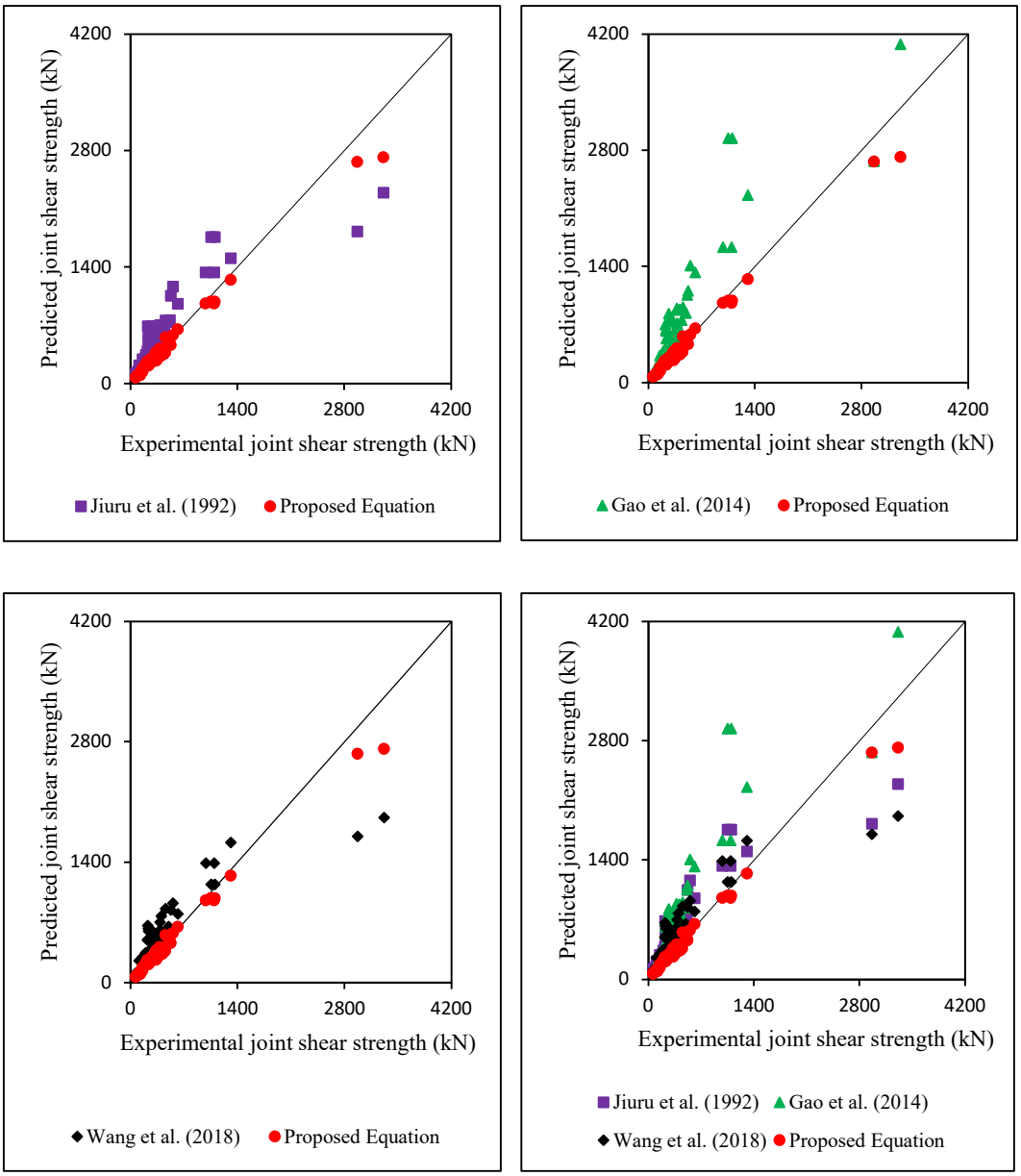

Figure 4.15. Comparison between the proposed equation and existing equations.

For SFRCC joints, as can be observed from Figure 4.15, the equations developed by other researchers tend to exhibit a tendency towards overestimation, which is not conservative. Zhang et al. (2022), also stated that the equations proposed by Gao et al. (2014) and Jiuru et al. (1992) often lead to an overestimation of the shear strength of steel FRCC beam-to-column joints.

The proposed equation has the highest accuracy and the least scatter in data, which demonstrates its reliability in predicting the shear strength of FRCC beam-to-column joints. Another advantage of the proposed prediction equation is that it can be used for FRCC joints constructed with any fiber type.

The shear strength prediction equations for FRCC joints constructed with any other fiber type are limited. Tingting et al. (2022) proposed a model for PVA-HPFRCC beam-to-column connection specimens including transverse beams and slab. The results of the Table 4.13 indicate that the proposed equation in this study, when compared to the prediction equation by Tingting et al. (2022), provides a more reliable estimation of joint shear strength, as it shows a smaller deviation from the experimental values. This implies that the proposed equation has a higher level of accuracy and precision in predicting the joint shear strength of the beam-to-column connections under consideration. Since TB and ε_t parameters were not defined in the article by Tingting et al. (2022), only the six specimens reported in the study are used for comparison. The only modification was the effective joint width taken as per ACI 318-19, as defined in Figure 2.3, to facilitate the comparison with the proposed equation.

Table 4.13 Comparison of proposed equation and the prediction by Tingting et al. (2022)

Specimen	**$V_{j,exp}$ (MPa)**	**$V_{j,proposed}$ (MPa)**	**$V_{j,Tingting}$ (MPa)**	**$AAE_{proposed}$**	**$AAE_{Tingting}$**
F1	8,92	9,09	8,20	2%	8%
F2	8,83	9,09	8,23	3%	7%
F3	9,22	9,09	8,51	1%	8%
F4	9,26	9,09	8,79	2%	5%
F5	8,83	9,09	8,46	3%	4%
F6	9,18	9,09	8,54	1%	7%
			Average:	**2%**	**6%**

The proposed equation in this study does not explicitly incorporate the influence of transverse beam and slab although these members will provide additional confinement to the joint. Despite this simplification, the proposed equation gives lower average absolute errors and standardized residuals when compared to the equation developed by Tingting et al. This finding indicates that the proposed equation captures and incorporates the relevant parameters and their effects on joint shear strength in an accurate manner.

CHAPTER 5

JOINT SHEAR STRESS vs. DEFORMATION RELATIONSHIP

5.1 Overview

The significance of joint shear deformation, particularly the joint shear strain, in the seismic behavior of beam-to-column joints is indisputable. These joints undergo substantial shear forces and experience significant deformations during seismic loading, affecting their structural response and potential failure mechanisms. The joint shear strain governs critical aspects such as load transfer mechanisms, energy absorption capacity, and overall seismic performance. Therefore, accurately predicting joint shear strain is essential for assessing the joint's capacity to withstand seismic forces, ensuring the structural integrity of the system. Thus, a thorough understanding and consideration of joint shear deformation are vital in promoting seismic resilience and ensuring adequate beam-to-column joint behavior.

Moreover, the proper evaluation of joint shear deformation plays a significant role in the overall seismic response of beam-to-column joints. By comprehending the relationship between shear forces and deformation, it is possible to interpret the load redistribution mechanisms and energy dissipation characteristics during seismic loading. Accurate prediction of joint shear strain enables a more comprehensive assessment of the joint performance under seismic forces, aiding in the design and evaluation of robust systems.

This chapter focuses on the modeling of beam-to-column connections, specifically examining their joint shear stress versus shear strain behavior. The initial step involves examining the experimental results and extracting the performance points, which represent key points for joint shear stress vs. shear strain values. It is important to note that the joint shear database provides limited data for this analysis, as joint

shear deformations or strains were not commonly recorded during testing, unlike the abundance of data available for joint shear strength estimations.

For each performance point, separate prediction equations are formulated and compared to the experimental data. The accuracy and reliability of the model are then assessed through a comprehensive verification process using the experimental results. The findings validate the accuracy of the developed model in capturing the joint shear stress versus deformation relationship.

5.2 Specimen Selection Criteria

The joint shear database consists of 117 specimens; however, only 36 specimens provide the joint shear stress versus shear deformation behavior. Moreover, among the 36 specimens with available data, only 30 specimens exhibited joint shear failure, while the remaining specimens failed due to beam flexural failure. Since the purpose of this study is to capture the joint shear behavior accurately, specimens that experienced beam flexural failure were not considered in the modeling process. Consequently, the modeling focused on a subset of 30 specimens that demonstrated joint shear failure.

5.3 Performance Points

To obtain the relationship between joint shear stress and deformation, five performance points were defined: cracking point, the onset of inelastic activity, the initial point of the plateau region, where the maximum strength is reached, the termination point of the plateau region, and the final point. Figure 5.1 demonstrates the points considered in this study.

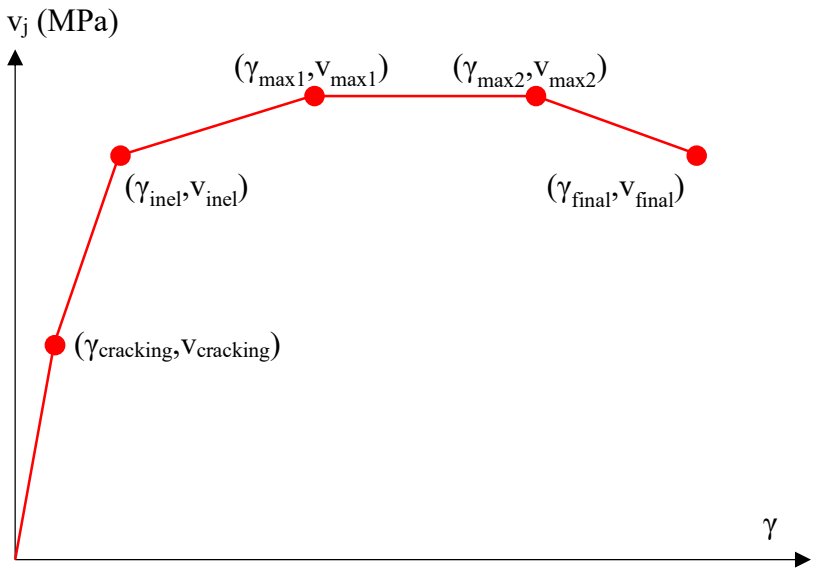

Figure 5.1. The performance points of the shear stress vs. deformation model.

5.3.1 Performance Points

In this section, each performance point will be elaborated in terms of definitions, and prediction equations. The key parameter of this modeling approach is the maximum joint shear strength obtained from the prediction equation, which predicts the maximum stress that a beam-to-column joint made of FRCC can be subjected to.

5.3.1.1 Definition of Performance Points

5.3.1.1.1 Cracking Point

At the cracking point, $(\gamma_{cracking},v_{cracking})$, micro-cracks begin to form within the joint due to the applied shear stress. Before reaching this point, the joint exhibits a linear shear stress vs. deformation relationship, with an increasing slope indicating the elastic behavior. However, as the cracking point is reached, there is a slight reduction in the slope of the curve, indicating the initiation of micro-crack formation. This

transition marks a departure from the linear behavior and signifies the onset of nonlinearity in the joint shear stress vs. strain response.

5.3.1.1.2 Onset of Inelastic Activity

The onset of inelastic activity, (γ_{inel},v_{inel}), is characterized by a significant reduction in the slope of the curve compared to the cracking point. At this point, the material undergoes a notable increase in plastic deformation, resulting in a more pronounced deviation from the initial linear relationship. The reduction in slope signifies a greater departure from the linear elastic behavior and indicates the transition to a nonlinear response, where the joint experiences permanent deformation and exhibits inelastic behavior.

5.3.1.1.3 Initial Point of The Plateau

The initial point of the plateau, (γ_{max1},v_{max1}), represents the location where the maximum shear stress is initially reached and maintained throughout the plateau region. It signifies the point at which the joint reaches its peak shear strength. This plateau continues until the termination point of the plateau, which marks the end of the sustained shear stress level. The region between the initial and termination points represents a relatively constant shear stress level.

5.3.1.1.4 Termination Point of The Plateau

The termination point of the plateau, (γ_{max2},v_{max2}), denotes the point at which the sustained shear stress level in the joint starts to reduce. It signifies the end of the stable phase where the shear stress remains relatively constant within the plateau region. Beyond this point, the joint may experience further deformation or failure, leading to a decline in the shear stress. In other words, any subsequent increase in

strain may result in a reduction of shear stress and potential structural damage or failure.

5.3.1.1.5 Final Point

The final point on the shear stress vs. shear strain graph, (γ_{final},v_{final}), represents the endpoint of the joint's response to the applied shear stress. After the termination of the plateau phase, the shear stress gradually reduces towards the final point. This reduction in shear stress is accompanied by a notable increase in the joint shear deformation, indicating a progressive deterioration of the joint's structural integrity.

5.3.1.2 Prediction of the Performance Points

The determination of relationships and the corresponding prediction equations for the performance points in the shear stress vs. deformation behavior of FRCC beam-to-column joints is a vital aspect of comprehending their structural response. In this study, a systematic approach was employed to establish these relationships and equations. Initially, the performance points were extracted from relevant experimental data for the 30 specimens under consideration. These points, including the cracking point, onset of inelasticity, plateau initial point, plateau termination point, and final point, were digitized using Engauge Digitizer Software (Mitchell, 2019), converting them into numerical data for further investigation. The digitization process involved obtaining the stress and strain values corresponding to selected five performance points.

Figure 5.2 demonstrates the process of determining the performance points for a given specimen. This illustration serves as a visual representation of the methodology employed to identify and locate the key points on the joint shear stress vs. deformation curve. By accurately pinpointing these performance points, a comprehensive understanding of the specimen's behavior and its response to applied shear stress can be obtained.

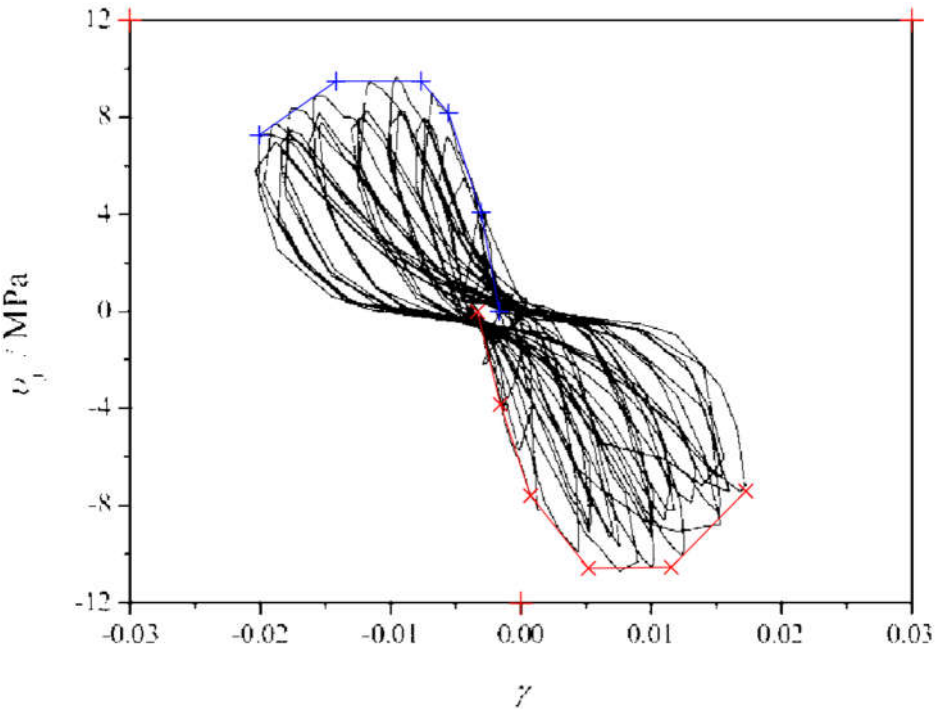

Figure 5.2. Digitization of the hysteresis curve using Engauge Digitizer.

Upon implementing the aforementioned process on all 30 specimens, the resulting data presented in Table 5.1 and Table 5.2 are derived. These tables serve as a comprehensive compilation of the performance points obtained for each specimen, comprising of the essential information regarding the joint shear stress vs. deformation behavior.

Table 5.1 Digitized joint shear stress values.

Researcher	Specimen	Experimental Joint Shear Stress (MPa)				
		Cracking	Inelastic	Max1	Max2	Final
Parra-Montesinos et al. (2005)	1	2.36	4.68	5.25	-	-
	2	3.25	6.10	6.63	6.63	5.67
Tingting et al. (2022)	F-1	3.67	6.37	8.92	8.92	6.14
	F-2	4.33	6.43	8.83	8.83	5.89
	F-3	3.37	7.08	9.22	9.22	5.68
	F-4	3.56	7.59	9.26	9.26	8.00
	F-5	3.44	7.30	8.83	8.83	6.52
	F-6	3.18	6.31	9.18	9.18	5.87
Lu & Liang (2020)	BC-2	4.37	6.17	8.86	8.86	5.84
	BC-3	3.52	7.70	8.42	8.42	5.74
Han & Lee (2022)	HC-JO-U	1.85	3.48	5.40	5.40	4.06
	HC-JX-U	1.44	3.11	4.62	4.62	3.77
Wang et al. (2018)	EJ-2	1.93	4.35	6.78	6.78	4.10
	EJ-3	2.71	5.17	7.57	7.57	3.63
	EJ-4	1.73	4.41	5.82	5.82	4.95
	EJ-5	2.76	5.18	7.82	7.82	4.90
	J-1	3.82	6.55	9.37	9.37	6.04
	J-2	3.76	6.92	10.26	10.26	5.46
	J-3	2.55	5.42	9.52	9.52	6.24
	J-4	3.44	6.68	9.48	9.48	6.19
Zhang et al. (2021)	IS1	2.72	7.52	8.93	8.93	6.82
	IS2	2.76	7.04	8.02	8.02	6.46
Choi & Bae (2019)	JNR-1-BTR	1.98	4.70	4.91	4.91	3.96
	JNR-2-BTR	2.04	5.03	5.72	5.72	5.41
	JTR-1-BNR	2.47	4.68	5.82	5.82	4.87
	JTR-2-BNR	2.17	5.66	6.14	6.14	4.22
Liu (2006)	SF-2	0.72	2.54	2.96	2.96	2.01
	SF-3	0.92	2.44	2.92	2.92	2.01
	SF-4	1.25	3.01	3.29	3.29	3.10
	SF-5	1.40	2.61	3.12	3.12	1.86

Table 5.2 Digitized joint shear distortion values.

Researcher	Specimen	Experimental Joint Shear Deformation				
		Cracking	Inelastic	Max1	Max2	Final
Parra-Montesinos et al. (2005)	1	1.2E-04	9.2E-04	1.3E-03	-	-
	2	2.7E-04	1.9E-03	3.7E-03	6.1E-03	7.9E-03
Tingting et al. (2022)	F-1	3.7E-03	8.5E-03	1.3E-02	2.0E-02	3.0E-02
	F-2	5.3E-03	1.0E-02	1.5E-02	2.1E-02	2.9E-02
	F-3	2.9E-03	7.2E-03	1.1E-02	1.7E-02	3.1E-02
	F-4	1.8E-03	7.0E-03	1.2E-02	1.8E-02	2.3E-02
	F-5	6.9E-04	5.8E-03	8.9E-03	1.4E-02	2.4E-02
	F-6	1.6E-03	4.0E-03	7.3E-03	1.4E-02	2.0E-02
Lu & Liang (2020)	BC-2	6.3E-03	1.3E-02	1.8E-02	2.6E-02	3.6E-02
	BC-3	5.3E-04	6.9E-03	8.8E-03	1.3E-02	1.8E-02
Han & Lee (2022)	HC-JO-U	3.7E-04	1.1E-03	2.6E-03	6.7E-03	7.8E-03
	HC-JX-U	1.1E-04	6.4E-04	2.2E-03	5.2E-03	1.4E-02
Wang et al. (2018)	EJ-2	2.7E-05	2.0E-04	3.8E-03	4.7E-03	5.5E-03
	EJ-3	1.1E-04	4.9E-04	1.2E-03	1.9E-03	5.3E-03
	EJ-4	2.1E-04	9.2E-04	1.9E-03	3.3E-03	5.6E-03
	EJ-5	2.0E-04	1.2E-03	2.2E-03	4.1E-03	5.4E-03
	J-1	9.3E-05	6.4E-04	1.8E-03	5.4E-03	1.6E-02
	J-2	1.3E-04	7.2E-04	1.6E-03	5.9E-03	2.4E-02
	J-3	3.7E-04	1.3E-03	3.7E-03	6.6E-03	8.7E-03
	J-4	7.0E-05	7.0E-04	1.9E-03	8.9E-03	1.7E-02
Zhang et al. (2021)	IS1	5.2E-04	3.0E-03	6.7E-03	2.4E-02	3.1E-02
	IS2	3.3E-04	1.7E-03	4.5E-03	9.9E-03	1.8E-02
Choi & Bae (2019)	JNR-1-BTR	4.7E-04	1.2E-03	2.0E-03	3.2E-03	7.8E-03
	JNR-2-BTR	5.8E-05	4.8E-04	9.9E-04	4.1E-03	6.8E-03
	JTR-1-BNR	2.3E-04	5.9E-04	1.7E-03	3.4E-03	5.2E-03
	JTR-2-BNR	3.8E-04	5.8E-04	7.8E-04	3.7E-03	7.8E-03
Liu (2006)	SF-2	4.6E-05	3.3E-04	4.8E-04	1.0E-03	1.0E-02
	SF-3	8.0E-05	2.2E-04	7.2E-04	2.2E-03	1.0E-02
	SF-4	5.1E-05	2.3E-04	5.3E-04	1.7E-03	3.6E-03
	SF-5	1.0E-04	2.7E-04	8.7E-04	3.1E-03	1.2E-02

With the obtained numerical data, the subsequent step focused on establishing prediction relationships for each performance point. The goal was to develop mathematical equations that could accurately predict the shear stress and shear strain values at these critical points. Nonlinear regression modeling, along with the software IBM SPSS, was employed to analyze the digitized data and determine the prediction equations.

The initial phase of the analysis involved establishing relationships between the actual stresses and strains obtained from the digitized data. The focus was first directed towards understanding the relationships among different stress values. Then, the relationships among the strain values were investigated.

A substantial correlation among the stresses associated with the five performance points was observed after examining the experimental data. This correlation could be accurately represented by multiplication constants, as indicated in Table 5.3, which presents the average and standard deviation of the stress transformation ratios between different performance points, highlighting the reliability of these relationships. This simplifies the modeling process by eliminating the need for complex prediction equations. It should be emphasized that the value of $\nu_{j,max1}$ is equal to $\nu_{j,max2}$, determined by using the joint shear strength prediction equation introduced in the preceding chapter.

Table 5.3 Statistical parameters for joint shear stress conversions based on tests.

Joint Type	**Parameter**	$\nu_{j,cracking}/\nu_{j,max1}$	$\nu_{j,inelastic}/\nu_{j,max1}$	$\nu_{j,final}/\nu_{j,max1}$
Interior	Average	39%	77%	70%
	Std. Dev.	7%	10%	9%
Exterior	Average	35%	79%	74%
	Std. Dev.	6%	11%	14%

This study prioritizes the development of conversion equations that are both accurate and practical to use. The low standard deviations presented in Table 5.3 further

support the feasibility of these equations. Accordingly, Equations **(5.1)** - **(5.4)** are proposed as conversion equations for the shear stress components for different joint performance points. It should be noted that the proposed conversion equations are applicable to both interior and exterior beam-to-column joints.

$$v_{j,cracking} = (0.35)v_{j,max1} \quad \textbf{(5.1)}$$

$$v_{j,inelastic} = (0.75)v_{j,max1} \quad \textbf{(5.2)}$$

$$v_{j,max2} = (1.00)v_{j,max1} \quad \textbf{(5.3)}$$

$$v_{j,final} = (0.70)v_{j,max1} \quad \textbf{(5.4)}$$

In contrast, the strain values displayed comparatively lower correlation without the inclusion of additional parameters, mainly related to fiber properties. This outcome is expected, as the deformation capacity of FRCC is known to be strongly influenced by key fiber properties. Parameters such as fiber volume fraction, aspect ratio, and mechanical properties play a significant role in determining the shear deformation of FRCC joints. Consequently, as a crucial step in the analysis, the investigation proceeded towards examining the strains and their highly correlated parameters.

The transition from stress estimations to strain estimations involves a fundamental equation that is strategically placed at the point of onset of inelastic activity. This choice is made due to the distinct behavior observed in the joint shear stress vs. deformation graph. Up until this critical point, the graph exhibits a predominantly linear relationship. However, unlike traditional reinforced concrete beam-to-column connections, FRCC beam-to-column connections demonstrate a unique response due to the presence of reinforcing fibers that effectively bridge any developing cracks. Consequently, the slope reduction observed at the cracking point is less pronounced compared to reinforced concrete structures. By specifically selecting the point of onset of inelastic activity as the transition point, we ensure that the first significant

slope reduction in the shear stress vs. shear deformation graph aligns with this critical phase.

To establish the relationship between the predicted shear stress and the experimental shear deformation at the point of onset of cracking, IBM SPSS and its nonlinear regression analysis tools are employed. Through this analysis, Equation **(5.5)**, which effectively captures the joint behavior, is obtained.

$$\gamma_{\mathrm{j,inelastic}} = c_1 . \frac{v_{\mathrm{j,inelastic}}}{2000\sqrt{f'_c}} . \left(\frac{h_b}{b_b}\right) . RI^{c_2} . \left(\frac{h_c}{b_b}\right) . \left(\frac{N}{A_s f_y}\right)_{mod} . \left(1 + 100\rho_{gross}\right)^{c_3} \quad \textbf{(5.5)}$$

In this equation, $v_{j,inel}$ denotes the predicted shear stress at the point of onset of inelastic activity, and is calculated with the combination of Equation **(4.33)** and Equation **(5.2)**, while the rest of the parameters were explained in the previous chapter. The coefficients c_1, c_2 and c_3 are specific coefficients that vary based on the joint type. The corresponding values for these coefficients are provided in Table 5.4.

Table 5.4 Coefficients utilized in the shear distortion prediction equation.

Joint Type	c_1	c_2	c_3
Interior	1.7	0.0	2.0
Exterior	1.0	-0.3	0.5

Note that the flexural strength ratio is an important factor that significantly influences the connection behavior. However, calculation of beam and column moment capacities are impractical for direct inclusion in the prediction equation. Additionally, incorporating the beam's longitudinal bars as a parameter is unfeasible due to their contribution to the shear demand. However, column longitudinal steel area is incorporated into the Equation **(5.5)** by a factor $\left(\frac{N}{A_s f_y}\right)_{mod}$ that is provided in Equation **(5.6)** to account for the influence of the axial load.

$$\left(\frac{N}{A_s f_y}\right)_{mod} = \begin{cases} \left(\frac{N}{A_s f_y}\right)^{0.5} & \text{if } \frac{N}{A_s f_y} \leq 2 \\ \left(\frac{N}{A_s f_y}\right)^{-0.5} & \text{if } \frac{N}{A_s f_y} > 2 \end{cases} \quad \textbf{(5.6)}$$

Following the determination of deformation at the point of onset of inelastic activity, further estimations of deformation at the remaining performance points are obtained through the application of the nonlinear regression method utilizing IBM SPSS. The resulting equations are presented in Equations **(5.7) - (5.10)**.

$$\gamma_{j,cracking} = (0.15)\gamma_{j,inelastic} \quad \textbf{(5.7)}$$

$$\gamma_{j,max1} = \begin{cases} (1.75)\gamma_{j,inelastic} & \text{for interior joints} \\ (2.75)\gamma_{j,inelastic} & \text{for exterior joints} \end{cases} \quad \textbf{(5.8)}$$

$$\gamma_{j,max2} = \begin{cases} (2.25)RI^{0.1}\gamma_{j,inelastic} & \text{for interior joints} \\ (7.25)RI^{0.1}\gamma_{j,inelastic} & \text{for exterior joints} \end{cases} \quad \textbf{(5.9)}$$

$$\gamma_{j,final} = \begin{cases} (4.00)\gamma_{j,inelastic} & \text{for interior joints} \\ (15.0)\gamma_{j,inelastic} & \text{for exterior joints} \end{cases} \quad \textbf{(5.10)}$$

5.4 Analytical Model

By considering the parameters that have an influence on the shear stress versus shear strain behavior of FRCC joints, an analytical model has been formulated to accurately predict the performance points.

Equations **(5.11)** and **(5.12)** provide the proposed equations formulated for the prediction of stress and strain components of performance points, respectively.

$$v_{j,max1} = \sigma_{cc}\left[1 + \left(0.30\frac{N}{f_c{}'A_g}\right)\right]\left[\gamma\left(\frac{b_b}{h_b}\right)^{1.1}\left(\frac{b_c}{h_c}\right)^{0.2}\left(\frac{h_c}{b_b}\right)^{0.7} RI^{\alpha} + 2\left(\rho_{gross}\right)^{0.5} RI^{\beta}\right]$$

$$v_{j,cracking} = (0.35)v_{j,max1}$$

$$v_{j,inelastic} = (0.75)v_{j,max1} \qquad \textbf{(5.11)}$$

$$v_{j,max2} = (1.00)v_{j,max1}$$

$$v_{j,final} = (0.70)v_{j,max1}$$

$$\gamma_{j,inelastic} = c_1.\frac{v_{j,inelastic}}{2000\sqrt{f_c'}}.BAR.RI^{c_2}.JAR.\left(\frac{N}{A_s f_y}\right)_{mod}.\left(1 + 100\rho_{gross}\right)^{c_3}$$

$$\gamma_{j,cracking} = (0.15)\gamma_{j,inelastic}$$

$$\gamma_{j,max1} = \begin{cases}(1.75)\gamma_{j,inelastic} & \text{for interior joints}\\ (2.75)\gamma_{j,inelastic} & \text{for exterior joints}\end{cases} \qquad \textbf{(5.12)}$$

$$\gamma_{j,max2} = \begin{cases}(2.25)RI^{0.1}\gamma_{j,inelastic} & \text{for interior joints}\\ (7.25)RI^{0.1}\gamma_{j,inelastic} & \text{for exterior joints}\end{cases}$$

$$\gamma_{j,final} = \begin{cases}(4.00)\gamma_{j,inelastic} & \text{for interior joints}\\ (15.0)\gamma_{j,inelastic} & \text{for exterior joints}\end{cases}$$

5.5 Verification of the Developed Model

To verify the accuracy of the proposed model, a thorough comparison was performed between the predicted results, given in Table 5.5 and Table 5.6, obtained from the model equations given in Equations **(5.11)** & **(5.12)**, and the corresponding experimental test data, provided in Table 5.1 and Table 5.2. The close agreement and consistency observed between the predicted and actual results serve as a strong verification of the reliability and effectiveness of the proposed model in capturing the shear stress versus shear strain behavior of FRCC joints.

Table 5.5 Predicted joint shear stress values.

Researcher	Specimen	Predicted Joint Shear Stress (MPa)				
		Cracking	Inelastic	Max1	Max2	Final
Parra-Montesinos et al. (2005)	1	2.06	4.41	5.87	5.87	4.11
	2	2.14	4.59	6.12	6.12	4.29
Tingting et al. (2022)	F-1	3.13	6.70	8.93	8.93	6.25
	F-2	3.13	6.70	8.93	8.93	6.25
	F-3	3.13	6.70	8.93	8.93	6.25
	F-4	3.13	6.70	8.93	8.93	6.25
	F-5	3.13	6.70	8.93	8.93	6.25
	F-6	3.13	6.70	8.93	8.93	6.25
Lu & Liang (2020)	BC-2	2.92	6.25	8.34	8.34	5.84
	BC-3	2.92	6.25	8.34	8.34	5.84
Han & Lee (2022)	HC-JO-U	2.19	4.69	6.25	6.25	4.38
	HC-JX-U	1.80	3.86	5.15	5.15	3.61
Wang et al. (2018)	EJ-2	2.54	5.43	7.25	7.25	5.07
	EJ-3	2.47	5.29	7.05	7.05	4.94
	EJ-4	2.14	4.58	6.11	6.11	4.28
	EJ-5	2.35	5.03	6.71	6.71	4.70
	J-1	3.49	7.48	9.97	9.97	6.98
	J-2	3.52	7.54	10.05	10.05	7.03
	J-3	3.51	7.52	10.02	10.02	7.01
	J-4	3.54	7.59	10.12	10.12	7.08
Zhang et al. (2021)	IS1	2.73	5.85	7.80	7.80	5.46
	IS2	2.73	5.85	7.80	7.80	5.46
Choi & Bae (2019)	JNR-1-BTR	1.57	3.37	4.49	4.49	3.14
	JNR-2-BTR	1.88	4.03	5.37	5.37	3.76
	JTR-1-BNR	1.78	3.82	5.09	5.09	3.56
	JTR-2-BNR	2.23	4.78	6.38	6.38	4.47
Liu (2006)	SF-2	0.90	1.94	2.58	2.58	1.81
	SF-3	1.18	2.53	3.37	3.37	2.36
	SF-4	1.18	2.53	3.37	3.37	2.36
	SF-5	1.19	2.55	3.40	3.40	2.38

Table 5.6 Predicted joint shear deformation values.

Researcher	Specimen	Predicted Joint Shear Deformation				
		Cracking	Inelastic	Max1	Max2	Final
Parra-Montesinos et al. (2005)	1	1.6E-04	1.1E-03	1.8E-03	3.1E-03	4.2E-03
	2	1.8E-04	1.2E-03	2.1E-03	3.6E-03	4.9E-03
Tingting et al. (2022)	F-1	1.2E-03	7.7E-03	1.4E-02	2.1E-02	3.1E-02
	F-2	1.2E-03	7.7E-03	1.4E-02	2.1E-02	3.1E-02
	F-3	8.4E-04	5.6E-03	9.9E-03	1.5E-02	2.3E-02
	F-4	8.0E-04	5.3E-03	9.3E-03	1.4E-02	2.1E-02
	F-5	9.6E-04	6.4E-03	1.1E-02	1.7E-02	2.6E-02
	F-6	8.2E-04	5.5E-03	9.6E-03	1.5E-02	2.2E-02
Lu & Liang (2020)	BC-2	9.0E-04	6.0E-03	1.1E-02	1.6E-02	2.4E-02
	BC-3	9.0E-04	6.0E-03	1.1E-02	1.6E-02	2.4E-02
Han & Lee (2022)	HC-JO-U	1.2E-04	7.9E-04	2.2E-03	6.9E-03	1.2E-02
	HC-JX-U	9.2E-05	6.1E-04	1.7E-03	5.3E-03	9.2E-03
Wang et al. (2018)	EJ-2	3.7E-05	2.5E-04	6.8E-04	1.8E-03	3.7E-03
	EJ-3	3.8E-05	2.5E-04	7.0E-04	1.8E-03	3.8E-03
	EJ-4	5.6E-05	3.7E-04	1.0E-03	2.6E-03	5.6E-03
	EJ-5	5.9E-05	3.9E-04	1.1E-03	2.8E-03	5.9E-03
	J-1	9.5E-05	6.3E-04	1.1E-03	1.4E-03	2.5E-03
	J-2	8.0E-05	5.3E-04	9.3E-04	1.2E-03	2.1E-03
	J-3	1.2E-04	8.0E-04	1.4E-03	1.8E-03	3.2E-03
	J-4	1.0E-04	6.7E-04	1.2E-03	1.5E-03	2.7E-03
Zhang et al. (2021)	IS1	2.6E-04	1.7E-03	3.0E-03	3.8E-03	6.9E-03
	IS2	2.6E-04	1.7E-03	3.0E-03	3.7E-03	6.8E-03
Choi & Bae (2019)	JNR-1-BTR	5.7E-05	3.8E-04	1.0E-03	2.6E-03	5.7E-03
	JNR-2-BTR	5.6E-05	3.7E-04	1.0E-03	2.7E-03	5.6E-03
	JTR-1-BNR	8.9E-05	5.9E-04	1.6E-03	4.1E-03	8.9E-03
	JTR-2-BNR	9.1E-05	6.0E-04	1.7E-03	4.5E-03	9.1E-03
Liu (2006)	SF-2	4.6E-05	3.1E-04	8.4E-04	2.1E-03	4.6E-03
	SF-3	4.4E-05	3.0E-04	8.1E-04	2.2E-03	4.4E-03
	SF-4	3.0E-05	2.0E-04	5.5E-04	1.4E-03	3.0E-03
	SF-5	3.0E-05	2.0E-04	5.5E-04	1.4E-03	3.0E-03

By comparing the experimental and predicted joint shear stresses presented in Table 5.1 & Table 5.5, and examining the experimental and predicted joint shear deformations in Table 5.2 & Table 5.6, a considerable level of correlation is observed. The correlations between the experimental and predicted values for each performance point are visually depicted in Figure 5.3 and Figure 5.4, respectively. These figures provide an illustration of the strong alignment between the observed and estimated behaviors, further validating the accuracy and reliability of the proposed model. It is important to note that measuring shear deformations during the tests presents inherent challenges, which naturally result in a higher expected error compared to the measurement of joint shear stresses. Nevertheless, the substantial agreement between the experimental and predicted values provides strong evidence for the efficiency of the proposed model in accurately capturing the behavior of the joints.

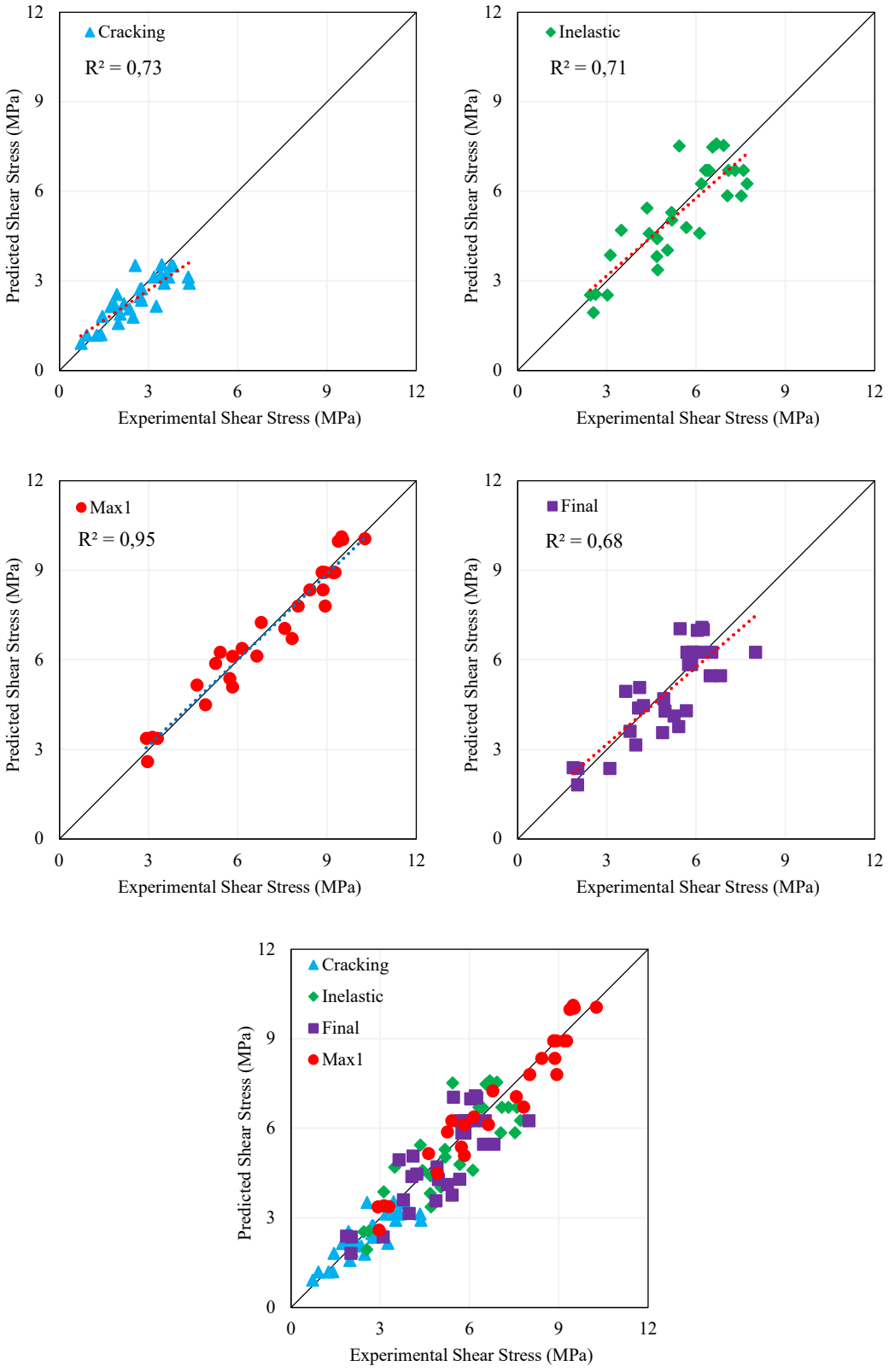

Figure 5.3. Comparison of predicted and experimental shear stresses.

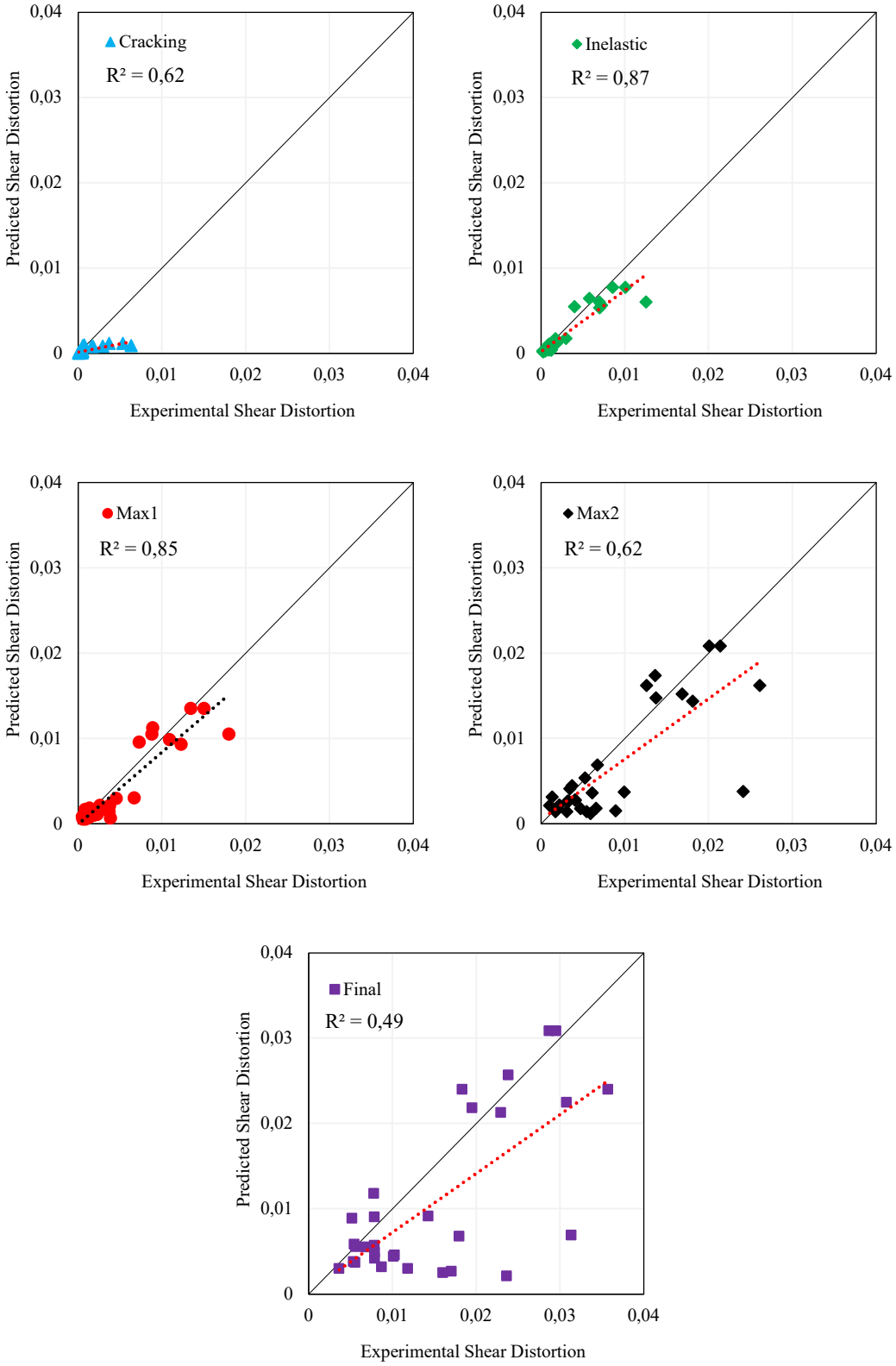

Figure 5.4. Comparison of predicted and experimental shear distortions.

Table 5.7 provides a comprehensive overview of the percent errors, for exterior and interior joints, at each performance point in terms of both shear stresses and shear distortions. As anticipated, the error associated with the stress predictions is significantly lower compared to the strain predictions. This discrepancy can be attributed to the inherent challenges in accurately measuring and predicting shear deformations. Nonetheless, the relatively lower errors for the stress predictions further affirm the robustness and effectiveness of the proposed model.

Table 5.7 Errors in predicting the shear stresses and distortions in each performance point.

Performance Point	**Error in the Stress Predictions**			**Error in the Distortion Predictions**		
	Exterior Joints	**Interior Joints**	**Overall**	**Exterior Joints**	**Interior Joints**	**Overall**
Cracking	18%	14%	16%	51%	50%	51%
Inelastic	16%	13%	14%	25%	22%	25%
Max1	9%	5%	7%	36%	32%	36%
Max2	9%	4%	7%	35%	42%	35%
Final	18%	12%	15%	39%	42%	39%

Predicting the cracking strain with high precision poses a significant difficulty due to the fiber contribution at the point of crack initiation. Nevertheless, the overall strain errors remain relatively low, which is a noteworthy outcome given the expected complexity in strain estimation. Furthermore, the estimation of the final distortion presents its own set of challenges as it depends extensively on the fiber contribution. Despite these difficulties, Table 5.7 indicates that even the error in the final shear distortion estimation is acceptable.

Figure 5.5 and Figure 5.6 provide comparisons of the predicted versus experimental shear stress versus distortion relationships. By comparing the predicted and experimental graphs, the accuracy and reliability of the proposed model can be evaluated.

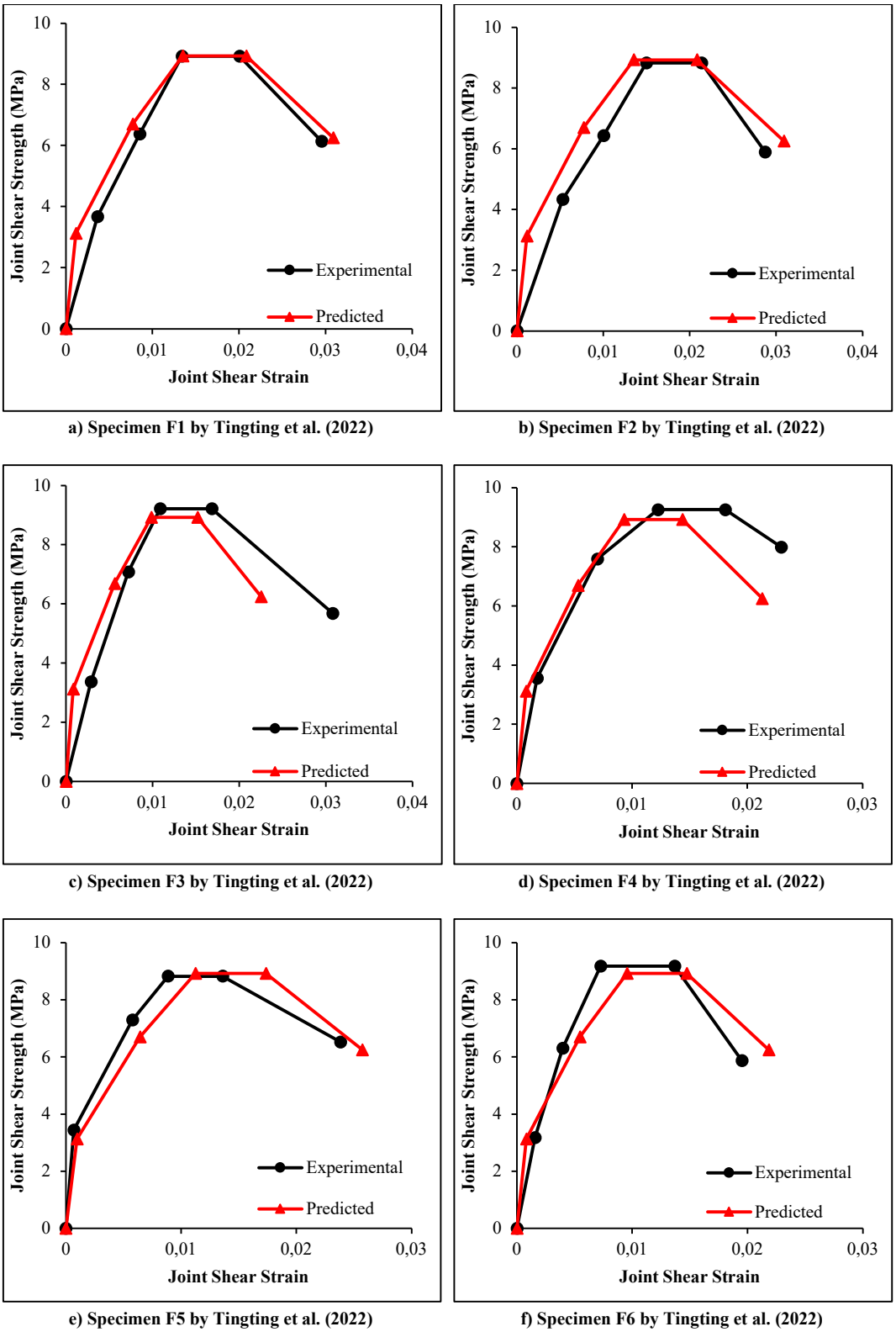

Figure 5.5. Comparison of predicted & experimental data for specimens of Tingting et al. (2022)

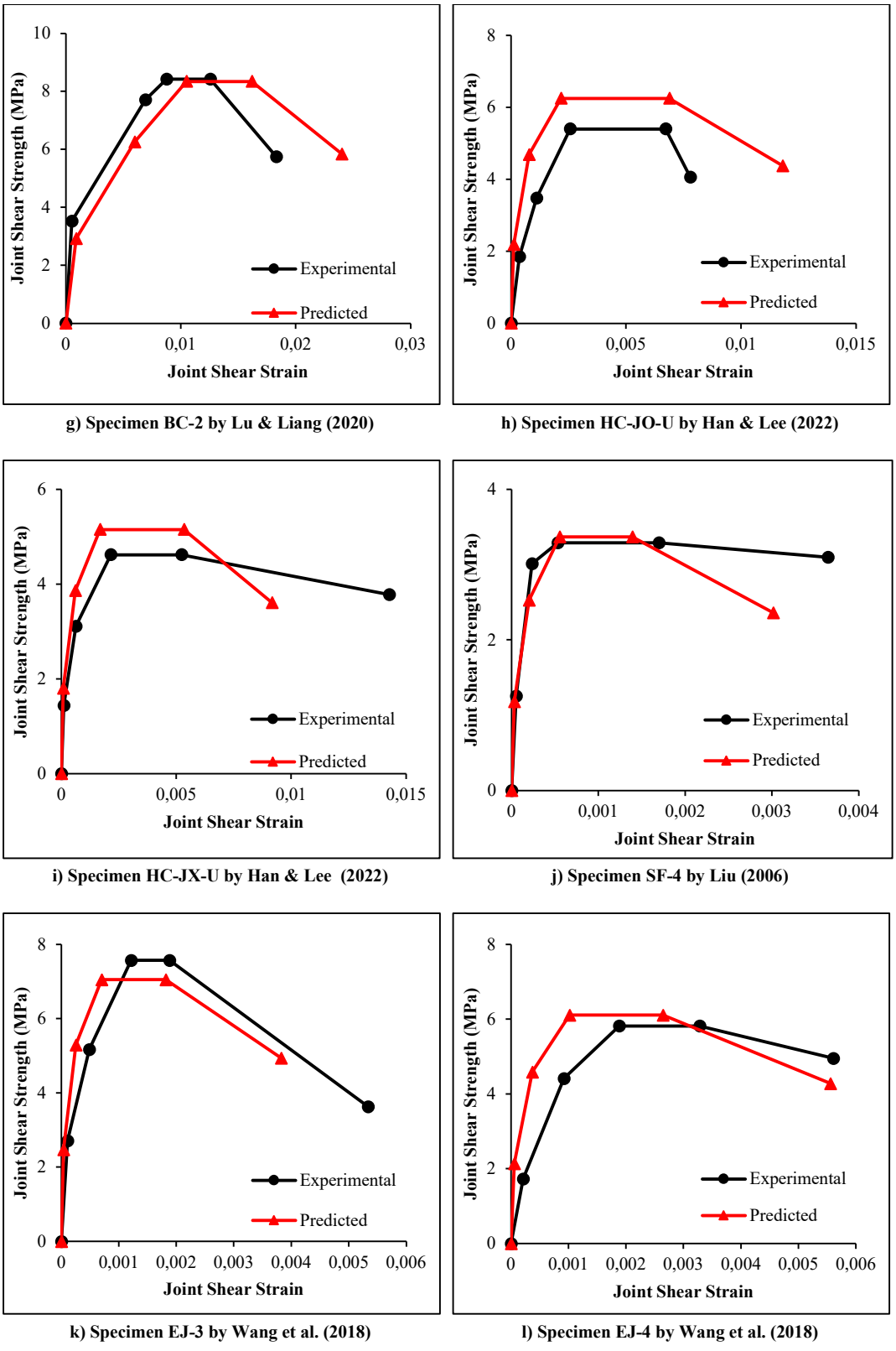

g) Specimen BC-2 by Lu & Liang (2020)

h) Specimen HC-JO-U by Han & Lee (2022)

i) Specimen HC-JX-U by Han & Lee (2022)

j) Specimen SF-4 by Liu (2006)

k) Specimen EJ-3 by Wang et al. (2018)

l) Specimen EJ-4 by Wang et al. (2018)

Figure 5.6. Comparison of predicted & experimental data for other several tests.

CHAPTER 6

SUMMARY AND CONCLUSIONS

6.1 Summary

The main objective of this study is to develop a comprehensive practical model that accurately predicts the shear strength and characterizes the relationship between shear stress and shear distortion of FRCC beam-to-column joints subjected to seismic loading. By incorporating different fiber types in the prediction, the model's applicability extends to a broad spectrum of FRCC applications in beam-to-column connections.

Within the scope of this study, a comprehensive database has been compiled by gathering and analyzing a diverse range of experimental data, with a specific focus on the seismic behavior of FRCC beam-to-column connections. The database contains a diverse range of data, including parameters such as specimen dimensions, fiber types, material properties, loading conditions, reinforcement detailing, and the resulting outcomes derived from these experimental investigations. Special attention has been given to tests that provide the joint shear stress vs. distortion relationships that will contribute to the development of a backbone curve, which can be used in nonlinear analysis.

The compiled database was utilized in the development of a joint shear prediction equation employing the analytical abilities of IBM SPSS to establish correlations of the stress and distortion values with the key parameters. Once the influencing parameters are identified, nonlinear regression techniques within IBM SPSS are applied to analyze and optimize the equation in an iterative manner, aiming to minimize the average absolute error between predicted and experimental values while maximizing their inherent correlation.

Following the development of the joint shear strength prediction equation, a systematic progression was undertaken to develop the joint shear stress vs. distortion model. To ensure the model's robustness and reliability, validation procedures were employed, utilizing additional experimental data.

6.2 Conclusions

After the detailed analytical investigation, the following conclusions are derived.

1. The correlation analysis identified key parameters influencing the shear strength of FRCC joints, including the compressive strength and tensile cracking strength of the composite, joint stirrup volumetric ratio, beam-to-column joint aspect ratio, and fiber properties such as volume fraction, aspect ratio, and reinforcing index.
2. The proposed joint shear strength prediction equation resulted in an average absolute error of 7.7%, demonstrating a strong correlation (coefficient of correlation: 0.97) between the predicted and experimental values. The equation outperformed other prediction models, displaying coefficients of correlation of 0.98 and 0.92 for exterior and interior joints, respectively.
3. The proposed shear strength prediction equation for FRCC beam-to-column joints offers the lowest error compared to existing prediction equations. It provides a simple and accurate tool that can be incorporated into structural design codes related to fiber reinforced cementitious composites and their application in beam-to-column connections.
4. An alternative joint shear strength prediction equation based on single-layer joint hoop ratio definition was explored but showed similar errors and coefficients of correlation. Thus, the gross volume approach was selected for simplicity and practicality.
5. The prediction equation mostly yields conservative estimates of joint shear strength, unlike other equations found in the literature that tend to overestimate.

6. Joint shear strength prediction equations recommended by ACI 352-02, ACI 318-19 and TSC2018 exhibit relatively homogenous scatter and lower errors than expected although they are explicitly developed for reinforced concrete structures.
7. The influence of beam longitudinal bars on joint shear capacity is not accounted for in the joint shear strength prediction equation, as it also affects the joint shear demand.
8. Since fibers are also confining the joint, the effect of transverse beams and slabs presence on joint shear strength is reduced. Although the confinement provided by the transverse beams and slabs is not considered, the proposed equation achieves a high level of accuracy.
9. Structural design codes currently lack provisions for the seismic behavior of FRCC beam-to-column connections, emphasizing the need for future enhancements in this area.
10. A backbone curve, capturing inelastic behavior of the joint, has been developed and validated utilizing experimental data. The use of this model in nonlinear analysis will provide more realistic results compared to rigid joint modeling in terms of internal forces and story drifts.
11. Proposed FRCC joint shear stress vs. distortion model is verified with the existing experimental data in terms of coefficient of correlation and average absolute error.
12. The proposed FRCC joint shear stress vs. strain model offers accurate representation of seismic behavior for composites with different fiber types, including hybrid FRCC, making it a pioneering study in this field.
13. The proposed joint shear stress vs. strain model is applicable to various fiber types, including hooked end steel fibers, straight steel fibers, PVA fibers, glass fibers, basalt fibers, PP fibers, PET fibers, PE fibers, and Aramid fibers, filling a gap in the literature.

6.3 Future Research Recommendations

Even though the current joint model yields satisfactory outcomes for the subassemblies in the database, there is room for further improvement to attain enhanced precision in the results.

Firstly, the number of tests conducted on knee connections and roof connections may be increased, as the existing literature lacks sufficient number of experiments in these areas. This will enable a more comprehensive evaluation, considering different types of joints.

Moreover, the experiments on the beam-to-column joints may be conducted on larger scales, preferably full scale. Smaller section dimensions reduce the likelihood of random fiber distribution, which may not accurately represent the actual behavior of the joints. Therefore, larger-scale experiments are needed to ensure realistic results.

Wide beam-to-column connections and eccentric specimens should also be tested and added to the database, as there is a lack of tests conducted on these joint types in the literature. Since these connection types are commonly encountered in real-life structures, it is crucial to explore their behavior both experimentally and analytically.

Furthermore, the number of tests that include transverse beams and slabs should be increased to further investigate the confining effect of these members in detail. This will provide a better understanding of their influence on the shear strength vs. distortion relationship of FRCC joints.

It is also significant to increase the number of tests on hybrid fiber FRCC specimens to explore the behavior of hybridization in more depth. The current number of tests in this area is insufficient, and increasing the research in hybrid fibers will contribute to a more comprehensive understanding of their influence.

Most importantly, incorporating plastic hinge models on beam and column ends near the joint faces would enable nonlinear analysis to be conducted. However, the existing literature lacks an adequate number of studies addressing this aspect. It is

recommended to conduct modeling studies on moment curvature behavior of FRCC members to complement the material testing and obtain accurate moment curvature relationships, for which the accurate modeling of tensile stress strain relationship is required. Therefore, investigation on modeling of tensile stress-strain behavior of FRCC materials in detail is required in this field, as there is a lack of tensile stress-strain models for FRCC with different fiber types. Comprehensive exploration of this material characteristic will contribute to a better understanding of its mechanical response under tensile loading.

REFERENCES

Abadel, A., Abbas, H., Almusallam, T., Al-Salloum, Y., & Siddiqui, N. (2016). Mechanical properties of hybrid fibre-reinforced concrete – analytical modelling and experimental behaviour. *Magazine of Concrete Research*, *68*(16), 823–843. https://doi.org/10.1680/jmacr.15.00276

Abbas, Y. M., Hussain, L. A., & Khan, M. I. (2022). Constitutive Compressive Stress–Strain Behavior of Hybrid Steel-PVA High-Performance Fiber-Reinforced Concrete. *Journal of Materials in Civil Engineering*, *34*(1). https://doi.org/10.1061/(ASCE)MT.1943-5533.0004041

Abbass, W., Khan, M. I., & Mourad, S. (2018). Evaluation of mechanical properties of steel fiber reinforced concrete with different strengths of concrete. *Construction and Building Materials*, *168*, 556–569. https://doi.org/10.1016/j.conbuildmat.2018.02.164

AbdelAleem, B. H., Ismail, M. K., & Hassan, A. A. A. (2020). Structural Behavior of Rubberized Engineered Cementitious Composite Beam-Column Joints under Cyclic Loading. *ACI Structural Journal*, *117*(2). https://doi.org/10.14359/51720194

ACI Committee 318. (2019). *ACI318-19 Building Code Requirements for Structural Concrete and Commentary*. American Concrete Institute. https://doi.org/10.14359/51716937

ACI Committee 544. (2017). *ACI544.9-17: Report on Measuring Mechanical Properties of Hardened Fiber-Reinforced Concrete*.

ACI Committee 544. (2018). *ACI544.4-18: Guide to Design with Fiber-Reinforced Concrete*.

ACI-ASCE Committee 352. (2002). *ACI352-02: Recommendations for Design of Beam-Column Connections in Monolithic Reinforced Concrete Structures(Reapp 2010)*.

Ahmad, J., Aslam, F., Martínez-García, R., de Prado-Gil, J., Abbas, N., & Hechmi EI Ouni, M. (2021). Mechanical performance of concrete reinforced with polypropylene fibers (PPFs). *Journal of Engineered Fibers and Fabrics*, *16*, 155892502110603. https://doi.org/10.1177/15589250211060399

Akin, U. (2011). *Seismic Assessment of Reinforced Concrete Beam-to-Column Connections under Reversed Cyclic Loading* [M.S. Thesis]. Middle East Technical University.

Al-Lebban, M. F., Khazaly, A. I., Shabbar, R., Jabal, Q. A., & Al Asadi, L. A. R. (2021). Effect of Polypropylene Fibers on some Mechanical Properties of Concrete and Durability against Freezing and Thawing Cycles. *Key Engineering Materials*, *895*, 130–138. https://doi.org/10.4028/www.scientific.net/KEM.895.130

Almusallam, T., Ibrahim, S. M., Al-Salloum, Y., Abadel, A., & Abbas, H. (2016). Analytical and experimental investigations on the fracture behavior of hybrid fiber reinforced concrete. *Cement and Concrete Composites*, *74*, 201–217. https://doi.org/10.1016/j.cemconcomp.2016.10.002

Alsadey, S. (2016). Effect of Polypropylene Fiber on Properties of Mortar. *International Journal of Energy Science and Engineering*, *2*(2).

Alsadey, S., & Salem, M. (2016). Effect of Polypropylene Fiber on Properties of Mortar. *American Journal of Engineering Research (AJER)*, *5*(7), 223–226.

Annadurai, A., & Ravichandran, A. (2016). Effects Of Hybrid Fiber Reinforced High- Strength Concrete in Exterior Beam – Column Joint Specimens. *Asian Journal of Civil Engineering (Building and Housing)*, *17*.

Architectural Institute of Japan. (1999). *Design Guidelines for Earthquake Resistant Reinforced Concrete Buildings Based on Inelastic Displacement Concept*.

Ayub, T., Khan, S. U., & Ayub, A. (2019). Analytical model for the compressive stress–strain behavior of PVA-FRC. *Construction and Building Materials*, *214*, 581–593. https://doi.org/10.1016/j.conbuildmat.2019.04.126

Ayub, T., Shafiq, N., & Nuruddin, M. F. (2014). Effect of Chopped Basalt Fibers on the Mechanical Properties and Microstructure of High Performance Fiber Reinforced Concrete. *Advances in Materials Science and Engineering*, *2014*, 1–14. https://doi.org/10.1155/2014/587686

Banu, W. B., Jaya, K. P., & Vidjeapriya, R. (2023). Seismic Behaviour of Exterior Beam-Column Joint Using Steel Fibre-Reinforced Concrete Under Reverse Cyclic Loading. *Arabian Journal for Science and Engineering*, *48*(4), 4635–4655. https://doi.org/10.1007/s13369-022-07139-z

Bayasi, Z., & Gebman, M. (2002). Reduction of Lateral Reinforcement in Seismic Beam-Column Connection via Application of Steel Fibers. *ACI Structural Journal*, *99*(6). https://doi.org/10.14359/12342

Bentur, A., & Mindess, S. (2006). *Fibre Reinforced Cementitious Composites* (Routledge, Ed.). CRC Press. https://doi.org/10.1201/9781482267747

Bhargava, P., Sharma, U. K., & Kaushik, Surendra. K. (2006). Compressive Stress-Strain Behavior of Small Scale Steel Fibre Reinforced High Strength Concrete Cylinders. *Journal of Advanced Concrete Technology*, *4*(1), 109–121. https://doi.org/10.3151/jact.4.109

Branston, J., Das, S., Kenno, S. Y., & Taylor, C. (2016). Mechanical behaviour of basalt fibre reinforced concrete. *Construction and Building Materials*, *124*, 878–886. https://doi.org/10.1016/j.conbuildmat.2016.08.009

Burak, B. (2005). *Seismic Behavior of Eccentric Reinforced Concrete Beam-Column-Slab Connections* [Ph.D. Thesis]. The University of Michigan.

Burak, B., & Wight, J. K. (2005). *Seismic Behavior of Eccentric Reinforced Concrete Beam-Column-Slab Connections* [Ph.D. Thesis]. The University of Michigan.

Cao, M., & Li, L. (2018). New models for predicting workability and toughness of hybrid fiber reinforced cement-based composites. *Construction and Building Materials*, *176*, 618–628. https://doi.org/10.1016/j.conbuildmat.2018.05.075

Chasioti, S. G., & Vecchio, F. J. (2017). Effect of Fiber Hybridization on Basic Mechanical Properties of Concrete. *ACI Materials Journal*, *114*(3). https://doi.org/10.14359/51689479

Chidambaram, S. R., & Agarwal, P. (2015). Seismic behavior of hybrid fiber reinforced cementitious composite beam–column joints. *Materials & Design*, *86*, 771–781. https://doi.org/10.1016/j.matdes.2015.07.164

Chidambaram, S. R., & Agarwal, P. (2018). Performance Evaluation of Metallic and Synthetic Fiber Hybridization on the Cyclic Behavior of Exterior Beam-Column Joint. *Advances in Civil Engineering Materials*, *7*(1), 20170137. https://doi.org/10.1520/ACEM20170137

Choi, C.-S., & Bae, B.-I. (2019). Effectiveness of Steel Fibers as Hoops in Exterior Beam-to-Column Joint Under Cyclic Loading. *ACI Structural Journal*, *116*(2). https://doi.org/10.14359/51712278

Chung, K. L., Ghannam, M., & Zhang, C. (2018). Effect of Specimen Shapes on Compressive Strength of Engineered Cementitious Composites (ECCs) with Different Values of Water-to-Binder Ratio and PVA Fiber. *Arabian Journal for Science and Engineering*, *43*(4), 1825–1837. https://doi.org/10.1007/s13369-017-2776-8

Cui, K., Liang, K., Chang, J., & Lau, D. (2022). Investigation of the macro performance, mechanism, and durability of multiscale steel fiber reinforced low-carbon ecological UHPC. *Construction and Building Materials*, *327*, 126921. https://doi.org/10.1016/j.conbuildmat.2022.126921

Disaster and Emergency Management Presidency. (2018). *TSC2018: Turkish Seismic Code - 2018*.

European Committee for Standardization (CEN). (2004). *Eurocode 8: Design of Structures for Earthquake Resistance - Part 1: General rules, Seismic Actions and Rules for Buildings, European Standard EN 1998-1*.

Ezeldin, A. S., & Balaguru, P. N. (1992). Normal- and High-Strength Fiber-Reinforced Concrete under Compression. *Journal of Materials in Civil Engineering*, *4*(4), 415–429. https://doi.org/10.1061/(ASCE)0899-1561(1992)4:4(415)

Fanella, D. A., & Naaman, A. E. (1985). Stress-Strain Properties of Fiber Reinforced Mortar in Compression. *ACI Journal Proceedings*, *82*(4). https://doi.org/10.14359/10359

Fang, H., Gu, M., Zhang, S., Jiang, H., Fang, Z., & Hu, J. (2022). Effects of Steel Fiber and Specimen Geometric Dimensions on the Mechanical Properties of Ultra-High-Performance Concrete. *Materials*, *15*(9), 3027. https://doi.org/10.3390/ma15093027

Faruk, O., Bledzki, A. K., Fink, H.-P., & Sain, M. (2014). Progress Report on Natural Fiber Reinforced Composites. *Macromolecular Materials and Engineering*, *299*(1), 9–26. https://doi.org/10.1002/mame.201300008

Filiatrault, A., Ladicani, K., & Massicotte, B. (1994). Seismic Performance of Code-Designed Fiber Reinforced Concrete Joints. *ACI Structural Journal*, *91*(5). https://doi.org/10.14359/4172

Filiatrault, A., Pineau, S., & Houde, J. (1995). Seismic Behavior of Steel-Fiber Reinforced Concrete Interior Beam-Column Joints. *ACI Structural Journal*, *92*(5). https://doi.org/10.14359/905

Ganesan, N., Indira, P. V., & Abraham, R. (2007). Steel Fibre Reinforced High Performance Concrete Beam-Column Joints Subjected to Cyclic Loading. *ISET Journal of Earthquake Technology*, *44*.

Gao, D., Guo, Y., Pang, Y., Chen, G., Shi, M., Ding, C., & Liu, D. (2023). Analysis and prediction of the compressive and splitting tensile performances for the novel multiple hooked-end steel fiber reinforced concrete. *Structural Concrete*, *24*(1), 1452–1470. https://doi.org/10.1002/suco.202200487

Gao, D., Shi, K., & Zhao, S. (2014). Calculation method for bearing capacity of steel fiber reinforced high-strength concrete beam-column joints. *Journal of Building Structures*, *35*(2), 71–79.

Gao, D., Yan, H., Yang, L., Pang, Y., & Sun, B. (2022). Analysis of bond performance of steel bar in steel-polypropylene hybrid fiber reinforced concrete with partially recycled coarse aggregates. *Journal of Cleaner Production*, *370*, 133528. https://doi.org/10.1016/j.jclepro.2022.133528

Gebman, M. (2001). *Application of Steel Fiber Reinforced Concrete in Seismic Beam-Column Joints* [M.Sc.Thesis]. San Diego State University.

Gefken, P. R., & Ramey, M. R. (1989). Increased Joint Hoop Spacing in Type 2 Seismic Joints Using Fiber Reinforced Concrete. *ACI Structural Journal*, *86*(2). https://doi.org/10.14359/2674

Gencoglu, M. (2000). *An Experimental Study on the Effective Zone of the Steel Fiber Reinforced Concrete Used in Exterior Beam-Column Connections Subjected to Bi-directional Reversals Cyclic Loadings* [Ph.D. Thesis]. Istanbul Technical University.

Gencoglu, M. (2007). The effects of stirrups and the extents of regions used SFRC in exterior beam-column joints. *Structural Engineering and Mechanics*, *27*(2), 223–241. https://doi.org/10.12989/sem.2007.27.2.223

Gencoglu, M., & Eren, İ. (2002). An experimental study on the effect of steel fiber reinforced concrete on the behavior of the exterior beam-column joints subjected to reversal cyclic loading. *Turkish Journal of Engineering and Environmental Sciences*, *26*(6), 493–502.

Ghosni, N., Samali, B., & Valipour, H. (2016). Evaluation of the Mechanical Properties of Steel and Polypropylene Fibre-Reinforced Concrete Used in Beam Column Joints. *Composite Construction in Steel and Concrete VII*, 401–407. https://doi.org/10.1061/9780784479735.030

Graybeal, B., & Davis, M. (2008). Cylinder or Cube: Strength Testing of 80 to 200 MPa (11.6 to 29 ksi) Ultra-High-Performance Fiber-Reinforced Concrete. *ACI Materials Journal*, *105*(6). https://doi.org/10.14359/20202

Guler, S., Yavuz, D., Korkut, F., & Ashour, A. (2019). Strength prediction models for steel, synthetic, and hybrid fiber reinforced concretes. *Structural Concrete*, *20*(1), 428–445. https://doi.org/10.1002/suco.201800088

Han, S. W., & Lee, S. H. (2022). Cyclic behavior of high-performance fiber-reinforced cementitious composite corner joints. *Journal of Building Engineering*, *47*, 103892. https://doi.org/10.1016/j.jobe.2021.103892

Hanif, F., & Kanakubo, T. (2017). Shear Performance of Fiber-Reinforced Cementitious Composites Beam-Column Joint Using Various Fibers. *Journal of the Civil Engineering Forum*, *3*(2), 383. https://doi.org/10.22146/jcef.26571

Henager, C. H. (1977). Steel Fibrous-Ductile Concrete Joint for Seismic-Resistant Structures. *ACI Symposium Publication*, *53*. https://doi.org/10.14359/17703

Hosseini, F., Gencturk, B., Aryan, H., & Cadaval, G. (2018). Seismic behavior of 3-D ECC beam-column connections subjected to bidirectional bending and torsion. *Engineering Structures*, *172*, 751–763. https://doi.org/10.1016/j.engstruct.2018.06.054

Ibrahim, S. M., Almusallam, T. H., Al-Salloum, Y. A., Abadel, A. A., & Abbas, H. (2016). Strain Rate Dependent Behavior and Modeling for Compression Response of Hybrid Fiber Reinforced Concrete. *Latin American Journal of Solids and Structures*, *13*(9), 1695–1715. https://doi.org/10.1590/1679-78252717

Ismail, M. K., Abdelaleem, B. H., & Hassan, A. A. A. (2018). Effect of fiber type on the behavior of cementitious composite beam-column joints under reversed cyclic loading. *Construction and Building Materials*, *186*, 969–977. https://doi.org/10.1016/j.conbuildmat.2018.08.024

Jalasutram, S., Sahoo, D. R., & Matsagar, V. (2017). Experimental investigation of the mechanical properties of basalt fiber-reinforced concrete. *Structural Concrete*, *18*(2), 292–302. https://doi.org/10.1002/suco.201500216

Jiang, C., Fan, K., Wu, F., & Chen, D. (2014). Experimental study on the mechanical properties and microstructure of chopped basalt fibre reinforced concrete. *Materials & Design*, *58*, 187–193. https://doi.org/10.1016/j.matdes.2014.01.056

Jiuru, T., Chaobin, H., Kaijian, Y., & Yongcheng, Y. (1992). Seismic Behavior and Shear Strength of Framed Joint Using Steel-Fiber Reinforced Concrete. *Journal of Structural Engineering*, *118*(2), 341–358. https://doi.org/10.1061/(ASCE)0733-9445(1992)118:2(341)

Jongvivatsakul, P., Thi, C. N., Tanapornraweekit, G., & Bui, L. V. H. (2020). Mechanical properties of aramid fiber-reinforced composites and performance on repairing concrete beams damaged by corrosion. *Songklanakarin Journal of Science and Technology (SJST)*, *42*(3), 637–644.

Kanda, T., & Li, V. C. (1999). Effect of Fiber Strength and Fiber-Matrix Interface on Crack Bridging in Cement Composites. *Journal of Engineering Mechanics*, *125*(3), 290–299. https://doi.org/10.1061/(ASCE)0733-9399(1999)125:3(290)

Kang, T. H.-K., Kim, S., Shin, J. H., & LaFave, J. M. (2019). Seismic Behavior of Exterior Beam-Column Connections with High-Strength Materials and Steel Fibers. *ACI Structural Journal*, *116*(4). https://doi.org/10.14359/51715568

Khabaz, A. (2014). Determination of Friction Coefficient between Glass Fiber and the Concrete Fri (GF.C). *International Journal of Materials Science and Applications*, *3*(6), 321. https://doi.org/10.11648/j.ijmsa.20140306.17

Khan, M., Cao, M., & Ali, M. (2020). Cracking behaviour and constitutive modelling of hybrid fibre reinforced concrete. *Journal of Building Engineering*, *30*, 101272. https://doi.org/10.1016/j.jobe.2020.101272

Kheni, D., Scott, R. H., Deb, S. K., & Dutta, A. (2015). Ductility Enhancement in Beam-Column Connections Using Hybrid Fiber-Reinforced Concrete. *ACI Structural Journal*, *112*(2). https://doi.org/10.14359/51687405

Kim, S. B., Yi, N. H., Kim, H. Y., Kim, J.-H. J., & Song, Y.-C. (2010). Material and structural performance evaluation of recycled PET fiber reinforced concrete. *Cement and Concrete Composites*, *32*(3), 232–240. https://doi.org/10.1016/j.cemconcomp.2009.11.002

Krishna, R., Kumar, R., & Srinivas, B. (2011). Effect of size and shape of specimen on compressive strength of glass fiber reinforced concrete (GFRC). *Facta Universitatis - Series: Architecture and Civil Engineering*, *9*(1), 1–9. https://doi.org/10.2298/FUACE1101001K

Li, V. C. (2008). Engineered Cementitious Composite (ECC): Material, Structural, and Durability Performance. In E. G. Nawy (Ed.), *Concrete Construction Engineering Handbook* (2nd Ed.). CRC Press.

Li, V. C., & Wu, H.-C. (1992). Conditions for Pseudo Strain-Hardening in Fiber Reinforced Brittle Matrix Composites. *Applied Mechanics Reviews*, *45*(8), 390–398. https://doi.org/10.1115/1.3119767

Li, Y., Zhao, R.-H., Li, D.-Y., & Qu, C. (2022). Study on Seismic Performance of Recycled Steel Fibers Locally Reinforced Cruciform Concrete Frame Beam-Column Joint. *Advances in Civil Engineering*, *2022*, 1–19. https://doi.org/10.1155/2022/8155038

Li, Y.-F., Huang, Y.-R., Syu, J.-Y., Tsai, Y.-K., & Huang, C.-H. (2022). A study on mechanical behavior of Kevlar fiber reinforced concrete under static and high-strain rate loading. *International Journal of Protective Structures*, 204141962211185. https://doi.org/10.1177/20414196221118596

Li, Y.-F., Wang, H.-F., Syu, J.-Y., Ramanathan, G. K., Tsai, Y.-K., & Lok, M. H. (2021). Mechanical Properties of Aramid/Carbon Hybrid Fiber-Reinforced Concrete. *Materials*, *14*(19), 5881. https://doi.org/10.3390/ma14195881

Liang, X., & Lu, T. (2018). Seismic evaluation of engineered cementitious composites beam-column-slab subassemblies with various column-to-beam flexural strength ratios. *Structural Concrete*, *19*(3), 735–746. https://doi.org/10.1002/suco.201600119

Liang, X., Wang, Y., Tao, Y., & Deng, M. (2016). Seismic performance of fiber-reinforced concrete interior beam-column joints. *Engineering Structures*, *126*, 432–445. https://doi.org/10.1016/j.engstruct.2016.08.001

Lin, C., Kanstad, T., Jacobsen, S., & Ji, G. (2023). Bonding property between fiber and cementitious matrix: A critical review. *Construction and Building Materials*, *378*, 131169. https://doi.org/10.1016/j.conbuildmat.2023.131169

Liu, C. (2006). *Seismic Behaviour of Beam-Column Joint Subassemblies Reinforced with Steel Fibres* [Master of Engineering Thesis]. University of Canterbury.

Liu, Z., Cao, M., & Xie, C. (2023). The Mechanical Properties of Mortar Blended with Steel-PVA Hybrid Fibers and CaCO3 Whiskers Under Freeze/Thaw Cycles Condition. *Arabian Journal for Science and Engineering*, *48*(4), 4451–4469. https://doi.org/10.1007/s13369-022-06917-z

Lu, T.-T., & Liang, X.-W. (2020). Effect of HPFRCC on Seismic Performance of Beam-Column-Slab Subassembly. *KSCE Journal of Civil Engineering*, *24*(12), 3785–3796. https://doi.org/10.1007/s12205-020-0097-z

Mansur, M. A., Chin, M. S., & Wee, T. H. (1999). Stress-Strain Relationship of High-Strength Fiber Concrete in Compression. *Journal of Materials in Civil Engineering*, *11*(1), 21–29. https://doi.org/10.1061/(ASCE)0899-1561(1999)11:1(21)

Marthong, C., & Marthong, S. (2016). An experimental study on the effect of PET fibers on the behavior of exterior RC beam-column connection subjected to reversed cyclic loading. *Structures*, *5*, 175–185. https://doi.org/10.1016/j.istruc.2015.11.003

Ministry of Construction of PR China. (1989). *GBJ 10-89: Code for the design of concrete structures*.

Mitchell, M. (2019). *Engauge Digitizer* (12.1).

Montgomery, D. C., Peck, E. A., & Vining, G. G. (2012). *Introduction to Linear Regression Analysis* (5th Edition). John Wiley & Sons, INC.

Mu, Y., Ando, M., Yasojima, A., & Kanakubo, T. (2018). *Influence of Fiber Orientation on Structural Performance of Beam-Column Joints Using PVA FRCC* (pp. 465–472). https://doi.org/10.1007/978-94-024-1194-2_54

Muthupriya, P., Boobalan, S. C., & Vishnuram, B. G. (2014). Behaviour of fibre-reinforced high-performance concrete in exterior beam-column joint. *International Journal of Advanced Structural Engineering*, *6*(3), 1–7. https://doi.org/10.1007/s40091-014-0057-2

Muthuswamy, K. R., & Thirugnanam, G. S. (2014). Structural behaviour of hybrid fibre reinforced concrete exterior BeamColumn joint subjected to cyclic loading. *International Journal of Civil And Structural Engineering*, *4*(3), 262–273.

Naaman, A. E. (2008). High Performance Fiber Reinforced Cement Composites. In C. Shi & Y. L. Mo (Eds.), *High-Performance Construction Materials* (Vol. 1). World Scientific. https://doi.org/10.1142/6793

Naaman, A. E. (2018). Fiber reinforced concrete: five decades of progress. *Proceedings of the 4th Brazilian Conference on Composite Materials*, 35–56. https://doi.org/10.21452/bccm4.2018.02.01

Naaman, A. E., & Reinhardt, H. W. (1996). Characterization of high performance fiber reinforced cement composites. In A. E. Naaman & H. W. Reinhardt (Eds.), *High Performance Fiber Reinforced Cement Composites 2* (pp. 1–24). E. and FN Spon.

Nataraja, M. C., Dhang, N., & Gupta, A. P. (1999). Stress–strain curves for steel-fiber reinforced concrete under compression. *Cement and Concrete Composites*, *21*(5–6), 383–390. https://doi.org/10.1016/S0958-9465(99)00021-9

Nawy, E. G. (2008). Fiber-Reinforced Composites. In E. G. Nawy (Ed.), *Concrete Construction Engineering Handbook* (2nd Ed.). CRC Press.

Nibudey, R. N., Nagarnaik, P. B., Parbat, D. K., & Pande, A. M. (2013a). Cube and cylinder compressive strengths of waste plastic fiber reinforced concrete. *International Journal of Civil and Structural Engineering*, *4*(2), 174–182.

Nibudey, R. N., Nagarnaik, P. B., Parbat, D. K., & Pande, A. M. (2013b). Strength and fracture properties of post consumed waste plastic fiber reinforced concrete. *International Journal of Civil, Structural, Environmental and Infrastructure Engineering Research and Development (IJCSEIERD)*, *3*(2), 9–16.

Niwa, J., Shakya, K., Matsumoto, K., & Watanabe, K. (2012). Experimental Study on the Possibility of Using Steel Fiber–Reinforced Concrete to Reduce Conventional Rebars in Beam-Column Joints. *Journal of Materials in Civil Engineering*, *24*(12), 1461–1473. https://doi.org/10.1061/(ASCE)MT.1943-5533.0000536

Nouri, A., Saghafi, M. H., & Golafshar, A. (2019). Evaluation of beam-column joints made of HPFRCC composites to reduce transverse reinforcements. *Engineering Structures*, *201*, 109826. https://doi.org/10.1016/j.engstruct.2019.109826

Nuruddin, Muhd. F., Ullah Khan, S., Shafiq, N., & Ayub, T. (2015). Strength Prediction Models for PVA Fiber-Reinforced High-Strength Concrete. *Journal of Materials in Civil Engineering*, *27*(12). https://doi.org/10.1061/(ASCE)MT.1943-5533.0001279

Ou, Y.-C., Tsai, M.-S., Liu, K.-Y., & Chang, K.-C. (2012). Compressive Behavior of Steel-Fiber-Reinforced Concrete with a High Reinforcing Index. *Journal of Materials in Civil Engineering*, *24*(2), 207–215. https://doi.org/10.1061/(ASCE)MT.1943-5533.0000372

P 3101 Concrete Design Committee for the Standards Council. (2006). *The New Zealand Concrete Structures Standard*.

Parra-Montesinos, G. J. (2005). High-Performance Fiber-Reinforced Cement Composites: An Alternative for Seismic Design of Structures. *ACI Structural Journal*, *102*(5). https://doi.org/10.14359/14662

Parra-Montesinos, G. J., Peterfreund, S. W., & Shih-Ho, C. (2005). Highly Damage-Tolerant Beam-Column Joints Through Use of High-Performance Fiber-Reinforced Cement Composites. *ACI Structural Journal*, *102*(3). https://doi.org/10.14359/14421

Patel, P. A., Desai, A. K., & Desai, J. A. (2013). Evaluation of RC and SFRC exterior beam–column joint under cyclic loading for reduction in lateral reinforcement of the joint region. *Magazine of Concrete Research*, *65*(7), 405–414. https://doi.org/10.1680/macr.12.00078

Pekgokgoz, R. K., & Avcil, F. (2022). Effect of steel fibres on reinforced concrete beam-column joints under reversed cyclic loading. *Journal of the Croatian Association of Civil Engineers*, *73*(12), 1185–1194. https://doi.org/10.14256/JCE.3092.2020

Pešić, N., Živanović, S., Garcia, R., & Papastergiou, P. (2016). Mechanical properties of concrete reinforced with recycled HDPE plastic fibres. *Construction and Building Materials*, *115*, 362–370. https://doi.org/10.1016/j.conbuildmat.2016.04.050

Qudah, S., & Maalej, M. (2014). Application of Engineered Cementitious Composites (ECC) in interior beam–column connections for enhanced seismic resistance. *Engineering Structures*, *69*, 235–245. https://doi.org/10.1016/j.engstruct.2014.03.026

Qureshi, L. A., & Muhammad, U. (2018). Effects of Incorporating Steel and Glass Fibers on Shear Behavior of Concrete Column-Beam Joints. *KSCE Journal of Civil Engineering*, *22*(8), 2970–2981. https://doi.org/10.1007/s12205-017-0037-8

Rajkumar, R., Umamaheswari, N., & Anand, S. V. (2021). Ductile Behaviour of Exterior Beam-Column Joints of High Strength Hybrid Fibre-Reinforced Concrete. *Oxidation Communications*, *44*(2), 451–463.

Ranade, R. (2014). *Advanced Cementitious Composite Development for Resilient and Sustainable Infrastructure* [Ph.D. Thesis]. The University of Michigan.

Ranade, R., Li, V. C., Stults, M. D., Heard, W. F., & Rushing, T. S. (2013). Composite Properties of High-Strength, High-Ductility Concrete. *ACI Materials Journal*, *110*(4). https://doi.org/10.14359/51685788

Rohm, C., Novák, B., Sasmal, S., Karusala, R., & Srinivas, V. (2012). Behaviour of fibre reinforced beam-column sub-assemblages under reversed cyclic loading. *Construction and Building Materials*, *36*, 319–329. https://doi.org/10.1016/j.conbuildmat.2012.04.114

Sachdeva, P., Danie Roy, A. B., & Kwatra, N. (2021). Behaviour of steel fibers reinforced exterior beam-column joint using headed bars under reverse cyclic loading. *Structures*, *33*, 3929–3943. https://doi.org/10.1016/j.istruc.2021.06.074

Sagar, B., & Sivakumar, M. V. N. (2021). Compressive properties and analytical modelling for stress-strain curves of polyvinyl alcohol fiber reinforced concrete. *Construction and Building Materials*, *291*, 123192. https://doi.org/10.1016/j.conbuildmat.2021.123192

Saghafi, M. H., Golafshar, A., Zareian, M. S., & Kashani, M. (2020). The effect of high-performance fiber-reinforced cementitious composites on the lateral behavior of reinforced concrete frames without seismic details. *Structures*, *26*, 801–813. https://doi.org/10.1016/j.istruc.2020.05.012

Saghafi, M. H., Golafshar, A., Zareian, M. S., & Mehri, A. H. (2021). Application of HPFRCC in beam–column joints to reduce transverse reinforcements. *Structures*, *31*, 805–814. https://doi.org/10.1016/j.istruc.2021.02.032

Saghafi, M. H., & Shariatmadar, H. (2018). Enhancement of seismic performance of beam-column joint connections using high performance fiber reinforced cementitious composites. *Construction and Building Materials*, *180*, 665–680. https://doi.org/10.1016/j.conbuildmat.2018.05.221

Saghafi, M. H., Shariatmadar, H., & Kheyroddin, A. (2019). Seismic Behavior of High-Performance Fiber-Reinforced Cement Composites Beam-Column Connection with High Damage Tolerance. *International Journal of Concrete Structures and Materials*, *13*(1), 14. https://doi.org/10.1186/s40069-019-0334-3

Said, S. H. (2016a). A Comparative Study of Conventional Concrete and Engineered Cementitious Composite (ECC) in Exterior RC Beam-Column Joints Subjected to Cyclic Loading. In N. Banthia, M. di Prisco, & S. Soleimani-Dashtaki (Eds.), *Proceedings of the 9th RILEM International Symposium on Fiber Reinforced Concrete*.

Said, S. H. (2016b). *Evaluation of Mechanical Properties of Engineered Cementitious Composite for Exterior Beam-Column Joints under Reversed Cyclic Loading* [Ph. D. Thesis]. University of Malaya.

Said, S. H. (2017). Effect of Replacing the Transverse Reinforcement with Engineered Cementitious Composite in RC Exterior Beam-Column Joints Subjected to Cyclic Loading. In T. Ibrahim, M. Alkhader, H. E. Kadi, & N. Qaddoumi (Eds.), *Eleventh International Conference on Composite Science and Technology*. College of Engineering, American University of Sharjah Sharjah, United Arab Emirates.

Said, S. H., & Razak, H. A. (2015). The effect of synthetic polyethylene fiber on the strain hardening behavior of engineered cementitious composite (ECC). *Materials & Design*, *86*, 447–457. https://doi.org/10.1016/j.matdes.2015.07.125

Sano, N., Yamada, H., Miyaguchi, M., Yasojima, A., & Kanakubo, T. (2015, July). Structural Performance of Beam-Column Joint Using DFRCC. *Proceedings of the 11th Canadian Conference on Earthquake Engineering*.

Sarmah, M., Roy, B., Mozumder, R. A., & Laskar, A. I. (2018a). Effect of Chopped Basalt Fibers on the Cyclic Behavior of RCC Beam–Column Subassemblies. *Arabian Journal for Science and Engineering*, *43*(4), 1865–1874. https://doi.org/10.1007/s13369-017-2801-y

Sarmah, M., Roy, B., Mozumder, R. A., & Laskar, A. I. (2018b). Effect of Chopped Basalt Fibers on the Cyclic Behavior of RCC Beam–Column Subassemblies. *Arabian Journal for Science and Engineering*, *43*(4), 1865–1874. https://doi.org/10.1007/s13369-017-2801-y

Sathishkumar, T., Navaneethakrishnan, P., Shankar, S., Rajasekar, R., & Rajini, N. (2013). Characterization of natural fiber and composites – A review. *Journal of Reinforced Plastics and Composites*, *32*(19), 1457–1476. https://doi.org/10.1177/0731684413495322

Shakya, K., Watanabe, K., Matsumoto, K., & Niwa, J. (2012). Application of steel fibers in beam–column joints of rigid-framed railway bridges to reduce

longitudinal and shear rebars. *Construction and Building Materials*, *27*(1), 482–489. https://doi.org/10.1016/j.conbuildmat.2011.07.016

Sharan, D. S., & Lal, A. (2016). Study the Effect of Polypropylene Fiber in Concrete. *International Research Journal of Engineering and Technology (IRJET)*, *3*(6), 616–619.

Sharma, R., Kaushik, R., & Sharma, T. (2014). Effect of PET Fibres Different Aspect Ratio on Fresh and Mechanical Properties of Cement Concrete. *The Asia-Pacific Young Researchers and Graduates Symposium (YRGS 2014)*.

Shi, K., Zhang, M., Zhang, T., Li, P., Zhu, J., & Li, L. (2021). Seismic Performance of Steel Fiber Reinforced High–Strength Concrete Beam–Column Joints. *Materials*, *14*(12), 3235. https://doi.org/10.3390/ma14123235

Song, P. S., & Hwang, S. (2004). Mechanical properties of high-strength steel fiber-reinforced concrete. *Construction and Building Materials*, *18*(9), 669–673. https://doi.org/10.1016/j.conbuildmat.2004.04.027

Suryanto, B., Tambusay, A., Suprobo, P., Bregoli, G., & Aitken, M. W. (2022). Seismic performance of exterior beam-column joints constructed with engineered cementitious composite: Comparison with ordinary and steel fibre reinforced concrete. *Engineering Structures*, *250*, 113377. https://doi.org/10.1016/j.engstruct.2021.113377

Suwannakarn, S. W. (2009). *Post-Cracking Characteristics of High Performance Fiber Reinforced Cementitious Composites* [Ph.D. Thesis]. The University of Michigan.

Thomas, J., & Ramaswamy, A. (2007). Mechanical Properties of Steel Fiber-Reinforced Concrete. *Journal of Materials in Civil Engineering*, *19*(5), 385–392. https://doi.org/10.1061/(ASCE)0899-1561(2007)19:5(385)

Tingting, L., Hao, Z., & Xingwen, L. (2022). Research on the mechanical properties of the joint of the beam-column subassembly. *Structures*, *35*, 873–881. https://doi.org/10.1016/j.istruc.2021.11.043

Tsonos, A.-D., Kalogeropoulos, G., Iakovidis, P., Bezas, M.-Z., & Koumtzis, M. (2021). Seismic Performance of RC Beam–Column Joints Designed According to Older and Modern Codes: An Attempt to Reduce Conventional Reinforcement Using Steel Fiber Reinforced Concrete. *Fibers*, *9*(7), 45. https://doi.org/10.3390/fib9070045

Unal, M. (2010). *Analytical Modeling of Reinforced Concrete Beam-to-Column Connections* [M.S. Thesis]. Middle East Technical University.

Unal, M., & Burak, B. (2012). Joint shear strength prediction for reinforced concrete beam-to-column connections. *Structural Engineering and Mechanics*, *41*(3), 421–440. https://doi.org/10.12989/sem.2012.41.3.421

Unal, M., & Burak, B. (2013). Development and analytical verification of an inelastic reinforced concrete joint model. *Engineering Structures*, *52*, 284–294. https://doi.org/10.1016/j.engstruct.2013.02.032

Van, T. T. T., & Trung, T. H. (2019). Evaluation of shear resistance for beam-column connections using ultra high performance steel fibre reinforced concrete (UHPSFRC) under cyclic loading by experimental research. *Journal of Physics: Conference Series*, *1425*(1), 012049. https://doi.org/10.1088/1742-6596/1425/1/012049

Wang, D., Ju, Y., Zheng, W., & Shen, H. (2018). Seismic Behavior and Shear Bearing Capacity of Ultra-High Performance Fiber-Reinforced Concrete (UHPFRC) Beam-Column Joints. *Applied Sciences*, *8*(5), 810. https://doi.org/10.3390/app8050810

Wang, Y., Liu, F., Yu, J., Dong, F., & Ye, J. (2020). Effect of polyethylene fiber content on physical and mechanical properties of engineered cementitious

composites. *Construction and Building Materials*, *251*, 118917. https://doi.org/10.1016/j.conbuildmat.2020.118917

Wille, K., El-Tawil, S., & Naaman, A. E. (2014). Properties of strain hardening ultra high performance fiber reinforced concrete (UHP-FRC) under direct tensile loading. *Cement and Concrete Composites*, *48*, 53–66. https://doi.org/10.1016/j.cemconcomp.2013.12.015

Wille, K., Kim, D. J., & Naaman, A. E. (2011). Strain-hardening UHP-FRC with low fiber contents. *Materials and Structures*, *44*(3), 583–598. https://doi.org/10.1617/s11527-010-9650-4

Wu, C. (2001). *Micromechanical Tailoring of PVA-ECC for Structural Applications* [Ph.D. Thesis]. The University of Michigan.

Yagmur, E. (2018). *Analytical modeling of Fiber Reinforced Composite Deep Beams* [Ph.D. Thesis]. Middle East Technical University.

Yamada, H., Ando, M., Yasojima, A., & Kanakubo, T. (2016). Effect of Fiber Types on Shear Performance of Precast Concrete Beam-Column Joints Using DFRCC. *The 7th International Conference of Asian Concrete Federation "Sustainable Concrete for Now and the Future"*.

Yang. K.H. (2011). Tests on Concrete Reinforced with Hybrid or Monolithic Steel and Polyvinyl Alcohol Fibers. *ACI Materials Journal*, *108*(6). https://doi.org/10.14359/51683470

Yuan, F., Pan, J., Xu, Z., & Leung, C. K. Y. (2013). A comparison of engineered cementitious composites versus normal concrete in beam-column joints under reversed cyclic loading. *Materials and Structures*, *46*(1–2), 145–159. https://doi.org/10.1617/s11527-012-9890-6

Yuliarti, K., Fehling, E., & Ismail, M. (2015). UHPC Compressive Strength Test Specimens: Cylinder or Cube? *Procedia Engineering*, *125*, 1076–1080. https://doi.org/10.1016/j.proeng.2015.11.165

Zainal, S. M. I. S., Hejazi, F., & Rashid, R. S. M. (2021). Enhancing the Performance of Knee Beam–Column Joint Using Hybrid Fibers Reinforced Concrete. *International Journal of Concrete Structures and Materials*, *15*(1), 20. https://doi.org/10.1186/s40069-021-00457-w

Zhang, J., Pei, Z., & Rong, X. (2022). Seismic performance of HSS reinforced interior beam-column joints with high-strength steel fiber concrete and enhanced reinforcements. *Journal of Building Engineering*, *48*, 103958. https://doi.org/10.1016/j.jobe.2021.103958

Zhang, L., Yao, J., Hu, Y., Gao, J., & Cheng, Z. (2022). Predicting shear strength of steel fiber reinforced concrete beam-column joints by modified compression field theory. *Structures*, *41*, 1432–1441. https://doi.org/10.1016/j.istruc.2022.05.072

Zhang, R., Matsumoto, K., Hirata, T., Ishizeki, Y., & Niwa, J. (2015). Application of PP-ECC in beam–column joint connections of rigid-framed railway bridges to reduce transverse reinforcements. *Engineering Structures*, *86*, 146–156. https://doi.org/10.1016/j.engstruct.2015.01.005

Zheng, Z. (1995). Synthetic fibre-reinforced concrete. *Progress in Polymer Science*, *20*(2), 185–210. https://doi.org/10.1016/0079-6700(94)00030-6

Zhu, H., Li, C., Gao, D., Yang, L., & Cheng, S. (2019). Study on mechanical properties and strength relation between cube and cylinder specimens of steel fiber reinforced concrete. *Advances in Mechanical Engineering*, *11*(4), 168781401984242. https://doi.org/10.1177/1687814019842423